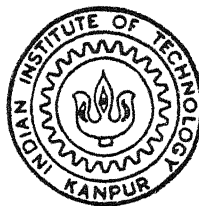# A DETAILED NUMERICAL STUDY OF THERMAL TRANSPORT PROCESSES IN THE METERING SECTION OF A SINGLE-SCREW PLASTICATING EXTRUDER

by

MANAB KUMAR DAS

DEPARTMENT OF MECHANICAL ENGINEERING

INDIAN INSTITUTE OF TECHNOLOGY, KANPUR

October, 1993

A DETAILED NUMERICAL STUDY OF THERMAL TRANSPORT PROCESSES IN THE METERING SECTION OF A SINGLE-SCREW PLASTICATING EXTRUDER

A Thesis Submitted
in Partial Fulfilment of the Requirements
for the Degree of
DOCTOR OF PHILOSOPHY

by
MANAB KUMAR DAS

to the

DEPARTMENT OF MECHANICAL ENGINEERING
INDIAN INSTITUTE OF TECHNOLOGY, KANPUR

OCTOBER, 1993

CERTIFICATE

It is certified that the work contained in the thesis entitled "A detailed numerical study of thermal transport processes in the metering section of a single-screw plasticating extruder", by Mr Manab Kumar Das, has been carried out under my supervision and that this work has not been submitted elsewhere for a degree

P S Ghoshdastidar

(Dr.P. S Ghoshdastidar)
Thesis Supervisor
Department of Mechanical
Engineering
I. I. T. Kanpur

Kanpur
October, 1993

TABLE OF CONTENTS

ABSTRACT

Extrusion is one of the most widely used manufacturing processes in industries dealing with materials such as plastics, polymers and pharmaceutical products In order to control the quality of these products and improve productivity, it is imperative to understand clearly the underlying mechanisms and determine heat transfer rates, residence time distributions, and the thermal and flow fields, etc within the extruder. In the present work, a detailed numerical study of the thermal transport processes in the metering section of a single screw plasticating extruder has been carried out The results are presented for a non-Newtonian material following power-law fluid behaviour The computations using finite-difference scheme has been performed for a uniform barrel temperature distribution and conducting screw A parametric study has also been performed.

Typically, a single screw extruder consists of a screw rotating uniformly inside a barrel maintained at a fixed temperature. At one end there is a hopper, through which plastic granules are fed in. The screw extruder can be divided into three sections, namely, (i) the feed section which is the section near the hopper, (ii) the heating and conveying section where the depth of the screw channel decreases gradually and heat is added raising the fluid pressure and temperature, and (iii) the metering section where the molten material is further heated, accompanied by

further increase in pressure and the material subjected to high shear thus enhancing the mixing

The material in the present study is low density polyethylene (LDPE) which is a highly viscous non-Newtonian fluid Its viscosity is assumed to be following the power-law model Thus, the viscosity of the said fluid is represented as a power law function of the local strain rate and an exponential function of temperature Therefore, the temperature and the velocity profiles are linked by the temperature dependence of viscosity. The conduction within the screw body has been considered leading to conjugate heat transfer between the fluid and the screw which is made of steel Hence, the momentum equations and the energy equation of the fluid and the energy equation of the screw are numerically solved simultaneously subject to satisfying compatibility requirements at the screw-fluid interface and the continuity equation

As the screw channel is shallow and long, and as inertial forces are small in comparison to viscous(since polymers have very high viscosity), creeping flow approximations are made for conservation of momentum. The effect of viscous dissipation is included in the energy equation of the fluid. The coordinate system is fixed to the screw and thus the barrel moves in a directin opposite to the screw rotation. The curvature effects have been neglected, and therefore, the screw is treated as unwound. Therefore, the cross-section of the screw channel is taken as rectangular. Also, the leakage across the screw flights

is ignored The screw is modelled as a semi-infinite body(i.e., semi-infinite in the direction perpendicular to the base of the screw channel) in a thin layer below the screw channel base while the rest of the screw body behaves as adiabatic This means that the present analysis is valid for large extruders having screw channel height to diameter ratio much less than one.

At this point, it is to be emphasized that the basic objective of this study is to develop a model which most accurately simulates the thermal transport processes in the metering section of the screw extruder To achieve this goal, a quasi two-dimensional model followed by a more complex fully two-dimensional model and most complex quasi three-dimensional model have been modelled The aforementioned models basically predict fluid velocities, pressure gradients, pressures, temperatures and screw body temperatures. Furthermore, the models compute the heat input from the barrel, local Nusselt numbers and bulk temperatures along the down-channel direction

In the quasi two-dimensional model, the flow is taken to be hydrodynamically developed but thermally undeveloped In the fully two-dimensional model, the flow is both hydrodynamically and thermally undeveloped. Consequently, the solution procedure for the latter is more involved. For the quasi two-dimensional model, the iterative Newton-Raphson method requiring initial guesses for the pressure gradients is used to satisfy the conditions on the total flow rates given by the integral forms of the continuity equation. The two most important fall-outs of the fully

two-dimensional model are. (a) to develop an efficient and novel numerical technique for computing the pressure gradients accurately, and (b) to show that the flow becomes locally fully developed at a short distance from the inlet, — thus confirming the earlier use of fully developed velocity profile in the quasi two-dimensional model as the inlet boundary condition to be not physically unrealistic.

However the main limitation of both the models is that they do not take into consideration the thermal convections normal to the screw flights as well as to the channel base and thus fail to predict accurately the screw surface temperature which should be nearly equal to barrel temperature in most part of the metering section The necessity of correct prediction of screw surface temperature and also pressure distributions leads to the development of the quasi three-dimensional model which, unlike in the quasi and fully two-dimensional models includes additionally, the conservation of momentum in the direction normal to the base of the channel as well as thermal convections in the direction normal to the screw flights and to the channel base. Also, the contribution of thermal conduction in the direction normal to the screw flights is included. As expected, the inclusion of the cross convection effects results in accurate representation of the screw surface temperature and pressure distribution although the numerical solution procedure becomes more involved requiring the use of SIMPLE algorithm for the solution of flow field in the cross-channel planes of the channel. The results show screw surface temperature rising rapidly to steady values equal to or

slightly higher than the barrel temperature in the greater part of the metering section This trend also tallies well with the reported experimental results of Marshall et al (1965) and Palit(1972) obtained from 63 5 mm (2 5 inch) extruders processing materials such as low density polyethylene, polypropylene and polyvinyl chloride These results support the use of barrel temperature as the thermal boundary condition at the screw surface by some authors in earlier quasi two-dimensional models.

Finally, a parametric study based on the quasi three-dimensional model has also been performed to see the effect of variations in dimensionless volumetric flow rate (q_v), power-law index (n) and screw speed (N) on the pressure gradient, pressure, local Nusselt number and bulk temperature in the downchannel direction of the extruder.

List Of Figures

List Of Tables

NOMENCLATURE

A $\qquad \dot{\gamma}^{n-1} e^{-\beta\theta}$

b $\qquad$ Temperature co-efficient of viscosity

C_p $\qquad$ Specific heat of the fluid at constant pressure

D $\qquad$ Barrel diameter

DXEP(I) $\qquad$ X(IP1)-X(I)

DXEPU(I) $\qquad$ XU(IP1)-XU(I)

DYNP(J) $\qquad$ Y(JP1)-Y(J)

DXPW(I) $\qquad$ X(I)-X(IM1)

DXPWU(I) $\qquad$ XU(I)-XU(IM1)

DYNPV(J) $\qquad$ YV(JP1)-YV(J)

DYPS(J) $\qquad$ Y(J)-Y(JM1)

DYPSV(J) $\qquad$ YV(J)-YV(JM1)

E $\qquad$ Factor used in under-relaxation process (VanDoormaal and Raithby, 1984)

G $\qquad$ Griffith number = $\bar{\mu} \, V_{bz}^{2} / (K_f (T_{b(ref)} - T_i))$

H $\qquad$ Height of the screw channel

H_d $\qquad$ Depth (below the screw surface interface) at which the co-ordinate systemn is fixed

I $\qquad$ Grid line number for an Y-constant line

IM1 $\qquad$ I-1

IP1 $\qquad$ I+1

J $\qquad$ Jacobian matrix. Grid line number for an X-constant line

JM1 $\qquad$ J-1

JP1	J+1
K_f	Thermal conductivity of the fluid
K_s	Thermal conductivity of the screw
L	Axial screw length
N	Screw speed, r p m
NI	Number of X-constant grid lines in the flow domain
NIM1	NI-1
NIM2	NI-2
NJ	Number of Y-constant grid lines in the flow domain
NJM1	NJ-1
NJM2	NJ-2
n	Power law index
p	Pressure along the helix for quasi two-dimensional and fully two-dimensional models Pressure in the transverse plane for quasi three-dimensional case
P_{av}	Space averaged pressure over a cross-section
$\bar{p}$	Reference pressure [$= \bar{\mu}\, V_{bz}/H$]
Pe	Peclet number ($= V_{bz}H/\alpha$)
Q	Total volumetric flow rate
q_v	Dimensionless volumetric flow rate or throughput parameter
q_{in}	Heat flux input at the barrel, Eq.(4.4)
R	$\Delta y_f/\Delta z$
SEW(I)	Distance separating the two constant X cell walls of a cell around a node
SEWU(I)	Distance separating the two constant X-cell walls of a u-cell
SNS(J)	Distance separating the two constant Y-cell walls

	of a cell around a node
SNSV(J)	Distance separating the two constant Y-cell walls of a v-cell
T	Temperature
$T_{b(ref)}$	Reference barrel temperature
T_i	Temperature at the inlet of the heating zone
T_o	Reference temperature
u	Velocity component in the x-direction
V_b	Tangential velocity of the barrel ($=\frac{\pi DN}{60}$)
V_{bx}	Component of V_b in x-direction [$=V_b\sin\phi$]
V_{bz}	Component of V_b in z-direction [$=V_b\cos\phi$]
v	Velocity component in y-direction
W	Width of the screw channel
w	Velocity component in the z-direction
x	Co-ordinate axis normal to the screw flights
X(I)	X- co-ordinate values of the X constant grid lines
X(IM1)	X(I-1)
X(IP1)	X(I+1)
XU(I)	X- co-ordinate values of the X constant grid lines through u-locations
XU(IM1)	XU(I-1)
XU(IP1)	XU(I+1)
y	Co-ordinate axis normal to the screw roots
Y(J)	Y co-ordinate values of the Y constant grid lines
Y(JM1)	Y(J-1)
Y(JP1)	Y(J+1)
YV(J)	Y co-ordinates values of the Y-constant grid lines
YV(JM1)	YV(J-1)

YV(JP1)	YV(J+1)
z	Co-ordinate axis along the screw channel
$\Delta y^*, \Delta z^*$	Grid spacing along y- and z-directions respectively

Greek Symbols

α_R	Under-relaxation parameter
β	Dimensionless b [$=b(T_{b(ref)}-T_i)$]
$\dot{\gamma}$	Strain rate
$\dot{\gamma}_0$	Reference strain rate
θ	Dimensionless temperature [$=(T-T_i)/(T_{b(ref)}-T_i)$]
μ_0	Reference viscosity
$\bar{\mu}$	Average viscosity $\{ =\mu_0[(V_{bz}/H)/\dot{\gamma}_0]^{n-1}e^{-b(T_i-T_0)} \}$
ρ	Density of the fluid
τ	Shear stress
ϕ	Screw helix angle, Fig 1(b)
ψ	$\partial p/\partial x$
η	$\partial p/\partial z$

Subscripts

b	Barrel
bulk	Bulk temperature
dev	Developed
e,w,n,s	Main control volume faces (Fig.5.5)
e'',w''	East and west faces of v-control volume
f	Fluid

i	Inlet
nb	Neighbouring points
P,E,W,N,	Main grid point locations, (Temperature, pressure,
S,SE,SW,	w-velocity located)
NE,NW	
$P',E',W',N',$	u-grid point locations
$S',S'E,S'W'$	
$,N'E,N'W'$	
$P'',E'',W'',$	v-grid point locations
$N'',S'',S''E'',$	
$S''W'',N''E'',$	
$N''W''$	
o	Reference quantity
s	Screw
s',n'	South and north faces of u-control volume

Superscript

*	Dimensionless quantity
'	u-control volume
''	v-control volume

ACKNOWLEDGEMENTS

etc Subir and Joydeep helped the author with plots and print outs often defying the late hours

The constant encouragement from the family could set the author to this point of his research career. It is the author's inability to put them down in good literary words.

Last but not the least, Mr B K Jain's excellent drafting quality is recorded who made all the tracing of this dissertation

Manab Kumar Das

CHAPTER 1

INTRODUCTION

CHAPTER 1

1.1 INTRODUCTION

Screw extrusion is widely used for the manufacture of plastics, polymers, pharmaceuticals and food products. In order to control the quality of these products and improve productivity, it is necessary to understand clearly the underlying mechanisms and determine heat transfer rates, residence time distributions, and the thermal and fluid flow fields, etc within the extruder

Typically a single screw extruder consists of a screw rotating uniformly inside a barrel maintained at a fixed temperature (Fig.1.1). At one end, there is a hopper through which plastic granules are fed in The extruder can be divided into three sections, namely (i) the feed section (relatively deep) which is the section near the hopper, (ii) the heating and conveying section where the depth of the screw channel decreases gradually and heat is added raising the fluid pressure and temperature, and (iii) the metering section (relatively shallow) accompanied by further increase in pressure and the material is subjected to high shear, thus enhancing the mixing While the bulk density of the feed solids is lower than that of the melt, the deep feed section enables solids to be conveyed at the same rate as the other section of the extruder. Otherwise the extruder may
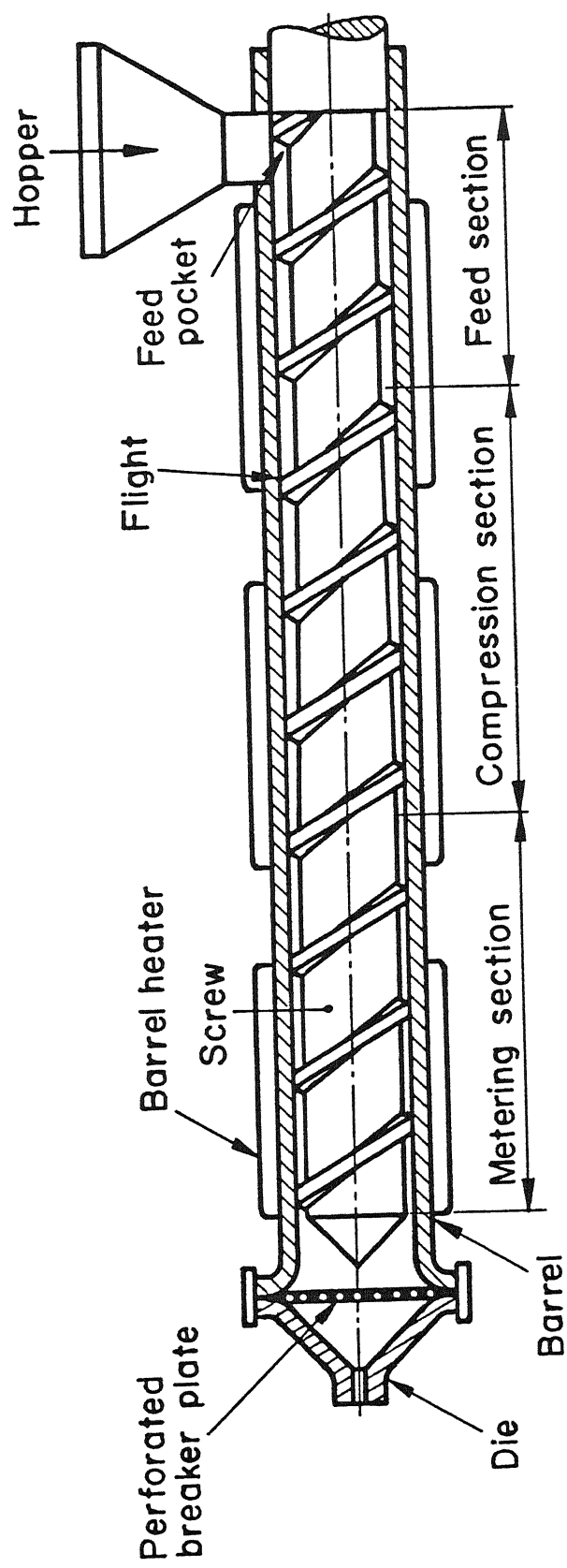
Fig.1.1 Sectional view of a typical single-screw plasticating extruder.

be 'starved', which means that certain portions of the space between the barrel and the screw will not be filled with polymer

The basic principle of screw extrusion is conveying solid materials and melting under the combined effects of barrel heating and viscous heat dissipation The screw extruder, in addition to being an efficient pump, is also a good solids conveying device and an excellent melt generator

An extruder fed by solid polymer is called a 'Plasticating extruder'. In this case, the extruder is more than an efficient pump, for it must also apply the heat energy to melt the polymer. There are two sources of energy for this purpose · (1) The hot barrel of the extruder which is equipped with heaters supplies thermal energy to polymer by conduction, and (2) through the rotating shaft, mechanical energy is introduced and converted by viscous dissipation to thermal energy

In addition to conveying the polymer to the die and melting the solids, the screw extruder also mixes and homogenizes the melt. Indeed, one measure of quality in the product is the temperature uniformity and homogeneity of the melt (i.e. the extrudate) leaving the extruder. The plasticating extruder can accomplish all these tasks despite a relatively short polymer residence time in the extruder, thus preventing the possibility of thermal degradation of the polymer.

The solids and melt are pumped forward by the relative

movement of screw and barrel The transporting mechanism is similar to a nut held in wrench with the screw rotating in the nut. Normally, the screw advances in the nut, but when the screw is physically prevented from advancing, as in the case of the extruder, the nut will slide in the wrench In a similar way the material 'slides' between the screw and the barrel The screw is turned by a motor through a gear box, but a thrust bearing prevents the screw from being pushed out of the barrel by the pressure that develops at the die Screws, usually single flighted, are made of steel and often hardened for protection. Barrels are also made of steel, and their inner surface is either hardened or often coated with special wear-resistant layers The screw 'floats' in the barrel with a small clearance and the polymer acts as a lubricant between the tip of the screw flights and the barrel.

The principal variables that can be controlled during operation are the screw r.p m., the barrel temperature, and the pressure at the die(e.g. with the aid of a valve). The screw r.p.m. depends on the size of the extruder and production rate requirements Typical plasticating screw extruders operate mostly in the range of 10-200 r.p m and, depending on their size, extruding upto 1600 kg/hr (higher flow rates for extruder with a diameter above 30 cm). The limiting factor in a given size extruder is quality. Higher screw speed will produce higher throughput, but will usually result in deterioration of quality (Tadmor and Klein, 1970).

Barrel temperature setting is selected according to the polymer extruded The temperature has to be high enough to melt the polymer without causing thermal degradation.

The main advantage of modelling plasticating extrusion process is that an analyst can computationally predict pressure, temperature, residence time distributions and degree of mixing or homogeneity of the extrudate and select optimum operating conditions without performing costly laboratory experiments.

In the present work, a detailed numerical study of the thermal transport processes in the metering section of a single screw plasticating extruder has been carried out. A comparative study of the results based on three computer models developed by the present author, namely quasi two-dimensional, fully two-dimensional and quasi three-dimensional is presented for low density polyethylene (LDPE) following non-Newtonian power-law fluid behaviour. However, the work is general enough to include other power-law fluids. The computations have been carried out for a uniform barrel temperature distribution and conducting screw. The plastic granules are assumed to have been completely melted at the inlet of the metering section of the screw extruder and therefore, melting has not been considered in the present analysis. The models discussed here can be used for design and optimization of screw extruders. However, in this work, no attempt has been made to design such extruders

It may be worthy of note that the models presented here for

the metering section of the plasicating screw extruder can also be used to design a 'melt extruder' where the polymer is fed in a molten form In such a case, the extruder contains only one functional zone, namely, the metering section. Melt extruders are used, for example, to pelletize a polymer fed straight from the polymerization reactor

1.2 REVIEW OF LITERATURE

In recent years, experimental and numerical studies have been done to understand the underlying physical phenomena in a screw extruder (Tadmor and Gogos, 1979, Fenner, 1979, Tadmor and Klein, 1970) However, most of the studies are preliminary in nature and entail varying degrees of approximation. Consequently, many aspects such as effect of conducting screw and transverse thermal convection on the thermal and flow field, warrant further investigation In one of the pioneering studies on the flow in a single screw extruder, Griffith (1962) solved the governing equations for the fully developed (both thermally and hydrodynamically) flow of an incompressible fluid through a screw extruder with velocity and temperature profiles essentially the same as those in a channel of infinite width and length. The effects of curvature and leakage, across the flights were ignored. He acknowledged the importance of transverse thermal convection i.e. convection normal to the screw flights in the recirculating channel flow (and the very small contribution of thermal conduction) in their choice of thermal boundary condition at the screw, by setting the temperature there equal to the barrel

temperature Martin's work (1969,1970) also confirmed Griffith's assumption Martin also demonstrated the potentially important effect of leakage flow over the screw flight, assuming that such flow occurs, on melt temperatures in the channel It may be noted that because of the intense shear in the clearance between the screw and the barrel, a significant amount of heat may be convected into the channel rather than be conducted into the barrel or flight tip surface although the no leakage condition appears to be reasonable for the purposes of computing velocity profiles in the channel (Martin, 1970). Marshall et al. (1965) and Palit (1974) reported detailed experimental results obtained from 63 5 mm (2 5 inch) extruders processing materials such as low density polyethylene, polypropylene and polyvinyl chloride which showed screw surface temperatures rising rapidly along the feed and compression sections to steady values slightly higher than the barrel temperature along most of the metering section Zamodits and Pearson (1969) obtained numerical solutions for a fully developed, two-dimensional, isothermal and non-Newtonian flow of polymer melts in infinitely wide rectangular screw channels. Rauwendaal (1985), and Lappe and Potente (1983) have discussed the relationship between the volume flow rate and presure for single screw extruders. Lidor and Tadmor (1976) and Bigg and Middleman (1974) have performed theoretical analyses to determine the residence time distribution function and strain distribution in screw extruders. Tadmor and Gogos (1980) and Fenner (1980) have obtained solutions for the flow of a polymeric material in the various sections of an extruder. Fenner (1977) also solved the case of temperature profile developing along the length of the

screw channel Elbirli and Lindt (1984) have reported the results
of a model in which temperature was allowed to develop along the
screw channel In these models the screw and the barrel were
assumed to be at the same temperature Agur and Vlachopoulus
(1982) have studied the flow of polymeric materials, which
included a model for flow of solids in the feed hopper, a model
for the solid conveying zone, and a model for the melt conveying
zone Mokhtarian and Erwin (1982) developed a mathematical model
for mixing in a single screw extruder

Recently, Karwe and Jaluria (1988,1990) have numerically
analysed by finite difference techniques the flow of a polymeric
material (following non-Newtonian power law fluid behaviour) in
the metering section of a single screw extruder. While in both the
papers the screw surface is assumed to be adiabatic, in the
former, the barrel is at a fixed temperature and in the latter, a
given barrel temperature distribution is specified. The velocity
profile is assumed to be fully developed at the inlet to the
metering zone. Their results indicate that the temperature in the
downstream direction has a small effect on the corresponding
velocity field, which is determined mainly by the total volume
flow rate Under certain circumstances, the fluid temperature near
the exit of the extruder in the vicinity of the barrel becomes
higher than the barrel temperature indicating transfer of heat
from fluid to the barrel. A numerical procedure is presented for
computing the residence time distribution (RTD). Screw
characteristics are presented in terms of bulk temperature rise
versus screw speed.

The studies of Gopalakrishna and Jaluria (1990) and Gopalakrishna et al (1992) are directed mainly at simulating heat and mass transfer inside the channel of a single screw extruder, for a power-law fluid Moisture is taken as the species for mass transfer, since it is of particular interest in food processing In this case, in addition to the strain rate and temperature, the viscosity of the fluid is dependent also on moisture As an application of this analysis to starch based food systems, the reactive nature of the food constituents is incorporated by including the rate of reaction (gelatinization) between moisture and food Strong viscous dissipation is found to arise for typical operating conditions The effect of various governing parameters on pressure build-up within the extruder channel is determined and discussed in terms of the underlying physical process The moisture contours indicate that starch gelatinization typically occurs first at the screw root Numerical results are validated experimentally.

Gupta and Kwon (1990) have investigated three dimensional flows of non-Newtonian viscous fluids in various geometries including screw channel using enriched finite element. Pressure flow and the temperature dependence of viscosity are not considered in their study. The channel width to depth ratio is taken as 2.50. Velocity vector distribution obtained with and without leakage at the top right corner are shown.

A few investigators have attemped to model the flow of food

stuffs in single screw extruders Bruin et al (1978) have discussed the flow of bio-polymers in an extruder Harper (1980) has discussed various aspects of food extrusion in single screw extruders Mohamed and Morgan (1986) have presented the results for average heat transfer coefficients in a single screw extruder, for the flow of non-Newtonian food materials.

1.3 OBJECTIVES OF THE PRESENT WORK

The above literature review reveals that .

(a) The recent computer models of the metering section of screw extruders are quasi two-dimensional in nature, i e the flow is hydrodynamically developed but thermally undeveloped at the entrance of the screw channel which is assumed to be infinitely wide.

(b) So far no attempt has been made by earlier researchers to take into account in their models the conjugate heat transfer i.e. the coupling of conduction between the fluid and the screw, which is the real situation.

(c) No work considers the effect of cross convection, i.e., the thermal convection normal to the screw flights The crosswise convection effect can only be included in a three dimensional model. Most researchers have acknowledged the contribution of this cross-convection by setting the screw surface temperature equal to the barrel temperature in their quasi two-dimensional models.

However, it must be noted that this is an approximate boundary condition, although close to reality

(d) For the reasons mentioned in (c), no researcher could numerically predict the screw surface temperature distribution

Keeping the aforementioned limitations of the previous works in mind, the main objective of the present study is to develop a model which would predict the flow and thermal characteristics of the polymer in the metering section of a single screw plasticating extruder in a most realistic manner. To acheive this goal, the present research is directed in the following way.

First, a quasi two-dimensional model considering conduction in the screw body is developed. The velocity, pressure, temperature, bulk temperature, local Nusselt number at various sections of the extruder along the screw helix are computed The same results are compared with those obtained on the basis of a fully two-dimensional model (i.e considering uniform velocity as well as temperature at the entrance of the metering section) also developed by the present author. The idea is to see whether assumption of fully developed velocity profile in quasi two-dimensional model is adequate or not It will be shown later in Chapter 4 that in a fully two-dimensional model, the flow becomes 'locally' fully developed at a very short distance from the inlet. Therefore, assummption of fully developed entry condition is quite justified. Finally, a quasi three-dimensional model (a fully three-dimensional one would result in additional

complexities in the model without appreciable difference in the output, thus straining tremendously the computer time and storage space) which assumes fully developed velocity profile at the inlet and finite width of the channel is developed taking into account the cross convection in addition to the convection in the downchannel direction To check the accuracy of this model, the screw surface temperature distribution is compared with those computed on the basis of quasi two-dimensional and fully two-dimensional models It will be shown in Chapter 6 that the quasi three-dimensional model predicts the screw surface temperature most realistically, i.e , the nature of the temperature distribution matches with that observed in earlier experimental works.

Furthermore, a parametric study has also been performed to see the effect of variations in dimensionless volumetric flow rate, power-law index and screw speed on the pressure gradient, pressure, local Nusselt number and bulk temperature in the downchannel direction of the extruder using the quasi three-dimensional model.

All results have been obtained for low density polyethylene (LDPE) and steel screw combination However the models are general enough to include other materials following non-Newtonian power-law fluid behavior and other screw materials

To sum up, the present thesis aims at (i) developing a rigorous computer model (starting with relatively simpler ones)

that includes conduction within the screw body and thermal convections normal to the screw flights as well as to the screw root, (ii) coming up with efficient and novel numerical solution procedures in the process and (iii) finally, checking the consistency of the model and understanding the complex physical processes within the extruder by performing a parametric study

1.4 MAJOR ASSUMPTIONS

(a) For ease of analysis, the coordinate system is fixed to the screw (Fig 1.2) and thus the barrel moves in a direction opposite to the screw rotation

(b) The curvature effects have been neglected, and therefore, the screw is treated as unwound (Fig.1.2).

(c) The fluid is considered to be homogeneous following non-Newtonian power-law behaviour and flow and heat transfer steady.

(d) As the screw channel is shallow and long, i e., H/W ≪ 1, and as convective effects are small in comparison to viscous, (since polymers have high viscosity) creeping flow approximations are made for conservation of momentum (Schlichting, 1979)

(e) The leakage across the screw flights have been neglected.

(f) There is good thermal contact between the melt and the
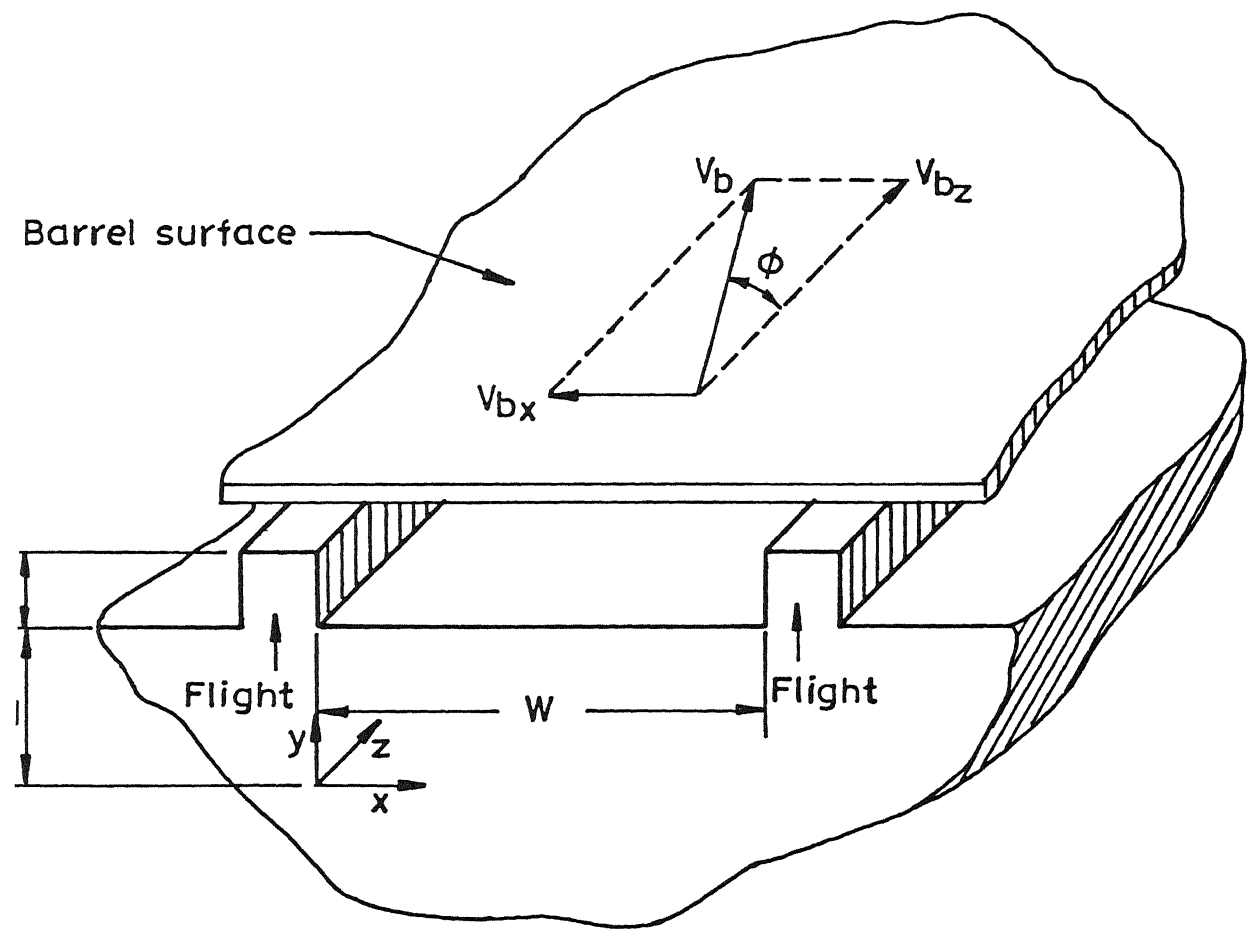
Fig. 1.2 Geometry of the unwound rectangular channel.

metal surfaces

(g) All properties of the fluid except viscosity are constant

(h) Viscosity of the fluid is represented as a power-law function of the local strain rate and an exponential function of temperature and is independent of pressure

CHAPTER 2

QUASI TWO-DIMENSIONAL   MODEL

CHAPTER 2

2.1 PHYSICAL DESCRIPTION OF THE QUASI TWO-DIMENSIONAL MODEL

The melt flow in the extruder channel has been modelled in a quasi two-dimensional domain The principal direction of flow is along the helical length of the channel Because of a cross component of the barrel velocity, there is a transverse circulation taking place also The flow is elliptic in the direction normal to the base of the screw root.

With suitable approximations, the three dimensional extruder channel is reduced to a quasi two-dimensional domain Variation in the direction perpendicular to the screw flight is neglected assuming that channel width is much longer than channel height. Similarly, lubrication approximation in the direction along the channel obviates any variation in this direction. But,the thermal convection in the downstream direction (it being very strong) is included in the energy equation of the fluid.

Therefore, essentially the flow becomes that of hydrodynamically developed but thermally undeveloped. The screw body is considered to be conducting, i.e., heat is conducted from the melt to the screw body. The screw is modelled as a semi-infinite body, i.e , semi-infinite in the direction perpendicular to the base of the screw channel. This is based on

the assumption that heat will penetrate from the fluid to the screw body (which is very thick compared to the height of the screw channel in a thin layer below the screw channel base while the rest of the screw behaves as adiabatic Fenner (1977) in a review of Martin's (1970) work regarding heat transfer between melt flow and a metal boundary, reported that the screw surface behaves as though almost thermally insulated. The screw depth in present observation has been taken as ten times the height of the channel depth The smalll curvature effect has been neglected.

The non-dimensional channel length has been taken as 250.0 following Karwe and Jaluria (1988,1990) At the entrance of the metering section, the flow is considered to be unidirectional and developed. Thus, at the inlet, the velocity in the direction normal to the screw flights (u) is considered to be zero, whereas the developed w-velocity profile along the channel is obtained by solving the momentum equation for isothermal fluid subject to satisfying the constraints on the volumetric flow rate.

2.2 GOVERNING EQUATIONS AND BOUNDARY CONDITIONS

The simplifications to the channel flow equations are introduced with the aid of the lubrication approximation. In essence, this involves the local replacement of the actual flow in the parallel gap between smooth surfaces by uniform flow between plane parallel surfaces. As the screw channel depth is constant in the downstream direction, it is reasonable to apply the lubrication approximation in the z-direction to velocities and

assume that velocities are fully developed in the downstream direction,

$$u = u(x,y) \qquad (2\ 1a)$$

$$v = v(x,y) \qquad (2\ 1b)$$

$$w = w(x,y) \qquad (2\ 1c)$$

The continuity equation becomes

$$\frac{\partial u}{\partial x} + \frac{\partial v}{\partial y} = 0 \qquad (2.2)$$

The momentum equations become:

$$\frac{\partial p}{\partial x} = P_x = \frac{\partial \tau_{xx}}{\partial x} + \frac{\partial \tau_{yy}}{\partial y} \qquad (2\ 3a)$$

$$\frac{\partial p}{\partial y} = P_y = \frac{\partial \tau_{yx}}{\partial x} + \frac{\partial \tau_{yy}}{\partial y} \qquad (2\ 3b)$$

$$\frac{\partial p}{\partial z} = P_z = \frac{\partial \tau_{zx}}{\partial x} + \frac{\partial \tau_{zy}}{\partial y} \qquad (2.3c)$$

where the pressure gradient P_z is independent of x and y .

Owing to the presence of significant thermal convection, it is much less reasonable to apply the lubrication approximation in the z-direction to temperatures So introducing lubrication approxinmation in the z-direction and simultaneously retaining the thermal convection term, the energy equation reduces to:

$$\rho\, C_p\left(u\frac{\partial T}{\partial x} + v\frac{\partial T}{\partial y} + w\frac{\partial T}{\partial z}\right) = K_f\left(\frac{\partial^2 T}{\partial x^2} + \frac{\partial^2 T}{\partial y^2}\right) + \tau_{xx}\frac{\partial u}{\partial x} + \tau_{yy}\frac{\partial v}{\partial y} +$$

$$\tau_{xy}\left(\frac{\partial u}{\partial y} + \frac{\partial v}{\partial x}\right) + \tau_{yz}\frac{\partial w}{\partial y} + \tau_{zx}\frac{\partial w}{\partial x} \qquad (2\ 4)$$

The next stage of simplification frequently employed is to apply the lubrication approximation in the x-direction. The channel depth is constant in this direction, except at the flight For the lubrication approximation to be valid, it is assumed that the influence of the flight is negligible and the flow may be treated as though the channel were infinitely wide Symbolically, H << W and Eqs (2.1)-(2 4) reduce to,

$$u=u(y) \qquad (2.5a)$$

$$v=0 \qquad (2\ 5b)$$

$$w=w(y) \qquad (2\ 5c)$$

$$\frac{\partial p}{\partial x} = P_x = \frac{\partial \tau_{xy}}{\partial y} \qquad (2\ 6a)$$

$$\frac{\partial p}{\partial y} = 0 \qquad (2.6b)$$

$$\frac{\partial p}{\partial z} = P_z = \frac{\partial \tau_{zy}}{\partial y} \qquad (2.6c)$$

Eq.(2.2) is automatically satisfied although continuity must be satisfied in terms of overall channel flow rate. The flow is not two dimensional in the sense that there are only two non-zero velocity componenets, u and w, which are functions of the third co-ordinate y.

Another very useful combination of assumptions, first employed by Yates (1968) is provided by taking velocity profiles to be locally fully developed in both the downstream and transverse directions and retaining the thermal convection in the downstream direction only The energy equation becomes

$$\rho \ C_p \ w \ \frac{\partial T_f}{\partial z} = K_f \frac{\partial^2 T_f}{\partial y^2} + \tau_{yx}\frac{\partial u}{\partial y} + \tau_{yz}\frac{\partial w}{\partial y} \qquad (2.7)$$

where,

$$\tau_{yx} = \mu\frac{\partial u}{\partial y} \qquad (2\ 7a)$$

$$\tau_{yz} = \mu\frac{\partial w}{\partial y} \qquad (2\ 7b)$$

In the energy equation of the fluid, viscous dissipation effects are strong as polymers have high viscosity Also this viscosity is an exponential function of temperature and a power-law function of the local strain rate as is shown in Eq.(2.8a).

$$\mu = \mu_0\left(\frac{\dot{\gamma}}{\dot{\gamma}_0}\right)^{n-1} e^{-b(T-T_0)} \qquad (2.8a)$$

where,

$$\dot{\gamma} = \left[\left(\frac{\partial u}{\partial y}\right)^2 + \left(\frac{\partial w}{\partial y}\right)^2\right]^{1/2} \qquad (2.8b)$$

The screw, which is assumed to be semi-infinite in the direction normal to the channel base, is considered to be as conducting up to a thin layer beyond which the screw is considered

to be adiabatic Let H_d is the depth Fig 1 2 upto which the screw is assumed to be conducting If $H_d \ll D$, then neglecting the small curvature effect, the portion of the screw which is conducting is unwound The screw then takes the shape of a rectangular slab Conduction in the direction perpendicular to the screw base is retained whereas, conduction both in the direction of the downstream as well as in the transverse are neglected for obvious reasons. So, the energy equation in the screw becomes.

$$\frac{\partial}{\partial y}\left(K_s \frac{\partial T_s}{\partial y}\right) = 0 \qquad (2\ 9)$$

where K_s is the conductivity of the screw material It may be noted that the screw is made of steel.

Except viscosity, all the properties are assumed to be constant.

The boundary conditions as shown in Fig (2 1) are

at y=0,

$$\frac{\partial T_s}{\partial y} = 0 \qquad (2.10a)$$

at $y = H_d$,

$$u = 0, \ w = 0,$$

$$T_f = T_s, \ K_f \frac{\partial T_f}{\partial y} = K_s \frac{\partial T_s}{\partial y} \qquad (2.10b)$$

Fully Developed Isothermal Flow at the Inlet

Die (Outlet)

Barrel at T_b

$u = V_{b_x}$, $w = V_{b_z}$, $T_f = T_b$

SCREEN CHANNEL

Q

$U = 0, W = 0$, $K_f \dfrac{\partial T}{\partial y}\Big|_f = K_s \dfrac{\partial T}{\partial y}\Big|_s$, $T_f = T_s$

SCREW BODY (Semi-infinite in y)

$\dfrac{\partial T_s}{\partial y} = 0$

W

$\displaystyle\int_{H_d}^{H_d + H} w\, dy = Q/W$, $\displaystyle\int_{H_d}^{H_d + H} u\, dy = 0$

H

H_d

z, w

y, v

$T_f = T_i$

x, u
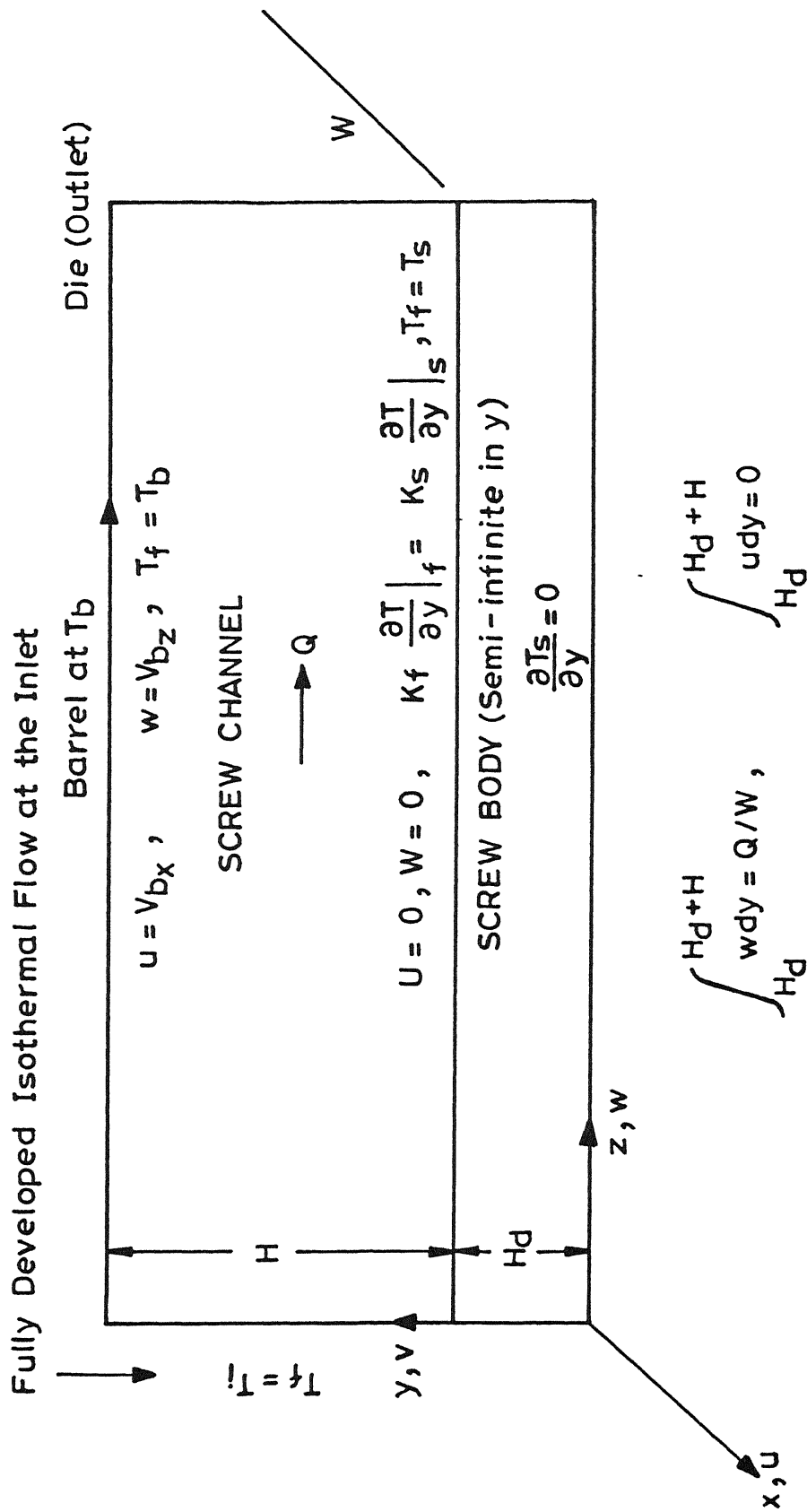
Fig.2.1 Boundary conditions for the quasi two-dimensional model.

at $y = H_d + H$,

$$u = V_{bx}, \quad w = V_{bz}, \quad T_f = T_b \qquad (2\ 10c)$$

at $z = 0$,

$$u = 0, \quad w = w_{dev}, \quad T_f = T_s = T_i \qquad (2\ 10d)$$

where the subscripts f refers to fluid, s refers to screw and i refers to the inlet conditions

At the inlet to the heating zone, the velocity in the x-direction (cross velocity) is taken as zero, following Agur and Vlachopoulus (1982) in which it is assumed that the solid bed is isothermal and the pressure varies only in the downchannel direction Thus the flow before the entrance is only uni-directional.

The two constraints on the flow are given as below,

$$\int_{H_d}^{H_d + H} u\,dy = 0 \qquad (2.11a)$$

$$\int_{H_d}^{H_d + H} w\,dy = Q/W \qquad (2.11b)$$

2.3 NON-DIMENSIONALISATION

The governing equations are non-dimensionalised in terms of the following dimensionless variables,

$$x^* = x/H, \quad y^* = y/H, \quad z^* = z/H \qquad (2\ 12a)$$

$$u^* = u / V_{bz}, \quad w^* = w / V_{bz} \qquad (2\ 12b)$$

$$\theta = \frac{T - T_i}{T_{b(ref)} - T_i} \qquad (2.12c)$$

$$p^* = \frac{p}{\bar{p}}, \quad \bar{p} = \bar{\mu}\,\frac{V_{bz}}{H} \qquad (2.12d)$$

$$\dot{\gamma}^* = \frac{\dot{\gamma}\,H}{V_{bz}}, \quad \bar{\mu} = \mu_0 \left[\frac{V_{bz}/H}{\dot{\gamma}_0}\right] e^{-b\left(T_i - T_0\right)} \qquad (2.12e)$$

$$\beta = b\left(T_{b(ref)} - T_i\right) \qquad (2.12f)$$

$$Pe = \frac{\rho\,C_p V_{bz}\,H}{K_f} \qquad (2.12g)$$

$$G = \frac{\bar{\mu}\,V_{bz}^{\;2}}{K_f(T_{b(ref)} - T_i)} \qquad (2.12h)$$

The dimensionless equations thus obtained are,

FLUID

X-MOMENTUM:

$$\frac{\partial p}{\partial x^*} = \frac{\partial}{\partial y^*}\left[\left(\dot{\gamma}^*\right)^{n-1} e^{-\beta\theta_f}\,\frac{\partial u}{\partial y^*}\right] \qquad (2.13a)$$

Z-MOMENTUM:

$$\frac{\partial p^*}{\partial z^*} = \frac{\partial}{\partial y^*}\left[\left(\dot{\gamma}^*\right)^{n-1} e^{-\beta\theta_f} \frac{\partial w}{\partial y^*}\right]$$ (2 13b)

ENERGY:

$$Pe\ w^* \frac{\partial\theta_f}{\partial z^*} = \frac{\partial^2\theta_f}{\partial y^{*2}} + G\left(\dot{\gamma}^*\right)^{n+1} e^{-\beta\theta_f}$$ (2 14)

SCREW:

ENERGY:

$$\frac{\partial^2\theta_s}{\partial y^{*2}} = 0$$ (2.15)

Similarly, the boundary conditions are also obtained in the non-dimensional form as:

at $y^* = 0$,

$$\frac{\partial\theta_s}{\partial y^*} = 0$$ (2.16a)

at $y^* = H_d/H$,

$$u^* = 0,\ w^* = 0,$$

$$\frac{\partial\theta_f}{\partial y^*} = \frac{K_s}{K_f} \frac{\partial\theta_s}{\partial y^*}\ ,\ \theta_s = \theta_f$$ (2.16b)

at $y^* = 1 + H_d/H$,

$$u^* = V_{bx}/V_{bz} = \frac{V_b \sin\phi}{V_b \cos\phi} = \tan\phi,\ w^* = 1,\ \theta_f = 1$$ (2.16c)

at z* =0,

$$u^* = 0, \quad w^* = \frac{w_{dev}}{V_{bz}} = w^*_{dev} \quad , \quad \theta_f = \theta_s = 0 \qquad (2\ 16d)$$

The constraint on the flow in the dimensionless form are,

$$\int_{H_d/H}^{1+H_d/H} u^* \, dy^* = 0 \qquad (2.17a)$$

$$\int_{H_d/H}^{1+H_d/H} w^* \, dy^* = q_v = \frac{Q}{HV_{bz}W} \qquad (2.17b)$$

Here, the parameter q_v represents the dimensionless volumetric flow rate, generally called the throughput emerging from the extruder. The parameter q_v expresses the ratio between the actual flow rate along the channel and the flow rate that would have been achieved if all the melt moved downstream with the same velocity as the barrel relative to the screw. It is therefore a measure of volumetric efficiency.

Thus for a given screw and temperature at the barrel, the parameters that govern the numerical solution are Pe, G, n, q_v, the viscosity parameter β and K_s/K_f.

2.4 Method of solutic

the inlet and boundary conditions given by Eqs (2 16a)-(2 16d) and constraints on the flow (Eqs (2.17a) and (2 17b)) are solved by means of finite difference techniques The computational domain in the y-z co-ordinate system is discretized to obtain the finite difference equations The pressure gradients in both the x- and z-directions are regarded as uniform over the depth of the channel. The computational domain is shown in Fig.2.2

2.4.1 THE FINITE DIFFERENCE EQUATIONS

The governing partial differential equations can be expressed in the following finite difference form In the subsequent discussions the superscripts (*) have been dropped. The x- and z-momentum equations (Eqs.(2 13a-b)) are discretized and solved in the channel domain. The energy equation for the channel and the screw are discretized. The compatibility conditions of equality of temperature and continuity of heat flux at the fluid-screw interface are used to obtain a discretized equation for the screw surface. Thus the energy equation is solved in the entire domain of screw body and the channel.

2.4.2 X-MOMENTUM EQUATION

The differential equation (Eq (2.13a)) is rewritten as:

$$\frac{\partial p}{\partial x} = \frac{\partial}{\partial y}\left[\left(\dot{\gamma}\right)^{n-1}e^{-\beta\theta}f\ \frac{\partial u}{\partial y}\right] \qquad (2.18)$$

With reference to Fig 2 2, using central difference method the discretized form of Eq (2.18) is obtained at grid form (i,j),

$$\left.\frac{\partial p}{\partial x}\right|_{i,j} = \frac{\dot{\gamma}^{n-1} e^{-\beta\theta_f} \left.\frac{\partial u}{\partial y}\right|_{i+1/2,j} - \dot{\gamma}^{n-1} e^{-\beta\theta_f} \left.\frac{\partial u}{\partial y}\right|_{i-1/2,j}}{\Delta y_f} \qquad (2.19)$$

Since the pressure gradient $(\partial p/\partial x)$ is constant over all i's in any j location, so instead of double subscript (i,j) for it, single subscript j is used . Please note that i is the grid point number in the y-direction and j is the grid point number in the z-direction. Eq (2.19) may further be resolved to obtain·

$$\left.\frac{\partial p}{\partial x}\right|_j = \frac{\dot{\gamma}^{n-1} e^{-\beta\theta_f}\Big|_{i+1/2} (u_{i+1,j} - u_{i,j})}{\Delta y_f^2} -$$

$$\frac{\dot{\gamma}^{n-1} e^{-\beta\theta_f}\Big|_{i-1/2} (u_{i,j} - u_{i-1,j})}{\Delta y_f^2} \qquad (2.20)$$

On rearranging,

$$\left.\frac{\partial p}{\partial x}\right|_j (\Delta y_f)^2 = u_{i-1,j}\, \dot{\gamma}^{n-1} e^{-\beta\theta_f}\Big|_{i-1/2} \quad -$$

$$u_{i,j} * \left[\dot{\gamma}^{n-1} e^{-\beta\theta_f}\Big|_{i-1/2,j} + \dot{\gamma}^{n-1} e^{-\beta\theta_f}\Big|_{i+1/2,j} \right] +$$

$$u_{i+1,j} * \dot{\gamma}^{n-1} e^{-\beta\theta_f}\Big|_{i+1/2,j} \qquad (2.21)$$
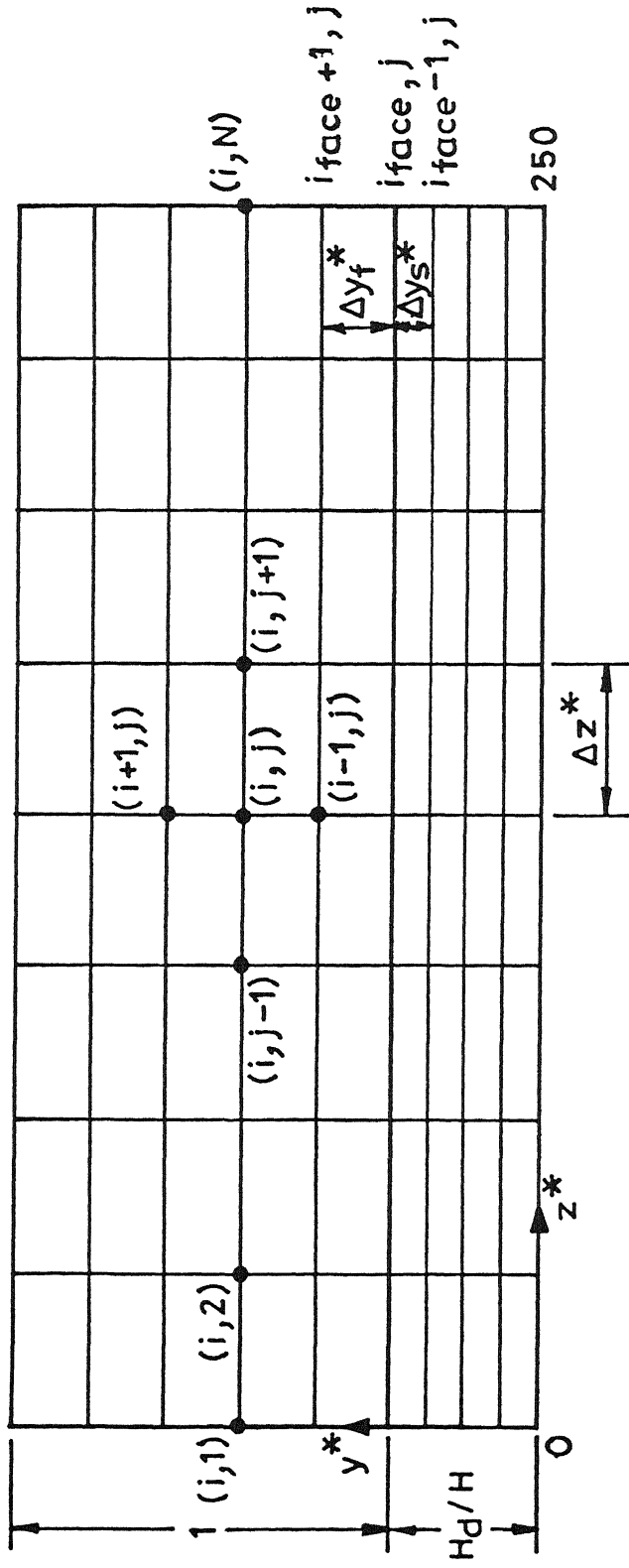
Fig.2.2 Computational domain and the finite difference grid for the quasi

two-dimensional model.

Discetization of $\dot{\gamma}^{\,n-1}\,e^{-\beta\theta}f$

$$\dot{\gamma}^{\,n-1}\,e^{-\beta\theta}f\Big|_{i-1/2,\,j} =$$

$$\left[\left(\frac{u_{i,j} - u_{i-1,j}}{\Delta y_f}\right) + \left(\frac{u_{i,j} - u_{i-1,j}}{\Delta y_f}\right)^2\right]^{\frac{n-1}{2}} e^{-\beta(\theta_{i,j} + \theta_{i-1,j})/2} \quad 0$$

$$(2\,22a)$$

$$\dot{\gamma}^{\,n-1}\,e^{-\beta\theta}f\Big|_{i+1/2,\,j} =$$

$$\left[\left(\frac{u_{i+1,j} - u_{i,j}}{\Delta y_f}\right) + \left(\frac{u_{i+1,j} - u_{i,j}}{\Delta y_f}\right)^2\right]^{\frac{n-1}{2}} e^{-\beta(\theta_{i+1,j} + \theta_{i,j})/2} \quad 0$$

$$(2.22b)$$

2.4.3 Z-MOMENTUM EQUATION

The differential equation (Eq.(2.12b)) is rewritten as:

$$\frac{\partial p}{\partial z} = \frac{\partial}{\partial y}\left[\left(\dot{\gamma}\right)^{n-1}e^{-\beta\theta}f \frac{\partial w}{\partial y}\right] \qquad (2\,23)$$

With reference to Fig (2.2), using central difference method the discretized form of Eq.(2.23) is obtained at grid point (i,j),

$$\frac{\partial p}{\partial z}\Big|_{i,j} = \frac{\dot{\gamma}^{\,n-1}\,e^{-\beta\theta}f \frac{\partial w}{\partial y}\Big|_{i+1/2,\,j} - \dot{\gamma}^{\,n-1}\,e^{-\beta\theta}f \frac{\partial w}{\partial y}\Big|_{i-1/2,\,j}}{\Delta y_f} \qquad (2.24)$$

The pressure gradient $\partial p/\partial z$ is constant over all i's in any j location Therefore instead of using double subscript (i,j) for it, single subscript j is used Eq (2 24) may further be expanded as

$$\frac{\partial p}{\partial z}\bigg|_j = \frac{\dot{\gamma}^{n-1} e^{-\beta\theta_f}\bigg|_{i+1/2} (w_{i+1,j} - w_{i,j})}{\Delta y_f^2} -$$

$$\frac{\dot{\gamma}^{n-1} e^{-\beta\theta_f}\bigg|_{i-1/2} (w_{i,j} - w_{i-1,j})}{\Delta y_f^2} \qquad (2\ 25)$$

Rearranging Eq (2.25),

$$\frac{\partial p}{\partial z}\bigg|_j (\Delta y_f)^2 = w_{i-1,j}\ \dot{\gamma}^{n-1} e^{-\beta\theta_f}\bigg|_{i-1/2,j} -$$

$$w_{i,j} \left[\dot{\gamma}^{n-1} e^{-\beta\theta_f}\bigg|_{i-1/2,j} + \dot{\gamma}^{n-1} e^{-\beta\theta_f}\bigg|_{i+1/2,j} \right] +$$

$$w_{i+1,j}\ \dot{\gamma}^{n-1} e^{-\beta\theta_f}\bigg|_{i+1/2,j} \qquad (2\ 26)$$

Discetization of $\dot{\gamma}^{n-1} e^{-\beta\theta_f}$

Since these two terms $\dot{\gamma}^{n-1} e^{-\beta\theta_f}\bigg|_{i-1/2,j}$ and $\dot{\gamma}^{n-1} e^{-\beta\theta_f}\bigg|_{i+1/2,j}$ are same for the x-momentum equations, Eqs.(2.22a-b) are used respectively.

2.4.4 ENERGY EQUATION

The energy equation is discretized separately for the extruder channel domain and the solid screw domain Using the compatibility conditions, a discretized equation for the fluid-screw interface is obtained

CHANNEL

The differential equation (Eq (2 12c)) is rewritten as:

$$Pe \ w \ \frac{\partial \theta_f}{\partial z} = \frac{\partial^2 \theta_f}{\partial y^2} + G \left(\dot{\gamma} \right)^{n+1} e^{-\beta \theta_f} \qquad (2 \ 27)$$

For convenience, the subscript f is dropped in the following discussions. In the z-direction (i.e , the downstream direction), the energy equation is parabolic. So the solution is obtained by marching procedure in the z-direction The discretization is carried out by the fully implicit marching technique

For a fully implicit condition, one may write,

$$\theta_{i,j} = \theta_{i,j-1} + \left(\frac{\partial \theta}{\partial z} \right) \Delta z \qquad (2.28)$$

where the current and the previous marching steps are denoted by j and j-1 respectively.

Substituting Eq.(2.27) in Eq.(2.28)

$$\theta_{i,j} = \theta_{i,j-1} + \left[\frac{1}{Pe\ w}\left(\frac{\partial^2\theta}{\partial y^2} + G\ \dot{\gamma}^{n+1}\ e^{-\beta\theta}\right)\right]_j \Delta z \qquad (2\ 29)$$

Further discretization is obtained using central difference technique.

$$\theta_{i,j} = \theta_{i,j-1} + \frac{1}{Pe\ w_{i,j}}\left[\frac{\theta_{i+1,j} - 2\ \theta_{i,j} + \theta_{i-1,j}}{\Delta y_f^2} + \right.$$
$$\left. G\left(\dot{\gamma}^{n+1}\ e^{-\beta\theta}\right)_{i,j}\right]\Delta z \qquad (2.30)$$

On rearrangement of Eq (2 30)

$$\theta_{i,j} - \frac{\Delta z}{Pe\ w_{i,j}\ \Delta y_f^2}\left[\theta_{i+1,j} - 2\ \theta_{i,j} + \theta_{i,j-1}\right] =$$
$$\theta_{i,j-1} + \frac{\Delta z}{Pe\ w_{i,j}}\ G\left(\dot{\gamma}^{n+1}\ e^{-\beta\theta}\right)_{i,j} \qquad (2.31)$$

Finally,

$$\theta_{i+1,j} - \left(2 + \frac{Pe\ w_{i,j}\ \Delta y_f^2}{\Delta z}\right)\theta_{i,j} + \theta_{i-1,j}$$
$$= -\frac{Pe\ w_{i,j}\ \Delta y_f^2}{\Delta z}\ \theta_{i,j-1} - G\ \Delta y_f^2\left(\dot{\gamma}^{n+1}\ e^{-\beta\theta}\right)_{i,j} \qquad (2.32)$$

where,

$$\dot{\gamma} = \left[\left(\frac{\partial u}{\partial y}\right)^2 + \left(\frac{\partial w}{\partial y}\right)^2\right]^{1/2} \qquad (2.33)$$

Discetization of $\dot{\gamma}^{n+1}\ e^{-\beta\theta}$

$$\dot{\gamma}^{n+1} e^{-\beta\theta} \Big|_{i,j} =$$

$$\left[\left(\frac{u_{i+1,j} - u_{i-1,j}}{2\Delta y_f} \right) + \left(\frac{w_{i+1,j} - w_{i-1,j}}{2\Delta y_f} \right)^2 \right]^{\frac{n+1}{2}} e^{-\beta\theta_{i,j}}$$

$$(2\ 34)$$

SCREW

The energy equation in the screw is rewritten from Eq.(2 14)as (subscript s is dropped).

$$\frac{\partial^2 \theta}{\partial y^2} = 0 \qquad\qquad (2\ 35)$$

Using central difference technique, the Eq (2 35) is discretized,

$$\theta_{i+1,j} - 2\,\theta_{i,j} + \theta_{i-1,j} = 0 \qquad\qquad (2.36)$$

2.4.5 DISCRETIZED EQUATION FOR THE INTERFACE

To obtain the discretized energy equation at the interface (i.e., at the screw surface separating the fluid and the screw body), referring to the Fig.2 2, $\theta_{iface+1,j}$ in the fluid and $\theta_{iface-1,j}$ in the screw body are expressed into Taylor series form dropping terms beyond second order (Carnahan et. al., 1969).

IN THE CHANNEL

From Taylor series expansion,

$$\theta_{i+1,j} = \theta_{i,j} + \left.\frac{\partial\theta}{\partial y}\right|_{i,j} \Delta y_f + \left.\frac{\partial^2\theta}{\partial y^2}\right| \Delta y_f^2/2 \qquad (2.37)$$

$$i\,e\,,\ \left.\frac{\partial\theta}{\partial y}\right|_{i,j} = \frac{\theta_{i+1,j} - \theta_{i,j}}{\Delta y_f} - \frac{\Delta y_f}{2}\left.\frac{\partial^2\theta}{\partial y^2}\right| \qquad (2.37a)$$

IN THE SCREW

From Taylor series expansion,

$$\theta_{i-1,j} = \theta_{i,j} - \left.\frac{\partial\theta}{\partial y}\right|_{i,j} \Delta y_s + \left.\frac{\partial^2\theta}{\partial y^2}\right|_{i,j} \Delta y_s^2/\,2 \qquad (2\ 38)$$

$$i.e.,\qquad \left.\frac{\partial\theta}{\partial y}\right|_{i,j} = \frac{\theta_{i,j} - \theta_{i-1,j}}{\Delta y_s} + \frac{\Delta y_s}{2}\left.\frac{\partial^2\theta}{\partial y^2}\right|_{i,j} \qquad (2.38a)$$

The compatibility condition at the interface is given by,

$$K_f \left.\frac{\partial\theta}{\partial y}\right|_f = K_s \left.\frac{\partial\theta}{\partial y}\right|_s \qquad (2.39a)$$

$$\theta_f = \theta_s \qquad (2.39b)$$

On substitution of $\left.\dfrac{\partial\theta}{\partial y}\right|_f$ and $\left.\dfrac{\partial\theta}{\partial y}\right|_s$ from Eq. (2.37a) and Eq. (2.38a) respectively in Eq. (2.39a),

$$\frac{K_f}{K_s} \left[\frac{\theta_{i+1,j} - \theta_{i,j}}{\Delta y_f} - \frac{\Delta y_f}{2} \frac{\partial^2 \theta}{\partial y^2}\bigg|_{i,j} \right]_f =$$

$$\left[\frac{\theta_{i,j} - \theta_{i-1,j}}{\Delta y_s} + \frac{\Delta y_s}{2} \frac{\partial^2 \theta}{\partial y^2}\bigg|_{i,j} \right]_s \qquad (2\ 40)$$

From Eq (2 27) one can write,

$$\frac{\partial^2 \theta}{\partial y^2}\bigg|_f = Pe\ w\ \frac{\partial \theta}{\partial z} - G\ \dot{\gamma}^{n+1} e^{-\beta\theta} \qquad (2.41)$$

Substituting Eqs (2 41) and Eq (2.35) in Eq (2 40) and dropping the subscripts f and s,

$$\frac{K_f}{K_s} \left[\frac{\theta_{i+1,j} - \theta_{i,j}}{\Delta y_f} - \frac{\Delta y_f}{2} \left\{ Pe\ w\ \frac{\partial \theta}{\partial z} - G\ \dot{\gamma}^{n+1} e^{-\beta\theta} \right\}_{i,j} \right] =$$

$$\left[\frac{\theta_{i,j} - \theta_{i-1,j}}{\Delta y_s} \right] \qquad (2.42)$$

Because of solid boundary at the interface of the channel and the screw, $w = 0$.

Rearranging the terms,

$$\frac{K_f}{K_s} \theta_{i+1,j} - \left(R + \frac{K_f}{K_s} \right) \theta_{i,j} + R\, \theta_{i,j} =$$

$$- \frac{K_f}{K_s} \frac{\Delta y_f}{2} G\, \dot{\gamma}^{\,n+1} e^{-\beta\theta} \bigg|_{i,j} \qquad (2\ 43)$$

where, $R = \dfrac{\Delta y_f}{\Delta y}$

Please note that with reference to Fig.(2.2) i=iface, i-1=iface-1 and i+1=iface+1.

2.4.6 SOLUTION SCHEME

The energy Eq.(2.32) is parabolic in the z-direction, i.e., direction along the helix Therefore, the boundary conditions are necessary only at z = 0 to allow marching in the z-directin, and thus obtain the solution in the entire domain The boundary conditions at z=0 are provided in terms of the developed velocity profiles at uniform temperature $T=T_i$ Since u is zero at the inlet, w_{dev} is obtained by solving Eq.(2 26)[modified by substituing $\theta=0$] by means of an implicit finite difference scheme. The iterative Newton-Rapson method is used to satisfy the conditions on the total flow rate given by Eq.(2 17b). This requires initial guess for $\partial p/\partial z$. The iteration is terminated when there is negligible change in $\partial p/\partial z$

At any j location downstream of the inlet, the pressure gradient $\partial p/\partial x$ is obtained in a way similar to that described in the previous paragraph for $\partial p/\partial z$. $\partial p/\partial x$ is obtaind by the

iterative Newton-Rapson method subject to satisfying the the constraint given by the Eq.(2 17a)

The overall solution algorithm is as follows

(1) Guess $\partial p/\partial x$, $\partial p/\partial z$, u, w, θ at downstream location $z_{i,j}$.

(2) Solve Eq (2.13a) and Eq (2 13b) to obtain u, w. This implies solution of Eq.(2.21) and Eq (2 26) in the channel domain

(3) Check whether Eqs (2 17a-b) are satisfied or not. If yes, go to Step 5.

(4) If not, improve the guess for $\partial p/\partial x$, $\partial p/\partial z$ by iterative Newton-Rapson method and go back to Step 2

(5) Solve Eq.(2 14) and Eq (2.15). This implies solution of Eq.(2.32), Eq (2.35) and Eq.(2.43) in the entire computational domain.

(6) If max $|\theta_{new} - \theta_{guess}| \leq 10^{-3}$, go to Step 8.

(7) Else, go to Step 2.

(8) Print u, w, θ, $\partial p/\partial x$, $\partial p/\partial z$

(9) Using u, w, θ at $z_{i,j}$, compute the same at $z_{i,j+1}$ and so on until z = 250 following Steps # 1-8.

Eq (2 21) and Eq (2 26) are solved by an implicit finite difference scheme The convergence criterion used for the pressure gradients is

$$\max \left[\Delta(\partial p/\partial x), \; \Delta(\partial p/\partial z) \right] \leq 10^{-4}$$

where Δ stands for the absolute fractional change between two consecutive iterations. This particular convergence criterion is not suitable when the values of the pressure gradients become small, i.e , close to zero Under such circumstances, only the absolute change in the values of the pressure gradients is considered for convergence

Eq.(2.32) is solved by unconditionally stable implicit scheme having an accuracy of the order (Δz^*) and $(\Delta y^*)^2$. However, to avoid numerical oscillations (characteristics of stable methods with rather large grid size in the parabolic diection) over a very short distance near the inlet, since there is a step change in the barrel temperature at the inlet from T_i to T_b, the barrel is assumed to be adiabatic very near the inlet

The adiabatic boundary condition at $y = 0$ (Fig.2 1)is represented by a three point forward difference scheme.

The computer program is tested with a wide range of governing parameters. A value of 0.3 for q_v is chosen as $q_v = 0.4 \sim 0.5$ corresponds to drag flow situation (no die situation), where

negative or no pressure gradient is generated Small values of q_v represent a die of smaller opening, which restricts the flow considerably Therefore, $q_v = 0\ 3$ is a resonable value to assume

CHAPTER 3

FULLY TWO-DIMENSIONAL MODEL

CHAPTER 3

3.1 PHYSICAL DESCRIPTION OF THE FULLY TWO-DIMENSIONAL MODEL

In the present analysis, a fully two-dimensional domain is considered (as shown in Fig 3.1) Variations in the transverse channel direction normal to the flights have been ignored because the width is assumed to be much larger as compared to the depth of the channel Following the well known lubrication approximation (Schlichting, 1979), the momentum equation in the y-direction can be omitted altogether because the component v is very small with respect to u and w The reason (also valid for quasi two-dimensional model) why lubrication approximation can be used in polymer processing in which 'films' of several orders of magnitude thicker than very very thin oil films are encountered is the fact that viscosity of polymeric melts is also several orders of magnitude higher than the viscosity of the lubricating oils

Unlike that in the quasi two-dimensional model described in Chapter 2, the effect of the variation in the z-direction has been considered Thus the model becomes fully elliptic in both the y- and z-directions. The inlet w-velocity along the channel is taken as uniform whereas the u-velocity (i.e., the velocity component in the direction normal to the screw flights) is assumed to have a zero value following Agur and Vlachopoulous (1982). The outflow

boundary conditions at the exit of the channel are satisfied as follows For both the u- and w-velocities, the first derivative with respect to z has been set equal to zero because axial diffusion terms in the x- and z-momentum equations approach almost zero values at the exit of the long channel It is to be noted that the first and not the second derivatives are set equal to zero because the coefficient of viscosity, μ, is not constant here For the energy equation, the axial diffusion term $(\partial^2 T/\partial z^2)$ at the channel outlet is set equal to zero on the assumption that axial diffusion is zero Also conduction within the screw body is considered   All computations have been carried out assuming a steady state flow and heat transfer.

3.2 GOVERNING EQUATIONS AND BOUNDARY CONDITIONS

The geometry of the unwound rectangular screw channel is shown in Fig 3 1.

As screw channel is shallow and long, i e., H/W ≪ 1, and as convective effects are small in comparison to viscous, creeping flow approximation (Schlichting, 1979) are made for the conservation of momentum equations. Variations in the y- and z-directions are important and considered here. The thermal convection is significant only along the channel length (z-direction). Unlike in the quasi two-dimensional model, thermal conduction in the fluid and the screw are significant in both the transverse direction y- and downchannel direction z. It is also acknowledged that thermal convection normal to the screw flights

Fig. 3.1 Boundary conditions for the fully two-dimensional model

(x-direction) does have considerable effect since there is a circulation in that direction which contributes to the mixing of the fluid However, the effect can be considered only in a three-dimensional model

Similar to that in the quasi two-dimensional model, the screw body is treated as semi-infinite in the y-direction.

With the foregoing assumptions, the momentum equations of the fluid and the energy equations of the fluid and the screw may be written as

MELT:

X-MOMENTUM :

$$\frac{\partial p}{\partial x} = \frac{\partial}{\partial y}\left(\mu\,\frac{\partial u}{\partial y}\right) + \frac{\partial}{\partial z}\left(\mu\,\frac{\partial u}{\partial z}\right) \tag{3 1a}$$

Z-MOMENTUM :

$$\frac{\partial p}{\partial z} = \frac{\partial}{\partial y}\left(\mu\,\frac{\partial w}{\partial y}\right) + \frac{\partial}{\partial z}\left(2\mu\,\frac{\partial w}{\partial z}\right) \tag{3.1b}$$

ENERGY EQUATION :

$$\rho\,C_p w\,\frac{\partial T_f}{\partial z} = \frac{\partial}{\partial y}\left(K_f\,\frac{\partial T_f}{\partial y}\right) + \frac{\partial}{\partial z}\left(K_f\,\frac{\partial T_f}{\partial z}\right) + \mu\,\phi \tag{3.2}$$

$$\text{where, } \phi = 2\left(\frac{\partial w}{\partial z}\right)^2 + \left(\frac{\partial u}{\partial y}\right)^2 + \left(\frac{\partial u}{\partial z}\right)^2 + \left(\frac{\partial w}{\partial y}\right)^2 \tag{3.2a}$$

In the energy equation of the fluid, viscous dissipation effect is strong as polymers have high viscosity This statement is also true for quasi two-dimensional model

$$\mu = \mu_0 \left(\frac{\dot{\gamma}}{\dot{\gamma}_0} \right)^{n-1} e^{-b(T-T_0)} \qquad (3\ 3)$$

where,

$$\dot{\gamma} = \left[2 \left(\frac{\partial w}{\partial z} \right)^2 + \left(\frac{\partial u}{\partial y} \right)^2 + \left(\frac{\partial u}{\partial z} \right)^2 + \left(\frac{\partial w}{\partial y} \right)^2 \right]^{1/2} \qquad (3\ 3a)$$

SCREW :

ENERGY EQUATION :

$$\frac{\partial}{\partial y} \left(K_s \frac{\partial T_s}{\partial y} \right) + \frac{\partial}{\partial z} \left(K_s \frac{\partial T_s}{\partial z} \right) = 0 \qquad (3\ 4)$$

At the outlet, the fully developed flow conditions exist if the channel were infinitely long In practice, such a condition can only be approximate However, the channel length in the screw extruders is usually about two orders of magnitude larger than the other dimensions Thus it is reasonably accurate to assume fully developed velocity conditions at the outlet This means that the axial diffusion terms become smaller downstream and their appropach to zero are used both in the boundary conditions for the momentum and the energy equations at the outlet (see Eqs.(3.5b-c) as well as Eqs (3.11b-c)).

The boundary conditions as shown in Fig 3 1 are

at z = 0,

$$u = 0, \quad w = Q/H, \quad T_f = T_s = T_i \tag{3 5a}$$

at z = L (exit),

$$\frac{\partial u}{\partial z} \longrightarrow 0 \tag{3.5b}$$

$$\frac{\partial w}{\partial z} \longrightarrow 0 \tag{3 5c}$$

$$\frac{\partial^2 T_f}{\partial z^2} \longrightarrow 0 \tag{3 5d}$$

$$\frac{\partial^2 T_s}{\partial z^2} \longrightarrow 0 \tag{3 5e}$$

at y=0,

$$\frac{\partial T_s}{\partial y} = 0 \tag{3.5f}$$

at $y = H_d$ (i e., at the interface),

$$u = 0, \quad w = 0,$$

$$T_f = T_s, \quad K_f \frac{\partial T_f}{\partial y} = K_s \frac{\partial T_s}{\partial y} \tag{3.5g}$$

at y=H_d + H,

$$u = V_{bx}, \quad w = V_{bz}, \quad T_f = T_b \tag{3.5h}$$

If the leakage across the screw flights is negligible, then for a total volumetric flow rate Q, the integral form of the continuity equation takes the form

$$\int_{H_d}^{H_d+H} u\,dy = 0 \tag{3 6a}$$

$$\int_{H_d}^{H_d+H} w\,dy = Q/W \tag{3 6b}$$

3.3 NON-DIMENSIONALISATION

The governing equations are non-dimensionalised in terms of the following dimensionless variables,

$$x^* = x/H, \quad y^* = y/H, \quad z^* = z/H \tag{3 7a}$$

$$u^* = u / V_{bz}, \quad w^* = w / V_{bz} \tag{3 7b}$$

$$\theta = \frac{T - T_i}{T_{b(ref)} - T_i} \tag{3 7c}$$

$$p^* = \frac{p}{\bar{p}} \,, \quad \bar{p} = \bar{\mu}\,\frac{V_{bz}}{H} \tag{3.7d}$$

$$\dot{\gamma}^* = \frac{\dot{\gamma}\,H}{V_{bz}}, \quad \bar{\mu} = \mu_0 \left[\frac{V_{bz}/H}{\dot{\gamma}_0}\right]^{-b} e^{-b\left(T_i - T_0\right)} \tag{3.7e}$$

$$\beta = b \left[T_{b(ref)} - T_i \right] \qquad (3\ 7f)$$

$$Pe = \frac{\rho\ C_p V_{bz}\ H}{K_f} \qquad (3\ 7g)$$

$$G = \frac{\bar{\mu}\ V_{bz}^2}{K_f(T_{b(ref)} - T_i)} \qquad (3.7h)$$

The dimensionless equations thus obtained are

MELT :

X-MOMENTUM :

$$\frac{\partial p^*}{\partial x^*} = \frac{\partial}{\partial y^*} \left[\left(\dot{\gamma}^* \right)^{n-1} e^{-\beta\theta_f} \frac{\partial u^*}{\partial y} \right] + \frac{\partial}{\partial z^*} \left[\left(\dot{\gamma}^* \right)^{n-1} e^{-\beta\theta_f} \frac{\partial u^*}{\partial y} \right] \qquad (3\ 8a)$$

Y-MOMENTUM :

$$\frac{\partial p^*}{\partial z^*} = \frac{\partial}{\partial y^*} \left[\left(\dot{\gamma}^* \right)^{n-1} e^{-\beta\theta_f} \frac{\partial w^*}{\partial y} \right] + 2 \frac{\partial}{\partial z^*} \left[\left(\dot{\gamma}^* \right)^{n-1} e^{-\beta\theta_f} \frac{\partial w^*}{\partial y} \right] \qquad (3\ 8b)$$

ENERGY EQUATION :

$$Pe\ w^* \frac{\partial \theta_f}{\partial z^*} = \frac{\partial^2 \theta_f}{\partial y^{*2}} + \frac{\partial^2 \theta_f}{\partial z^{*2}} + G \left(\dot{\gamma}^* \right)^{n+1} e^{-\beta\theta_f} \qquad (3.9)$$

SCREW :

ENERGY EQUATION :

$$\frac{\partial^2 \theta_s}{\partial y^{*2}} + \frac{\partial^2 \theta_s}{\partial z^{*2}} = 0 \qquad (3\ 10)$$

Similarly, the boundary conditions are also obtained in the non-dimensional form as

at $z^* = 0$,

$$u^* = 0, \quad w^* = \frac{Q / H}{W V_{bz}} = q_v, \quad \theta_f = \theta_s = 0 \qquad (3.11a)$$

at $z^* = L / H = 250\ 0$ (exit),

$$\frac{\partial u^*}{\partial z^*} \longrightarrow 0 \qquad (3\ 11b)$$

$$\frac{\partial w^*}{\partial z} \longrightarrow 0 \qquad (3\ 11c)$$

$$\frac{\partial^2 \theta_f}{\partial z^{*2}} \longrightarrow 0 \qquad (3.11d)$$

$$\frac{\partial^2 \theta_s}{\partial z^{*2}} \longrightarrow 0 \qquad (3.11e)$$

at $y^* = 0$,

$$\frac{\partial \theta_s}{\partial y^*} = 0 \qquad (3.11f)$$

at $y^* = H_d/H$,

$$u^* = 0, \quad w^* = 0, \tag{3 11g}$$

$$\left. \begin{array}{l} \dfrac{\partial \theta_f}{\partial y^*} = \dfrac{K_s}{K_f} \dfrac{\partial \theta_s}{\partial y^*}, \\[2em] \theta_s = \theta_f \end{array} \right\} \quad \text{Compatibility Conditions} \tag{3 11h}$$

at $y^* = 1 + H_d/H$,

$$u^* = V_{bx}/V_{bz} = \frac{V_b \sin\phi}{V_b \cos\phi} = \tan\phi, \quad w^* = 1, \quad \theta_f = 1 \tag{3 11i}$$

The constraints on the flow in the dimensionless form are,

$$\int_{H_d/H}^{1+H_d/H} u^* \, dy^* = 0 \tag{3 12a}$$

$$\int_{H_d/H}^{1+H_d/H} w^* \, dy^* = q_v = \frac{Q}{H V_{bz} W} \tag{3 12b}$$

Thus the parameters that govern the numerical solution are Pe, G, n, q_v, the viscosity parameter β and the thermal conductivity ratio (K_s / K_f).

3.4 METHOD OF SOLUTION

The computational domain is shown in Fig 3 2 The governing dimensionless Eqs (3 8)-(3 10) are solved by means of finite difference techniques For the sake of simplicity, in the subsequent discussions of this chapter, the superscript (*) has been dropped from the dimensionless equations Also, the subscript of θ have been deleted

3.4.1 X-MOMENTUM EQUATION

The Eq (3 8a) is rewritten as,

$$\frac{\partial p}{\partial x} = \frac{\partial}{\partial y} \left[\dot{\gamma}^{n-1} e^{-\beta\theta} \frac{\partial u}{\partial y} \right] + \frac{\partial}{\partial z} \left[\dot{\gamma}^{n-1} e^{-\beta\theta} \frac{\partial u}{\partial z} \right] \qquad (3.13)$$

Let $\dot{\gamma}^{n-1} e^{-\beta\theta} = A$

By central difference scheme, the Eq (3 13) is discretized as,

$$\left.\frac{\partial p}{\partial x}\right|_j = \frac{A \left.\frac{\partial u}{\partial y}\right|_{i+1/2,j} - A \left.\frac{\partial u}{\partial y}\right|_{i-1/2,j}}{\Delta y_f^2} - \frac{A \left.\frac{\partial w}{\partial z}\right|_{i-1/2,j} - A \left.\frac{\partial w}{\partial z}\right|_{i,j-1/2}}{\Delta z^2}$$

(3 14)

Further expanding the terms,
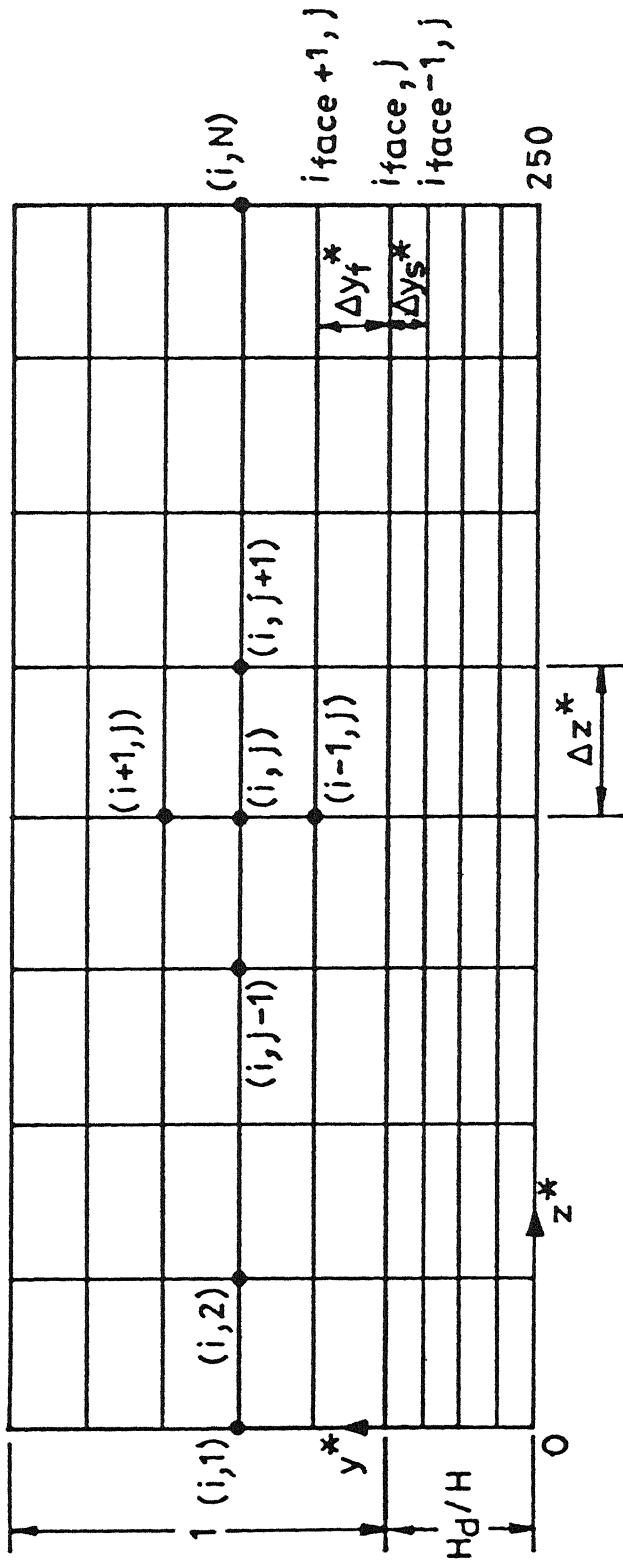
Fig. 3.2 Computational domain and the finite difference grid for the fully

two-dimensional model.

$$\left.\frac{\partial p}{\partial x}\right|_j = \frac{A_{i+1/2,j}\,(u_{i+1\ j} - u_{i,j}) - A_{i-1/2,j}\,(u_{i,j} - u_{i-1,j})}{\Delta y_f^2} +$$

$$\frac{A_{i,j+1/2}\,(u_{i\ j+1} - u_{i,j}) - A_{i,j-1/2}\,(u_{i,j} - u_{i,j-1})}{\Delta z^2} \qquad (3\ 15)$$

Rearranging the terms,

$$\left.\frac{\partial p}{\partial x}\right|_j \Delta y_f^2 = A_{i+1/2,j}\,u_{i+1,j} + A_{i-1/2,j}\,u_{i-1.,j}$$

$$+ R^2 \left\{ A_{i,j+1/2}\,u_{i,j+1} + A_{i,j-1/2}\,u_{i,j-1} \right\} -$$

$$\left[A_{i+1/2,j} + A_{i-1/2,j} + R^2 \left\{ A_{i,j+1/2} + A_{i,j-1/2} \right\} \right] u_{i,j}$$

$$(3\ 16)$$

where, $R = \dfrac{\Delta y_f}{\Delta z}$

3.4.2 Z-MOMENTUM EQUATION

The Eq (3 8b) is rewritten as,

$$\left.\frac{\partial p}{\partial z}\right|_j = \frac{\partial}{\partial y}\left[\dot{\gamma}^{n-1}\,e^{-\beta\theta}\,\frac{\partial w}{\partial y} \right] + 2\frac{\partial}{\partial z}\left[\dot{\gamma}^{n-1}\,e^{-\beta\theta}\,\frac{\partial w}{\partial z} \right]$$

$$(3.17)$$

Let $\quad \dot{\gamma}^{n-1}\,e^{-\beta\theta} = A$

By central difference scheme, the Eq (3 13) is discretized as,

$$\left.\frac{\partial p}{\partial z}\right|_j = \frac{A\left.\frac{\partial w}{\partial y}\right|_{i+1/2,j} - A\left.\frac{\partial w}{\partial y}\right|_{i-1/2,j}}{\Delta y_f^2} -$$

$$2\;\frac{A\left.\frac{\partial w}{\partial z}\right|_{i+1/2,j} - A\left.\frac{\partial w}{\partial z}\right|_{i-1/2,j}}{\Delta z} \tag{3 18}$$

Further expanding the terms,

$$\left.\frac{\partial p}{\partial z}\right|_j = \frac{A_{i+1/2,j}\,(w_{i+1,j} - w_{i,j}) - A_{i-1/2,j}\,(w_{i,j} - w_{i-1,j})}{\Delta y_f^2} +$$

$$\frac{A_{i,j+1/2}\,(w_{i,j+1} - w_{i,j}) - A_{i,j-1/2}\,(w_{i,j} - w_{i,j-1})}{\Delta z^2}$$

$$\tag{3 19}$$

Rearranging the terms,

$$\left.\frac{\partial p}{\partial z}\right|_j \Delta y_f^2 = A_{i+1/2,j}\,w_{i+1,j} + A_{i-1/2,j}\,w_{i-1.,j}$$

$$+\;2\,R^2\left\{A_{i,j+1/2}\,w_{i,j+1} + A_{i,j-1/2}\,w_{i,j-1}\right\} -$$

$$\left[A_{i+1/2,j} + A_{i-1/2,j} + 2\,R^2\left\{A_{i,j+1/2} + A_{i,j-1/2}\right\}\right]w_{i,j}$$

$$\tag{3.20}$$

where, $R = \dfrac{\Delta y_f}{\Delta z}$

3.4.3 ENERGY EQUATIONS

MELT :

The energy equation of the fluid (or melt) i e , Eq.(3.9) may be rewritten,

$$Pe \; w \; \frac{\partial \theta}{\partial z} = \frac{\partial^2 \theta}{\partial y^2} + \frac{\partial^2 \theta}{\partial z^2} + G \; \dot{\gamma}^{n+1} \; e^{-\beta \theta} \qquad (3.21)$$

Let $\dot{\gamma}^{n+1} \; e^{-\beta \theta} = A$

Using central diffeence scheme, the Eq.(3 21) is discretized as,

$$\left(Pe \; w \; \frac{\partial \theta}{\partial z} \right)_{i,j} = \frac{\theta_{i+1,j} - 2\theta_{i,j} + \theta_{i-1,j}}{\Delta y_f^2} +$$

$$\frac{\theta_{i,j+1} - 2\theta_{i,j} + \theta_{i,j-1}}{\Delta z^2} + G \; A_{i,j} \qquad (3\ 22)$$

The convective term $(Pe \; w \; \partial\theta/\partial z)_{i,j}$ in Eq (3.22) is discretized using backward difference scheme because the velocity w in the downchannel direction is always positive and the convective effects will be carried in the downstream direction. In other words, a first order upwind scheme is used to discretize the convective term, it being much more dominant than the diffusion

(or conduction) term in the z-direction as the Peclet number is large

With this, the final discretized form is,

$$\text{Pe } w_{i,j} \frac{\theta_{i,j} - \theta_{i,j-1}}{\Delta z} \Delta y_f^2 = \theta_{i+1,j} - 2\theta_{i,j} + \theta_{i-1,j}$$

$$+ R^2 * \left(\theta_{i,j+1} - 2\theta_{i,j} + \theta_{i,j-1} \right) \tag{3.23}$$

Rearranging the terms,

$$\theta_{i+1,j} + \theta_{i-1,j} + R^2 \theta_{i,j+1} + \left(\frac{\text{Pe } w_{i,j} \Delta y_f^2}{\Delta z} + R^2 \right) \theta_{i,j-1} - $$

$$\left\{ 2 + 2 R^2 + \frac{\text{Pe } w_{i,j} \Delta y_f^2}{\Delta z} \right\} \theta_{i,j} = - G A_{i,j} \Delta y_f^2 \tag{3.24}$$

SCREW :

The energy equation of the screw (Eq (3 10)) is rewritten as,

$$\frac{\partial^2 \theta}{\partial y_s^2} + \frac{\partial^2 \theta}{\partial z^2} = 0 \tag{3.25}$$

Using central difference scheme, the equation is discretized as shown in Fig.3.2

$$\frac{\theta_{i+1,j} - 2\theta_{i,j} + \theta_{i-1,j}}{\Delta y_s^2} + \frac{\theta_{i,j+1} - 2\theta_{i,j} + \theta_{i,j-1}}{\Delta z^2} = 0 \tag{3.26}$$

Rearranging the terms,

$$\theta_{i+1,j} - 2\theta_{i,j} + \theta_{i-1,j} + \left(\frac{\Delta y_s}{\Delta z}\right)^2 \left\{\theta_{i,j+1} - 2\theta_{i,j} + \theta_{i,j-1}\right\} = 0$$

(3.27)

The final form becomes,

$$\theta_{i+1,j} + \theta_{i-1,j} + \left(\frac{\Delta y_s}{\Delta z}\right)^2 \left\{\theta_{i,j+1} + \theta_{i,j-1}\right\} -$$

$$\left\{2 + \left(\frac{\Delta y_s}{\Delta z}\right)^2\right\} \theta_{i,j} = 0$$

(3.28)

3.4.4 DERIVATION OF THE MELT-SCREW INTERFACE EQUATION

To obtain the discretized energy equation at the interface (i e , at the screw surface separating the fluid and the screw body), referring the Fig 3.2, $\theta_{i+1,j}$ in the fluid and $\theta_{i-1,j}$ in the screw body are expanded into Taylor series form dropping terms beyond second order (Carnahan et al., 1969).

CHANNEL :

From Taylor Series expansion,

$$\theta_{i+1,j} = \theta_{i,j} + \left.\frac{\partial\theta}{\partial y}\right|_{i,j} \Delta y_f + \left.\frac{\partial^2\theta}{\partial y^2}\right|_{i,j} \frac{\Delta y_f^2}{2}$$

(3.29)

Rearranging,

$$\left.\frac{\partial\theta}{\partial y}\right|_{i,j} = \frac{\theta_{i+1,j} - \theta_{i,j}}{\Delta y_f} - \left.\frac{\partial^2\theta}{\partial y^2}\right|_{i,j} \frac{(\Delta y_f)}{2} \qquad (3\ 30)$$

SCREW :

From Taylor Series expansion,

$$\theta_{i-1,j} = \theta_{i,j} - \left.\frac{\partial\theta}{\partial y}\right|_{i,j} \Delta y_s + \left.\frac{\partial^2\theta}{\partial y^2}\right|_{i,j} \frac{\Delta y_s^2}{2} \qquad (3\ 31)$$

Rearranging,

$$\left.\frac{\partial\theta}{\partial y}\right|_{i,j} = \frac{\theta_{i,j} - \theta_{i-1,j}}{\Delta y_s} + \left.\frac{\partial^2\theta}{\partial y^2}\right|_{i,j} \frac{\Delta y_s}{2} \qquad (3\ 32)$$

The compatibility conditions obtained from Eq (3 11) are:

$$\left.\frac{\partial\theta}{\partial y}\right|_f = \frac{K_s}{K_f} \left.\frac{\partial\theta}{\partial y}\right|_s \qquad (3.33)$$

and,

$$\theta_f = \theta_s$$

$\left.\dfrac{\partial\theta}{\partial y}\right|_f$ and $\left.\dfrac{\partial\theta}{\partial y}\right|_s$ are substituted from Eq (3 30) and Eq.(3.32)

respectively in Eq.(3.33) to obtain,

$$\left[\frac{\theta_{i+1,j} - \theta_{i,j}}{\Delta y_f} - \frac{\partial^2\theta}{\partial y^2} \frac{\Delta y_f}{2} \right]_f =$$

$$\frac{K_s}{K_f} \left[\frac{\theta_{i+1,j} - \theta_{i,j}}{\Delta y_s} - \frac{\partial^2\theta}{\partial y^2} \frac{\Delta y_s}{2} \right]_s \qquad (3.34)$$

From Eq (3 21)

$$\left.\frac{\partial^2 \theta}{\partial y^2}\right|_f = Pe \ w \ \frac{\partial \theta}{\partial z} - \frac{\partial^2 \theta}{\partial z^2} - G \ \dot{\gamma}^{n+1} \ e^{-\beta\theta} \qquad (3.35)$$

and from Eq (3 25)

$$\frac{\partial^2 \theta}{\partial y^2} = - \frac{\partial^2 \theta}{\partial z^2} \qquad (3\ 36)$$

On substitution of Eqs (3 35) and Eq (3 36) in Eq.(3 34),

$$\frac{\theta_{i+1,j} - \theta_{i,j}}{\Delta y_f} - \left(Pe \ w \ \frac{\partial \theta}{\partial z} - \frac{\partial^2 \theta}{\partial z^2} - G \ \dot{\gamma}^{n+1} \ e^{-\beta\theta} \right)_{i,j} \frac{\Delta y_f}{2}$$

$$= \frac{K_s}{K_f} \left[\frac{\theta_{i,j} - \theta_{i-1,j}}{\Delta y_s} - \left.\frac{\partial^2 \theta}{\partial z^2}\right|_{i,j} \frac{\Delta y_s}{2} \right] \qquad (3.37)$$

On the solid interface, w = 0 Eq.(3 37) is further discretized using central difference,

$$\frac{\theta_{i+1,j} - \theta_{i,j}}{\Delta y_f} + \left\{ \frac{\theta_{i,j+1} - 2\theta_{i,j} + \theta_{i,j-1}}{\Delta z^2} + G \ \dot{\gamma}^{n+1} \ e^{-\beta\theta} \right|_{i,j} \right\} \frac{\Delta y_f}{2}$$

$$= \frac{K_s}{K_f} \left[\frac{\theta_{i,j} - \theta_{i-1,j}}{\Delta y_s} - \frac{\theta_{i,j+1} - 2\theta_{i,j} + \theta_{i,j-1}}{\Delta z^2} \frac{\Delta y_s}{2} \right]$$

$$(3.38)$$

On rearrangement,

$$\frac{\theta_{i+1}}{\Delta y_f} + \left(\frac{K_s}{K_f \, \Delta y_s} \right) \theta_{i-1,j} +$$

$$\left\{ \frac{\Delta y_f}{2 \, (\Delta z)^2} + \frac{K_s}{K_f} \frac{\Delta y_s}{2 \, (\Delta z)^2} \right\} \left(\theta_{i,j+1} + \theta_{i,j-1} \right) -$$

$$\left\{ \frac{\Delta y_f}{(\Delta z)^2} + \frac{1}{\Delta y_f} + \frac{K_s}{K_f} \frac{1}{\Delta y_s} + \frac{K_s}{K_f} \frac{\Delta y_s}{(\Delta z)^2} \right\} \theta_{i,j} =$$

$$- \frac{\Delta y_f}{2} \, G \, \dot{\gamma}^{\,n+1} \, e^{-\beta\theta} \Big|_{i,j}$$

$$(3 \; 39)$$

Please note that with reference to Fig 3 2 i=iface, i-1=iface-1 and i+1=iface+1.

3.4.5 SOLUTION SCHEME

The overall solution algorithm is as follows

(1) Guess u,w,θ at all interior grid points in the computational domain. ∂p/∂x, and ∂p/∂z are guessed at all z-locations. Note that the pressure gradients are constant over the height of the channel.

(2) Solve Eq.(3.8a) and Eq.(3.8b) to obtain u and w. This implies solution of Eq.(3.16) and Eq.(3.20) using G-S iterative method using SOR.

(3) With the values of u and w thus obtained from step 2, solve Eq (3.9) and Eq (3 10) simultaneously to obtain θ_f, θ_s This implies solution of Eq.(3 24), Eq (3 39) and Eq (3 28) using G-S iterative method with SOR to obtain θ in the entire computational domain.

(4) Check whether Eqs (3 12a) and (3 12b) are satisfied at each z-locatin. If yes, go to step 6.

(5) If not, improve the guess for $\partial p/\partial x$, and $\partial p/\partial z$ Return to step 2 with the new values of u, w, θ and $\partial p/\partial x$, and $\partial p/\partial z$

(6) Print u, w, θ_f, θ_s, $\partial p/\partial x$, and $\partial p/\partial z$.

(7) Compute p, bulk temperature θ_{bulk}, local Nusselt number Nu_H

(8) STOP

The convergence criterion used for the pressure gradient is,
$$\max \left[\Delta(\partial p/\partial x), \ \Delta(\partial p/\partial z) \right] \leq 10^{-4}$$
where Δ stands for the absolute fractional change between two consecutive iterations in the values of the pressure gradient To facilitate convergence, an efficient technique has been used to improve the guesses for the pressure gradients in subsequent iterations. This method is described next in the subsection 3 4.6.

3.4.6 METHOD OF PRESSURE GRADIENT CORRECTION

Referring to Fig 3 2, the pressure gradients $\partial p/\partial x$ and $\partial p/\partial z$ at the z-locations starting from the second to the last grid point $(2, \cdots, N)$ are guessed in the beginning. First grid point (i.e , $z = 1$) is omitted because it is the inlet boundary where u and w velocities are known.

Eq.(3 8a) and Eq (3.8b) are solved using the guessed pressure gradients In the next step, the pressure gradient $\partial p/\partial x$ (ψ) is perturbed by a very small amount at $z = 2$ Again Eq (3.8a) and Eq (3 8b) are solved. Now, the first column of the Jacobian matrix, 'J' shown in Eq.(3.46) is calculated The $\partial p/\partial z$(η) is perturbed, Eq (3.8a) and Eq (3.8b) are solved and the second column of matrix, 'J' is obtained The same procedure is repeated at successive z-stations until the exit of the channel i.e., $z = 250$ (the grid point number, N). Now the full Jacobian matrix, 'J', is generated. The Newton-Rapson scheme is used to get the improved guesses for the pressure gradients The aforementioned procedure is repeated in subsequent iterations till the convergence criterion specified in Eq.(3 40) is satisfied. The mathematical details are given below.

$$f(\partial p/\partial x, \partial p/\partial z) = \int_{H_d/H}^{1+H_d/H} u\,dy \qquad (3.41)$$

$$g(\partial p/\partial x, \partial p/\partial z) = \int_{H_d/H}^{1+H_d/H} w\,dy \; - \; q_v \qquad (3.42)$$

Convergence is obtained when the LHS of Eq (3 41) and Eq (3 42) are simultaneously zero or very close to zero

Putting $\psi = \partial p/\partial x$, and $\eta = \partial p/\partial z$, Eq (3 41) and Eq.(3.42) respectively becomes,

$$f_j = f(\psi_j, \eta_j) = \left[\int_{H_d/H}^{1+H_d/H} u\,dy \right]_{i,j} \tag{3.43}$$

$$g_j = g(\psi_j, \eta_j) = \left[\int_{H_d/H}^{1+H_d/H} w\,dy - q_v \right]_{i,j} \tag{3.44}$$

where, $j = 2, 3, \cdots, N$

Using Newton-Rapson scheme,

$$\underset{\sim}{pg}^{n+1} = \underset{\sim}{pg}^{n} - \left[J \right]^{-1} \left\{ \underset{\sim}{F} \right\} \tag{3.45}$$

where,

$\underset{\sim}{pg}^{n+1}$ = Column matrix $\left\{ \left(2N - 2 \right) \times 1 \right\}$ containing new

      pressure gradients

$\underset{\sim}{pg}^{n}$ = Column matrix $\left\{ \left(2N - 2 \right) \times 1 \right\}$ containing old

      pressure′gradients

$\underset{\sim}{F}$ = Column matrix $\left\{ \left(2N - 2 \right) \times 1 \right\}$ containing

      functions f_j, g_j to be made zero.

$$J = \text{Jacobian matrix} \left\{ \left(2N - 2 \right) \times \left(2N - 2 \right) \right\} \text{ shown in}$$

Eq 3 46

$$J = \begin{bmatrix} \dfrac{\partial f_2}{\partial \psi_1} & \dfrac{\partial f_2}{\partial \eta_1} & \cdots\cdots & \dfrac{\partial f_2}{\partial \psi_N} & \dfrac{\partial f_2}{\partial \eta_N} \\[2ex] \dfrac{\partial g_2}{\partial \psi_1} & \dfrac{\partial g_2}{\partial \eta_1} & \cdots\cdots & \dfrac{\partial g_2}{\partial \psi_N} & \dfrac{\partial g_2}{\partial \eta_N} \\[2ex] \cdots & \cdots & \cdots\cdots & \cdots & \cdots \\ \cdots & \cdots & \cdots\cdots & \cdots & \cdots \\ \cdots & \cdots & \cdots\cdots & \cdots & \cdots \\[1ex] \dfrac{\partial f_N}{\partial \psi_1} & \dfrac{\partial f_N}{\partial \eta_1} & \cdots\cdots & \dfrac{\partial f_N}{\partial \psi_N} & \dfrac{\partial f_N}{\partial \eta_N} \\[2ex] \dfrac{\partial g_N}{\partial \psi_1} & \dfrac{\partial g_N}{\partial \eta_1} & \cdots\cdots & \dfrac{\partial g_N}{\partial \psi_N} & \dfrac{\partial g_N}{\partial \eta_N} \end{bmatrix} \qquad (3\ 46)$$

CHAPTER 4

A COMPARATIVE STUDY OF THE TWO-MODELS

CHAPTER 4

In the present Chapter, a comparative study of the two models, namely, quasi two-dimensional and fully two-dimensional models, developed by the present author and discussed in Chapter 2 and Chapter 3 respectively has been carried out based on the results obtained by using the same for a typical non-Newtonian fluid (low density polyethylene) following power-law behaviour having $n=0.5$, for $G=10.0$, $Pe=5000~0$, $\beta=1~61$, $q_v=0.3$, $\phi=16.54$, $K_f=0.3$ W/m-K and $K_s=45$ W/m-K The aforementioned input parameters (other than K_s) have been taken from Karwe and Jaluria (1990). The value of K_s has been taken from Holman (1981).

4.1 TEMPERATURE AND VELOCITY FIELDS

Fig 4 1 shows isotherms in the screw channel computed on the basis of the quasi two-dimensional and fully two-dimensional model. A comparison reveals an almost identical fluid tenperature distributoin in the upper half of the channel. However, in the lower half, the fluid temperatures for the fully two-dimensional case are higher than those for the quasi two-dimensional case. A close inspection of the isotherms in the lower half also indicates that in the fully two-dimensional situation, heat flows mainly in the negative downchannel direction which means that very little heat is conducted to the screw body. This is also confirmed by the isotherms in the screw body depicted in the Fig.4.2 for the two
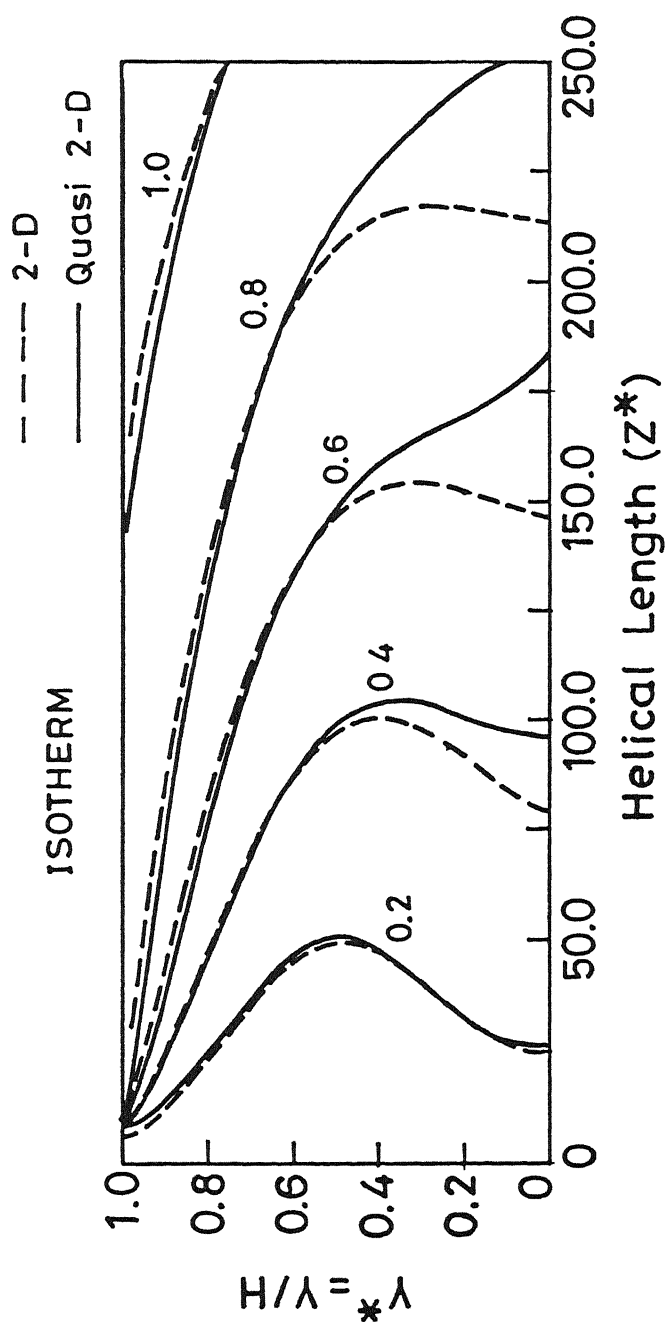
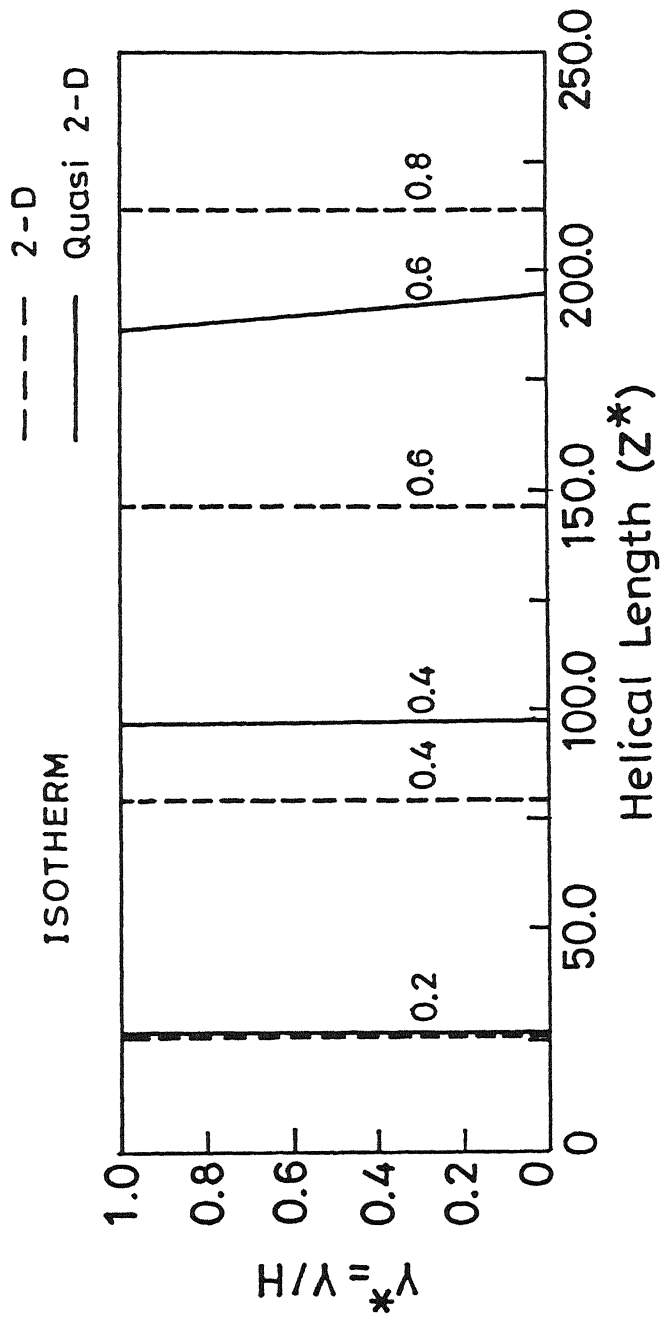Fig. 4.1 Isotherms in the screw channel for the quasi two-dimensional and fully two-dimensional models

Fig. 4.2 Isotherms in the screw body for the quasi two-dimensional and fully two-dimensional models.

models Fig 4 2 also shows that the nature of the isotherms in the screw body for the quasi two-dimensional case is consistent with those in the channel (Fig 4 1). The higher fluid temperatures in the downchannel direction for the fully two-dimensional case may be attributed to the axial diffusion effect. In other words, very small amount of heat is conducted out into the screw body resulting in rise in the fluid temperature

Fig.4.3 depicts the isovelocity (w^*) lines in the screw channel for the quasi two-dimensional and fully two-dimensional case The isovelocity lines are almost parallel, particularly at the outlet. It is clear that except near the inlet, the flow pattern is identical for both the cases From Fig.4.3, it is obvious that for the fully two-dimensional model, the flow becomes 'locally' developed at a very short distance from the inlet. This also shows that axial diffusion in the downchannel direction has very little effect on the velocity field The aforementioned revelations confirm that the use of fully developed inlet velocity profile in the quasi two-dimensional model is not physically unrealistic.

Fig.4.4 and Fig.4.5 show a comparison of transverse temperature profiles at four downstream locations in the fluid and the screw body respectively for the quasi two-dimensional and fully two-dimensional cases. For both the models, the rate of change of temperature along z^* is faster near the inlet and slows down towards the exit of the channel when 'almost' fully developed temperature profile exists. In the lower half of the channel, the

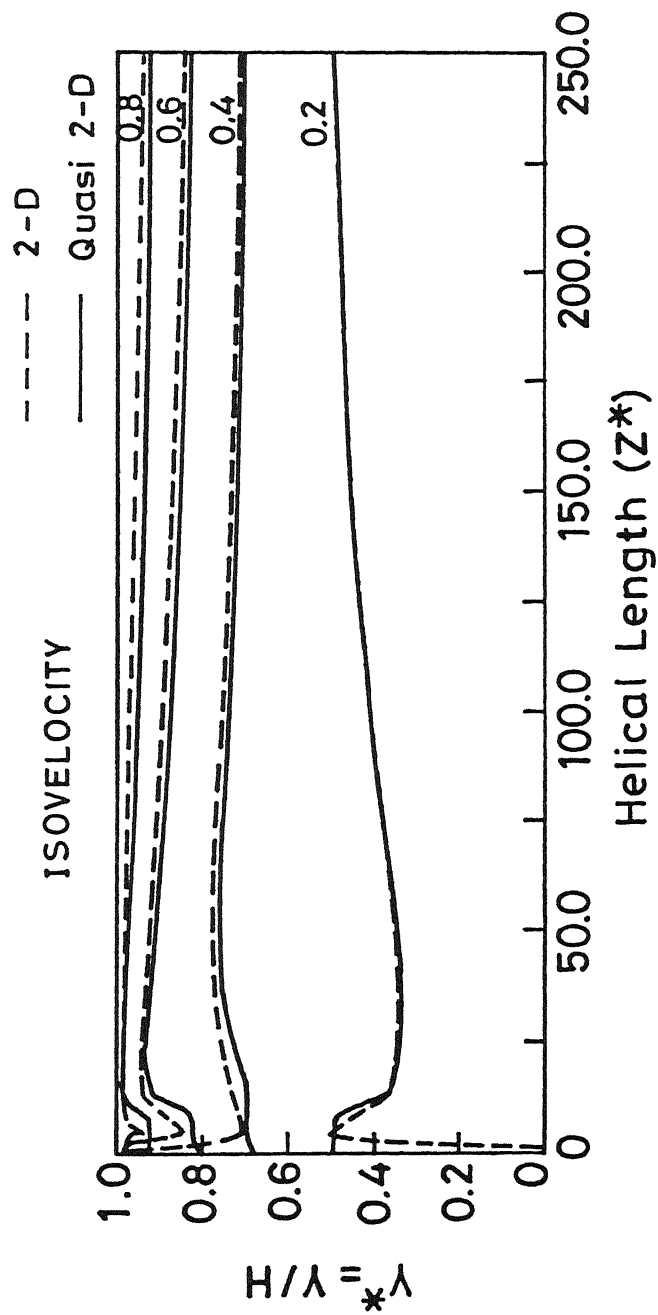Fig. 4.3 Lines of constant velocity components w* for the quasi two-dimensional and fully two-dimensional model.
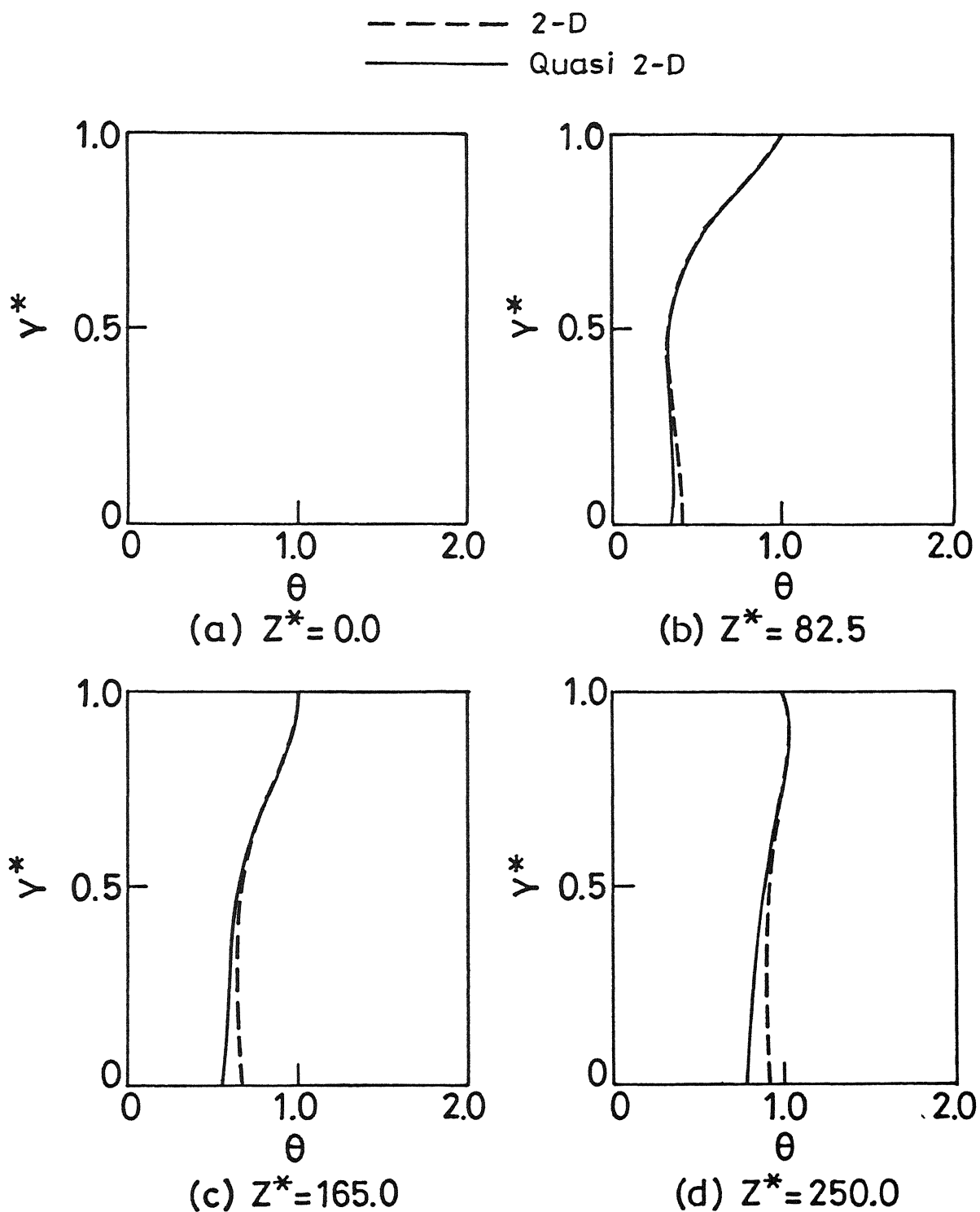
Fig. 4.4 Transverse temperature profiles in the screw channel at four downstream locations based on the quasi two-dimensional and fully two-dimensional models.
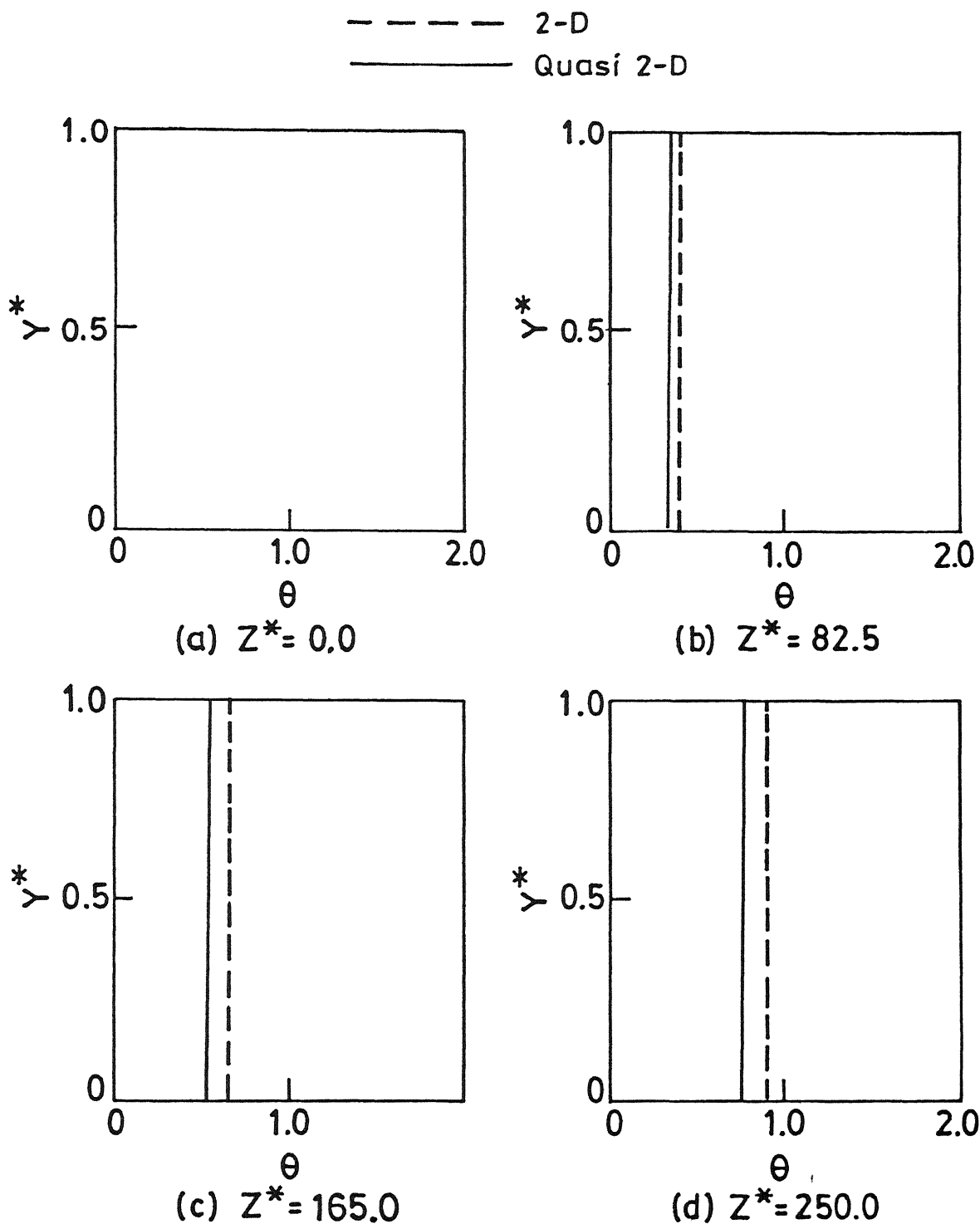
Fig. 4.5 Transverse temperature profiles in the screw
body at four downstream locations based on
the quasi two-dimensional and fully
two-dimensional models.

transverse fluid temperature in the fully two-dimensional model is nearly uniform at the downstream locations particularly away from the inlet. For obvious reasons, the same trend is seen in the screw body Fig 4 4 also reveals that in the initial portion, the fluid temperature is high near the barrel, and becomes more uniform with increasing downstream distance In fact, as seen from Fig.4 4, the temperature of the flow increases above the barrel temperature, $\theta > 1.0$, near the exit region due to the effect of viscous dissipation. However, the corresponding changes in the velocity fields are found to be less significant, as seen in Fig 4.6 and Fig 4.7

Fig.4.6 and 4.7 depict the development of downchannel and cross-channel velocities, i e., w^* and u^* respectively, along the screw channel. While the flow becomes 'locally' fully developed at a very short distance from the inlet for the fully two-dimensional case, except for a slightly higher velocities in the two-dimensional model, there is little difference in the velocity profiles computed on the basis of quasi two-dimensional and fully two-dimensional models. However, both w^* and u^* velocity profiles in both cases keep on changing in the downstream direction as because the temperature profiles are also developing in that direction. As in the case of transverse temperature profiles, the rate of development of velocity profiles is higher near the inlet than towards the outlet. Fig.4.7 also indicates that a circulation exists in the x-direction as the velocity component u^*'s are positive in the upper portion of the channel and negative in the lower portion. This actually creates appreciable thermal

Fig. 4.6 Down channel velocity $\overset{'}{w}{}^*$ profiles at four
downstream locations based on the quasi
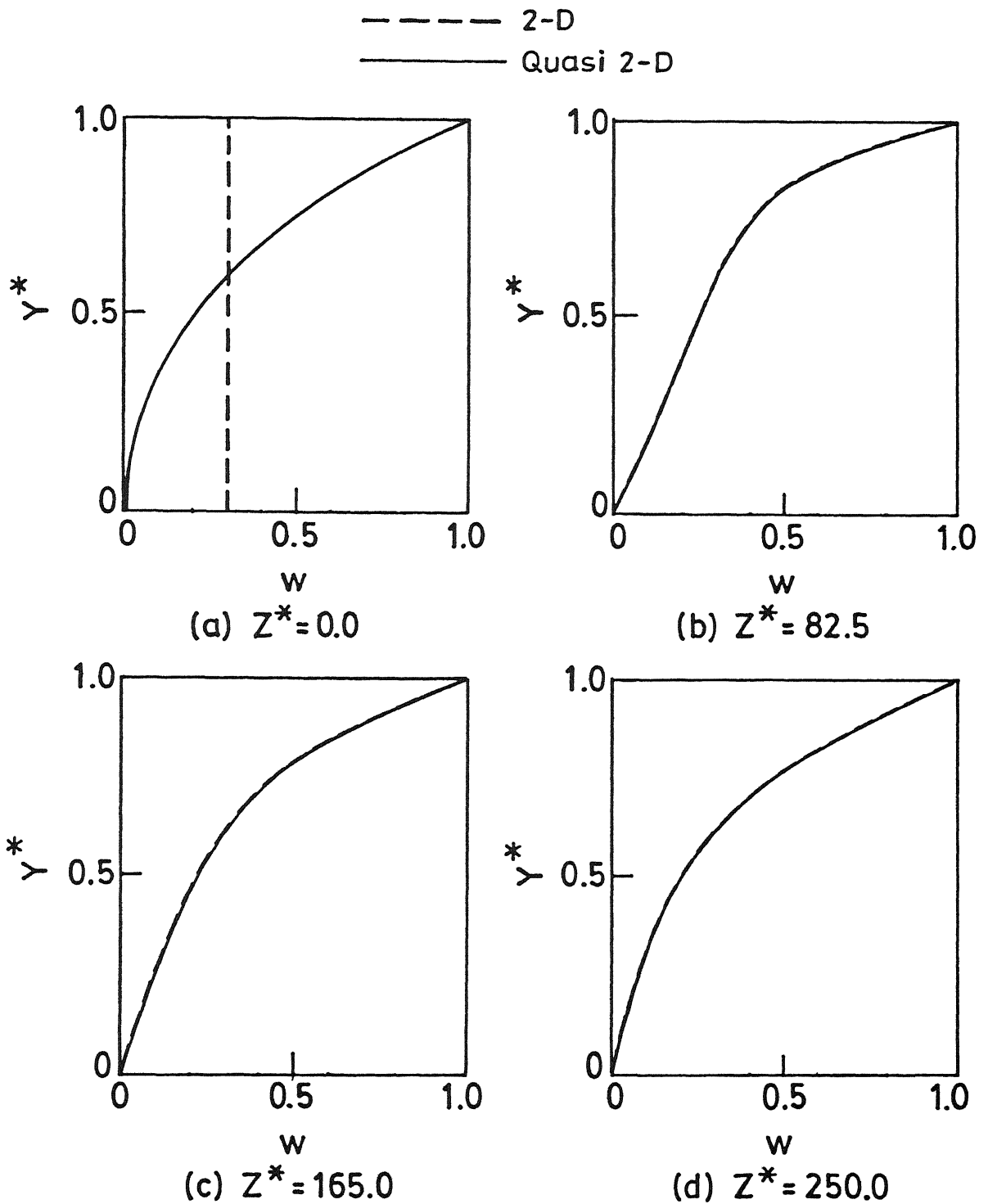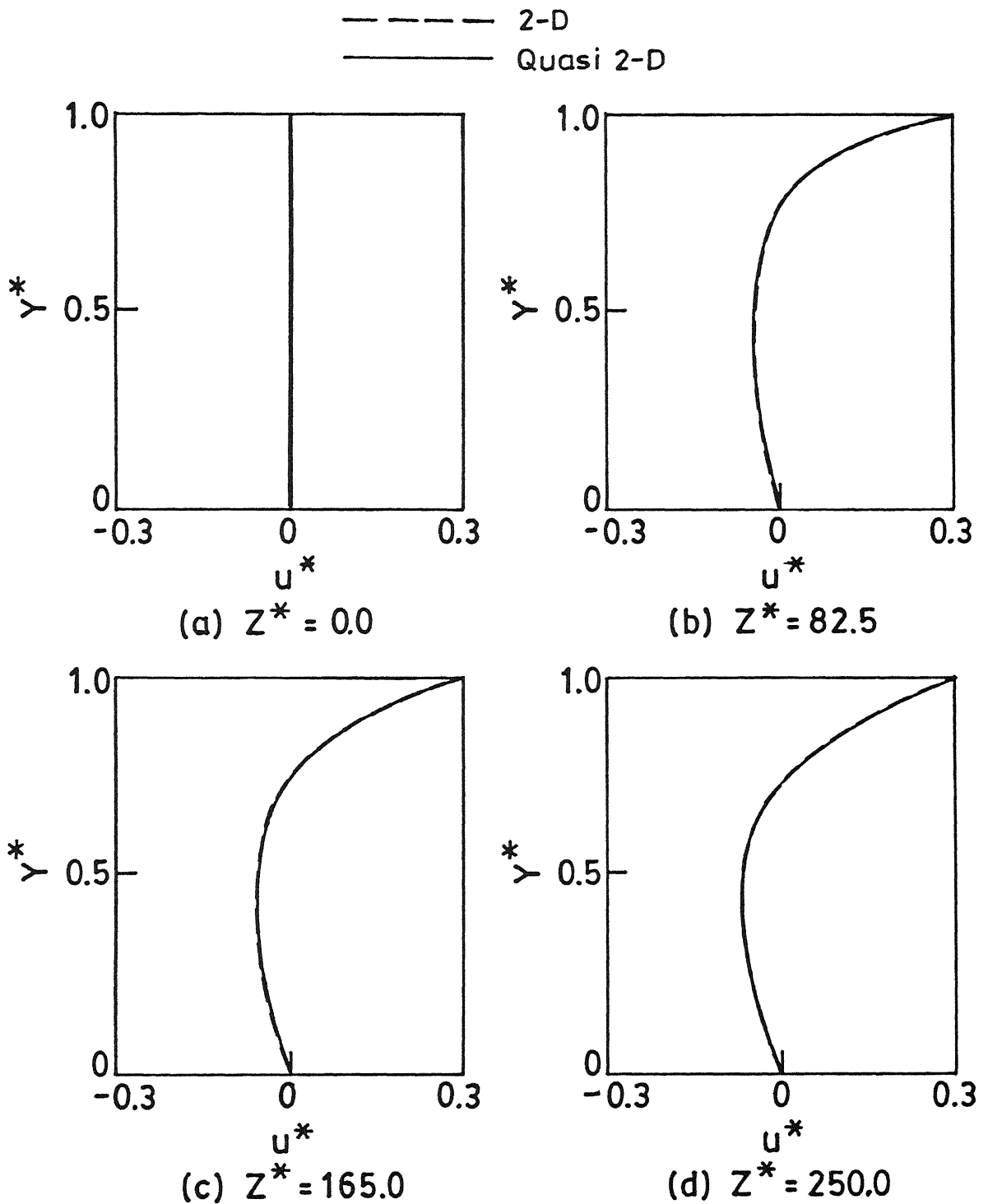two-dimensional and fully two-dimensional
models.

Fig. 4.7 Crosschannel velocity u* profiles at four downstream locations based on the quasi two-dimensional and fully two-dimensional models.

convection in the direction normal to the screw flights and facilitates mixing of the fluid The aforesaid crosswise convection keeps the screw surface temperature close to the barrel temperature But, Fig 4 8 show that the screw surface temperature is lower than the barrel temperature although the fully two-dimensional model performs better in this respect showing screw surface temperature closer to barrel temperature as compared to the quasi two-dimensional model As discussed earlier in the section on Review of Literature in Chapter 1, the reported experimental results of Marshall et al (1965) and Palit (1974) indicate that screw surface temperature settles to steady values slightly higher than the barrel temperature along most of the metering section The failure of the present quasi two-dimensonal and the fully two-dimensonal models to predict correctly the screw surface temperature can be explained by the fact that the thermal convection in the x-direction has not been taken into account in the present quasi two-dimensonal and the fully two-dimensonal models as all variations with respect to x has been neglected Only a three dimensional model could consider this effect

4.2 PRESSURE GRADIENTS AND PRESSURES

Fig 4 9 and Fig.4 10 show the corresponding pressure gradients $\partial p^*/\partial z^*$ and the local pressure values respectively obtained at various downstream locations for the quasi two-dimensonal and the fully two-dimensonal model models. As seen from Fig 4 9, slightly higher pressure gradients are required in the case of the fully two-dimensonal model. This is because of
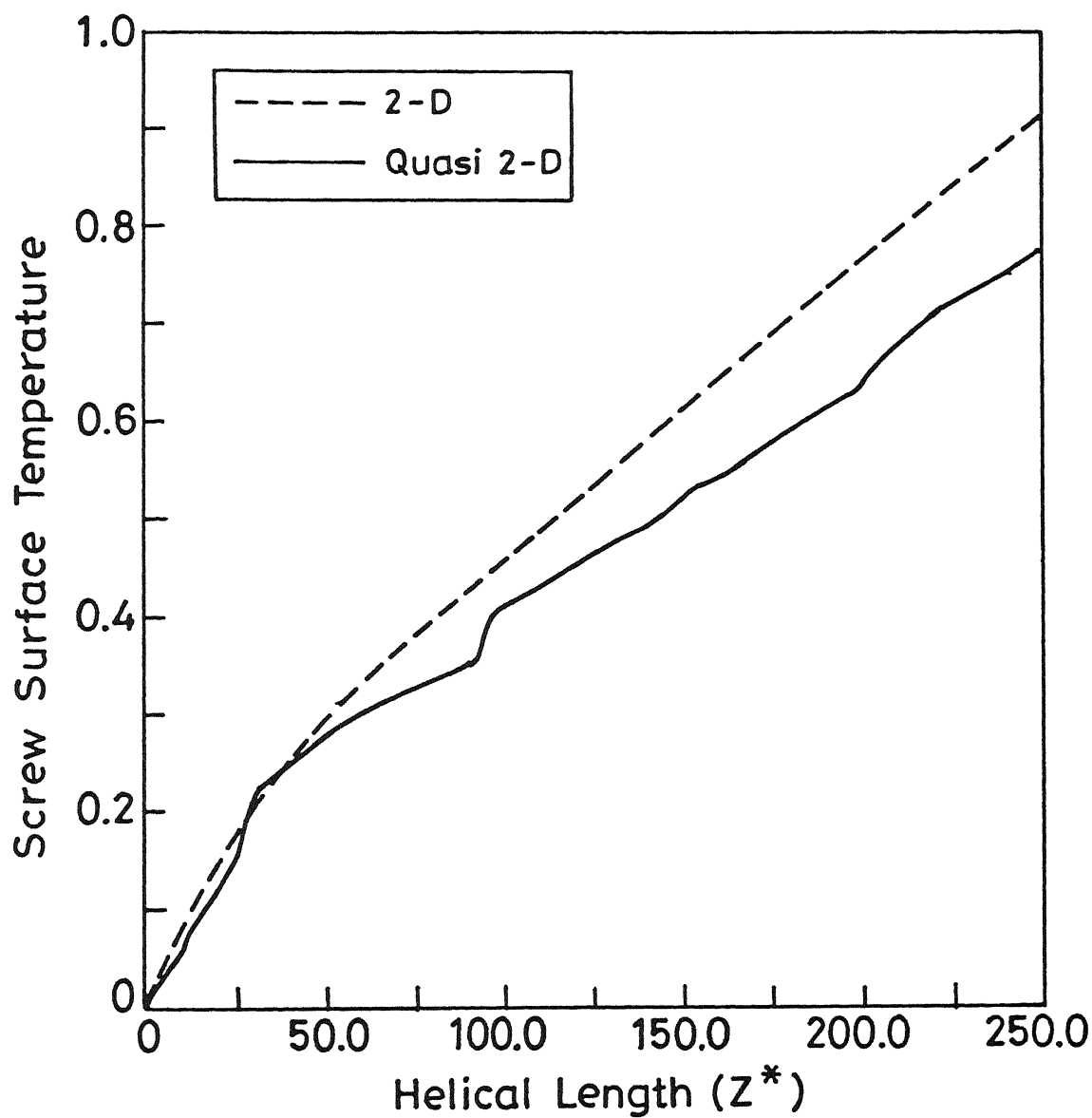
Fig. 4.8 Screw surface temperature variations along the helical length for the quasi two-dimensional and fully two-dimensional models.

Fig. 4.9 Variations of the dimensionless pressure
        gradients along the helical length for the
        quasi two-dimensional and two-dimensional
        models.

Fig. 4.10 Variations of the dimensionless pressure along the helical length for the quasi two-dimensional and fully two-dimensional models.

greater fluid temperature in the fully two-dimensonal case resulting in drop in viscosity which in turn increases the velocity Thus the shear rate γ^* increases which again increases the viscous drag Therefore slightly larger pressure gradients are required to overcome the higher viscous drag in the case of the fully two-dimensional model The greater negative pressure gradients in some part of the metering section near the inlet in the quasi two-dimensional case can be explained by the fact that although viscosity is higher because of lower temperature in the fluid, the shear rates are much smaller Thus the overall result is the larger negative pressure gradient in some portion of the metering section of the screw As expected, the pressure distribution curve for the fully two-dimensional model lies above that for the quasi two-dimensional case (Fig 4 10) The nature of the pressure curves is consistent with the pressure gradient distributions and tallies with Karwe and Jaluria (1990) who used an adiabatic screw boundary condition However, in an actual situation one would expect pressure to continously rise from the inlet of the metering section to the exit instead of a rise followed by a drop and then rise again This discrepancy may be attributed to the non-inclusion of the cross convection terms which can only be done in a three-dimensional model

4.3 BULK TEMPERATURE AND HEAT INPUT AT THE BARREL

Fig 4.11 and Fig.4.12 show the local dimensionless bulk temperature θ_{bulk} and the Nusselt number Nu_H at the barrel, each corresponding to the present quasi two-dimensional model and fully
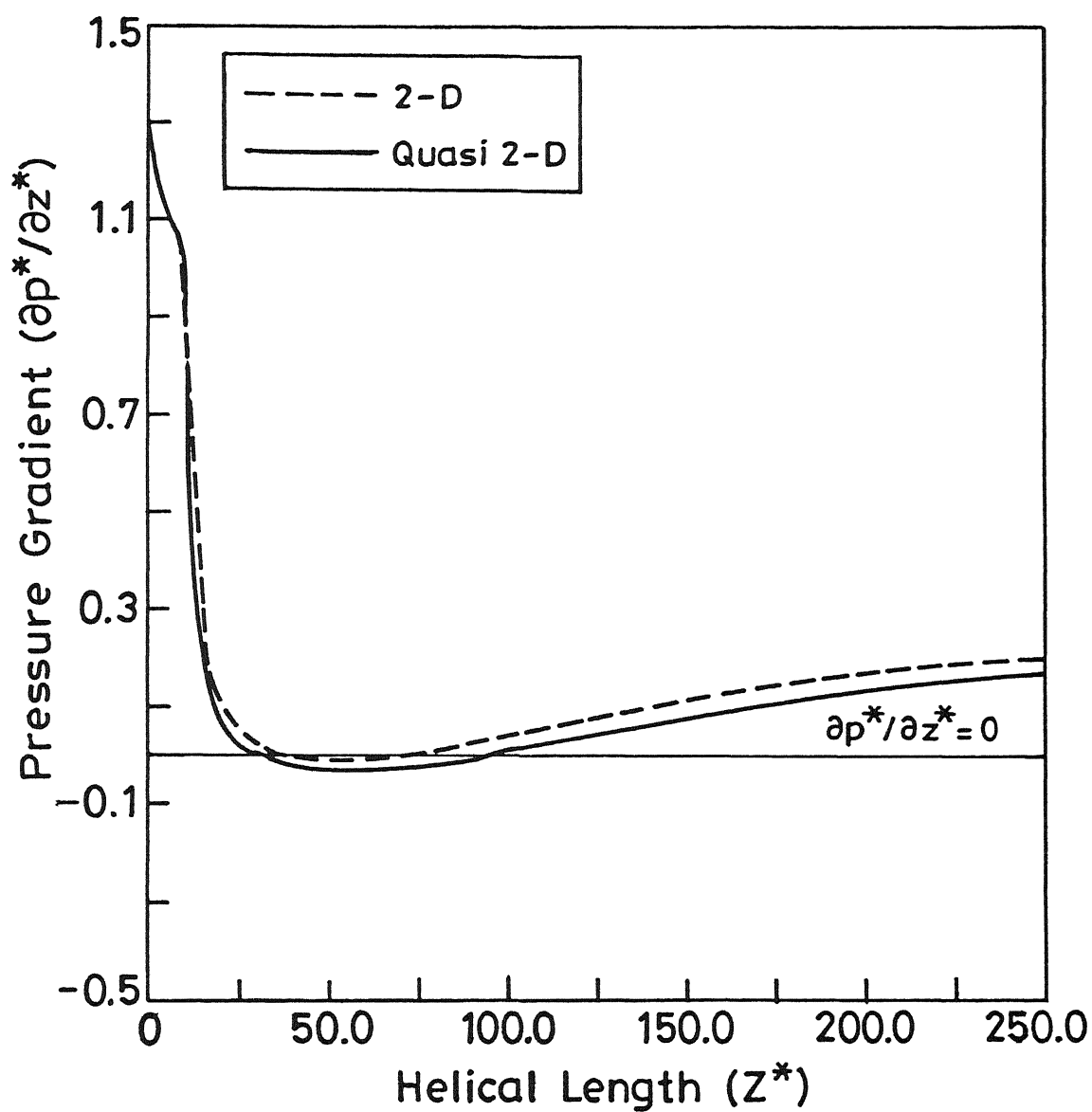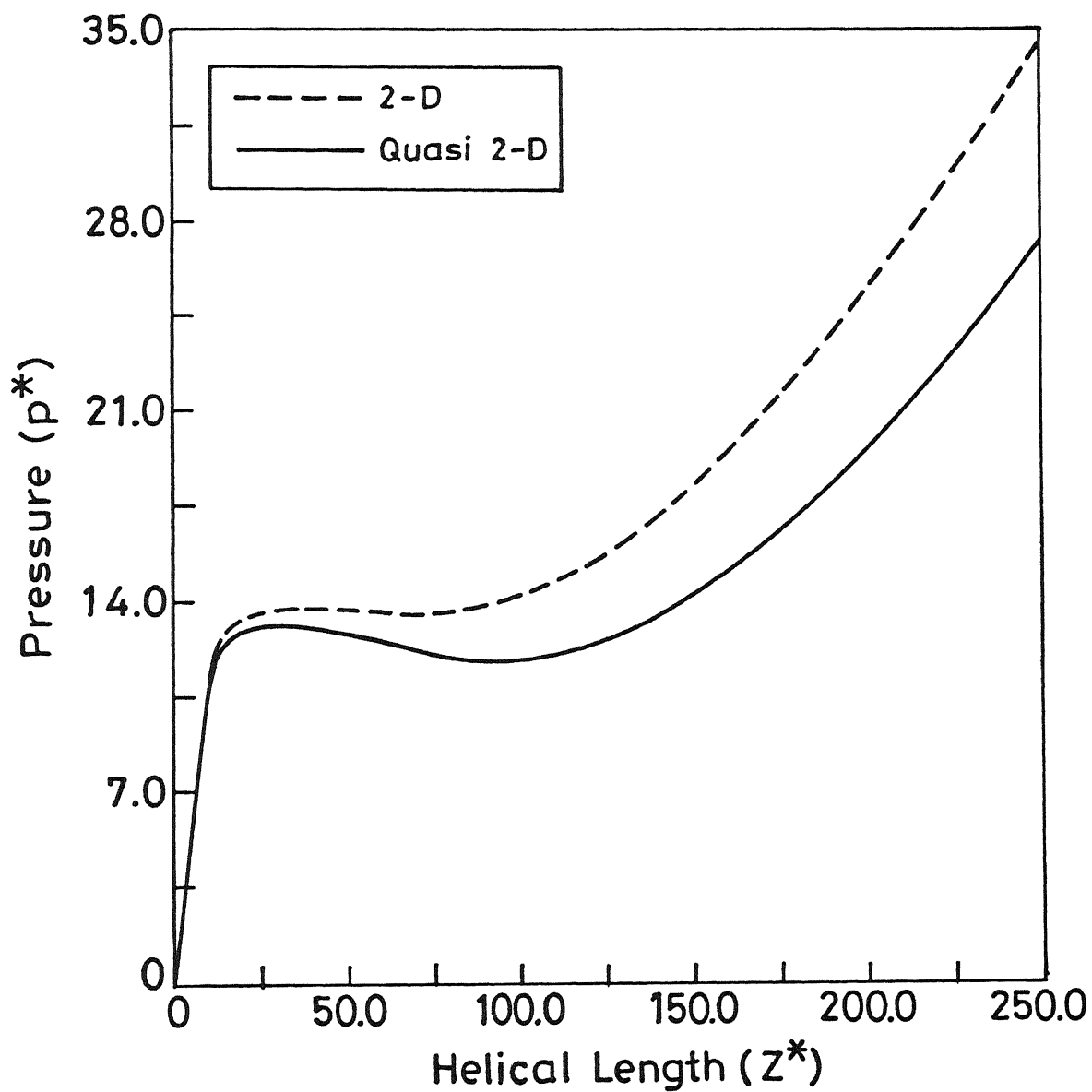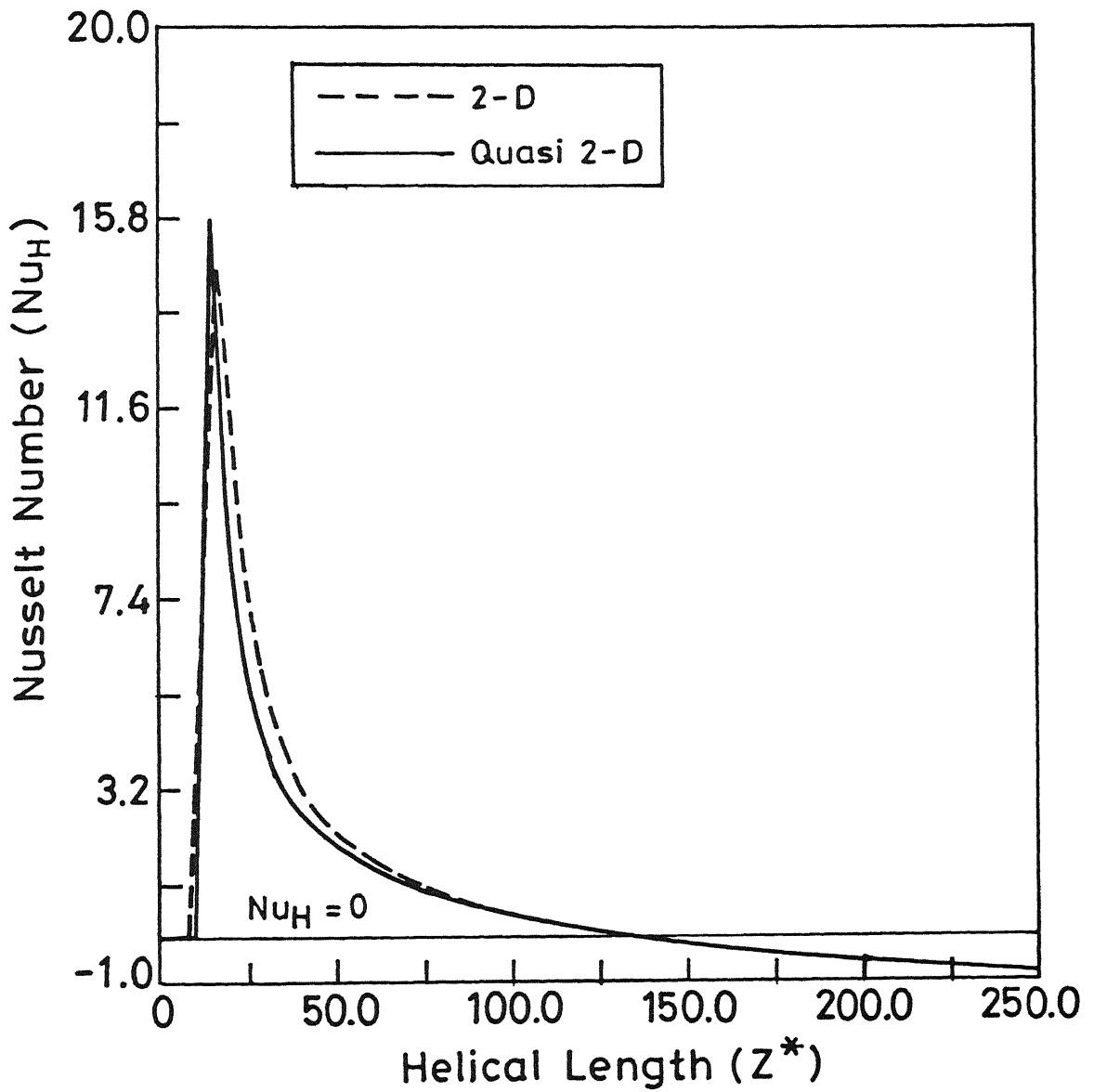
Fig. 4.12 Variations of Nusselt number along the
helical length for the quasi two-dimensional
and fully two-dimensional models.

two-dimensional model respectively The local bulk temperature T_{bulk} and the Nusselt number Nu_H at the barrel are defined as follows

$$T_{bulk} = \left[\int_{H_d}^{H_d+H} w\, T_f\, dy \middle/ \int_{H_d}^{H_d+H} w\, dy \right] \qquad (4\ 1)$$

$$\theta_{bulk} = \frac{1}{q_v} \int_{H_d/H}^{1+H_d/H} w^*\, \theta_f\, dy^* \qquad (4\ 2)$$

$$Nu_H = \frac{q_{in} H}{K_f(T_{b(ref)} - T_i)} \qquad (4\ 3)$$

where,

$$q_{in} = K_f \left. \frac{\partial T_f}{\partial y} \right|_b \qquad (4\ 4)$$

is the heat input flux at the barrel.

As expected, Fig.4.11 shows the bulk temperature in the fully two-dimensional model is slightly higher than that in the quasi two-dimensional model. In both the cases, bulk temperature exceeds barrel temperature near the outlet. Fig.4.12 shows higher Nusselt number near the inlet corresponding to the fully two-dimensional model As seen from Fig.4.12, the Nusselt number Nu_H is very high near the inlet location where a steep change in the barrel temperature occurs. With increasing downstream distance z^*, the value of heat flux q_{in}, and hence the value of Nu_H, drops rapidly. The heat loss by the barrel is convected downstream by the flow. Therefore a smaller amount of heat needs to supplied to the barrel

downstream in order to maintain it at a constant temperature If the heat generation due to viscous dissipation is substantial, so that fluid temperature rises above the barrel temperature, then the heat must be removed from the barrel in order to maintain it at a fixed value This is indicated by the negative Nusselt numbers near the outlet

4.4 THE CONCLUSIONS FROM THE STUDY OF THE TWO MODELS

The three most important achievements of the study of the quasi two-dimensional and the fully two-dimensional models are

(i) Development of an efficient and novel numerical technique for computing pressure gradients accurately for the fully two-dimensional model

(ii) Showing that the flow becomes 'locally' fully developed at a short distance from the inlet, - thus confirming the earlier use of fully developed velocity profile in the quasi two-dimensional model as the inlet boundary condition to be not physically unrealistic

(iii) Showing that axial diffusion has a very little effect on the fluid velocities and some but not significant effect on temperature and pressure

However, the limitations of the models that should be kept in mind are :

(i) Fully two-dimensional model is much too computer-time intensive

(ii) Both the models fail to predict realistically the screw surface temperature

(iii) None of the two models shows completely realistic pressure distribution along the downchannel direction

4.5 NEED FOR A THREE-DIMENSIONAL MODEL

As is evident from the discussions in this chapter, the main limitation of both the models presented so far is that they do not include the thermal convections normal to the screw flights as well as to the channel base and therefore fail to predict realistically the screw surface temperature distribution which should be close to or slightly greater than the barrel temperature in most part of the metering section. It is obvious that the aforementioned cross-convection terms can only be included in a three dimensional model. From the previous experience of the author with the fully two-dimensional model, it is possible to anticipate extremely large computer execution time and very complex solution procedure for a fully three-dimensional model. A quasi three-dimensional model on the other hand would be expected to give more or less similar results as those based on fully three-dimensional model but with much less computational effort. Therefore, in this study, a quasi three-dimensional model has been

proposed The readers are referred to the subsequent Chapters for a detailed discussion on the quasi three-dimensional model and a parametric study based on the same

CHAPTER 5

QUASI THREE-DIMENSIONAL MODEL

CHAPTER 5

5.1 PHYSICAL DESCRIPTION OF THE MODEL

Now that the need for a quasi three-dimensional model is established, the present discussion is directed towards the physical aspects of the said model Subsequent sections of this Chapter deal with the numerical modelling and the solution procedure.

The primary difference between a quasi two-dimensional model and a quasi three-dimensional model is the inclusion in the latter of the cross convection terms i e , thermal convections normal to the screw flights as well as to the base of the screw channel. Obviously, in contrast with the quasi two-dimensional model, the channel width is finite in this case Also, thermal conduction in the x- and y-directions are considered Furthermore, unlike in two-dimewnsional analyses which neglect y-momentum following hydrodynamic bearing lubrication approximation, in the quasi three-dimensional model y-momentum is taken into account as transverse convection normal to the channel base arising out of the v-velocity is to be accounted for Similar to the quasi two-dimensional analysis, the flow is assumed to be

hydrodynamically developed but thermally undeveloped That is, the flow is fully developed and the temperature of the melt is uniform at the entrance of the metering section in the x-y plane The solution is obtained at the next x-y plane and so on Thus the solution advances in the z-direction by a suitable marching procedure

Both the x-boundaries are assumed to be insulated considering that a negligible amount of heat is conducted between the melt and the uncooled screw (Fenner, 1977) Also, two-dimensional conduction is assumed to be present in the x-y plane of the screw body with both the boundaries in the x-direction acting as insulated considering that the screw body is sufficiently thick in that direction

As before, conjugate heat transfer at the fluid-screw interface is modelled by assuming the screw body (being much thicker compared to channel height) behaving like a semi-infinite solid with heat transfer taking place in a very thin layer below the screw surface and the rest of the screw remaining adiabatic As in earlier two models, the non-dimensional channel length is taken as 250

5.2 Governing Equations and the Boundary Conditions

The governing dimensional equations are as follows:

CONTINUITY :

$$\frac{\partial u}{\partial x} + \frac{\partial v}{\partial y} = 0 \qquad (5\ 1)$$

X-MOMENTUM :

$$\frac{\partial p}{\partial x} = 2 \frac{\partial}{\partial x}\left(\mu\frac{\partial u}{\partial x} \right) + \frac{\partial}{\partial y}\left[\mu\left(\frac{\partial u}{\partial y} + \frac{\partial v}{\partial x} \right) \right] \qquad (5\ 2a)$$

Y-MOMENTUM :

$$\frac{\partial p}{\partial y} = 2 \frac{\partial}{\partial y}\left(\mu\frac{\partial v}{\partial y} \right) + \frac{\partial}{\partial x}\left[\mu\left(\frac{\partial u}{\partial y} + \frac{\partial v}{\partial x} \right) \right] \qquad (5.2b)$$

Z-MOMENTUM :

$$\frac{\partial p_{av}}{\partial z} = \frac{\partial}{\partial x}\left(\mu\frac{\partial w}{\partial x} \right) + \frac{\partial}{\partial y}\left(\mu\frac{\partial w}{\partial y} \right) \qquad (5.2c)$$

Energy equations of the fluid and the screw may be written as follows :

FLUID :

$$\rho\ C_p\left\{ u\frac{\partial T}{\partial x} + v\frac{\partial T}{\partial y} + w\frac{\partial T}{\partial z} \right\} = \frac{\partial}{\partial x}\left(K\frac{\partial T}{\partial x} \right) + \frac{\partial}{\partial y}\left(K\frac{\partial T}{\partial y} \right) + \mu\ \phi$$

$$(5.3)$$

where ϕ is the viscous dissipation term given by

$$\phi = 2\left[\left(\frac{\partial u}{\partial x} \right)^2 + \left(\frac{\partial v}{\partial y} \right)^2 \right] + \left(\frac{\partial v}{\partial x} + \frac{\partial u}{\partial y} \right)^2 + \left(\frac{\partial w}{\partial y} \right)^2 + \left(\frac{\partial w}{\partial x} \right)^2 \qquad (5.3a)$$

SCREW :

$$\frac{\partial^2 T}{\partial x^2} + \frac{\partial^2 T}{\partial y^2} = 0 \qquad (5\ 4)$$

The boundary conditions as shown in Fig.5 1 are

at z = 0,

$$u = u_{dev}, \ v = v_{dev}, \ w = w_{dev},$$

$$T_f = T_s = T_i \qquad (5.5a)$$

at y=0,

$$\left.\frac{\partial T}{\partial y}\right|_s = 0 \qquad (5.5b)$$

at y = H_d (i e , at the interface),

$$u = 0, \ v = 0, \ w = 0,$$

$$T_f = T_s, \ K_f \left.\frac{\partial T}{\partial y}\right|_f = K_s \left.\frac{\partial T}{\partial y}\right|_s \qquad (5\ 5c)$$

at y=H_d + H,

$$u = V_{bx}, \ v = 0, \ w = V_{bz}, \ T_f = T_b \qquad (5.5d)$$

Fig. 5.1 Boundary conditions for the quasi three-dimensional model.

at $x = 0$, and W

$$u = 0, \quad v = 0, \quad w = 0,$$

$$\frac{\partial T}{\partial x} = 0 \quad (\text{ adiabatic condition }) \tag{5 5e}$$

The constraint on the flow in the downstream direction.

$$\int_0^W \int_{H_d}^{H_d+H} w \, dy \, dx = Q \tag{5 6}$$

5.2.1 THE UNCOUPLING OF LONGITUDINAL AND LATERAL PRESSURE GRADIENTS (PATNKAR AND SPALDING, 1972, RAITHBY AND SCHNEIDER, 1979)

A point to note is that the symbol p_{av} used for the pressure in the z-momentum Eq.(5.1c) is different from the symbol p in the momentum equations in x- and y-directions This is a reminder of the fact that in our calculation procedure, an inconsistency is deliberately introduced into the treatment of pressure and that the quantities p_{av} and p are calculated separately. The pressure p_{av} can be thought of as a form of space-averaged pressure over the cross-sectional plane. The gradient $\partial p_{av}/\partial z$ is calculated after the lateral pressure gradients are obtained.

5.3 Non-dimensionalisation

The governing equations are non-dimensionalised in terms of the following dimensionless variables,

$$x^* = x/H, \quad y^* = y/H, \quad z^* = z/H \tag{5 7a}$$

$$u^* = u \, / \, V_{bz}, \quad v^* = v \, / \, V_{bz}, \quad w^* = w \, / \, V_{bz} \tag{5 7b}$$

$$\theta = \frac{T - T_i}{T_{b(ref)} - T_i} \tag{5.7c}$$

$$p^* = \frac{p}{\bar{p}} \,, \quad \bar{p} = \bar{\mu} \, \frac{V_{bz}}{H} \tag{5 7d}$$

$$\dot{\gamma}^* = \frac{\dot{\gamma} \, H}{V_{bz}}, \quad \bar{\mu} = \mu_0 \left[\frac{V_{bz} \, / \, H}{\dot{\gamma}_0} \right] e^{-b\left(T_i - T_0 \right)} \tag{5.7e}$$

$$\beta = b \left(T_{b(ref)} - T_i \right) \tag{5.7f}$$

$$Pe = \frac{\rho \, C_p V_{bz} \, H}{K_f} \tag{5.7g}$$

$$G = \frac{\bar{\mu} \, V_{bz}^{\,2}}{K_f (T_{b(ref)} - T_i)} \tag{5.7h}$$

The dimensionless equations thus obtained are

MELT :

CONTINUITY :

$$\frac{\partial u^*}{\partial x^*} + \frac{\partial v^*}{\partial y^*} = 0 \tag{5.8}$$

X-MOMENTUM :

$$\frac{\partial p^*}{\partial x^*} = 2 \frac{\partial}{\partial x^*} \left[\left(\dot{\gamma}^* \right)^{n-1} e^{-\beta \theta} f \frac{\partial u^*}{\partial x} \right] +$$

$$\frac{\partial}{\partial y^*} \left[\left(\dot{\gamma}^* \right)^{n-1} e^{-\beta \theta} f \left(\frac{\partial u^*}{\partial y^*} + \frac{\partial v^*}{\partial x^*} \right) \right] \tag{5 9a}$$

Y-MOMENTUM :

$$\frac{\partial p^*}{\partial y^*} = 2 \frac{\partial}{\partial y^*} \left[\left(\dot{\gamma}^* \right)^{n-1} e^{-\beta \theta} f \frac{\partial v^*}{\partial y^*} \right] +$$

$$\frac{\partial}{\partial x^*} \left[\left(\dot{\gamma}^* \right)^{n-1} e^{-\beta \theta} f \left(\frac{\partial u^*}{\partial y^*} + \frac{\partial v^*}{\partial x^*} \right) \right] \tag{5.9b}$$

Z-MOMENTUM :

$$\frac{\partial p^*_{av}}{\partial z^*} = \frac{\partial}{\partial x^*} \left[\left(\dot{\gamma}^* \right)^{n-1} e^{-\beta \theta} f \frac{\partial w^*}{\partial x^*} \right] + \frac{\partial}{\partial y^*} \left[\left(\dot{\gamma}^* \right)^{n-1} e^{-\beta \theta} f \frac{\partial w^*}{\partial y^*} \right]$$

$$\tag{5.9c}$$

ENERGY :

FLUID :

$$Pe \left(u^* \frac{\partial \theta_f}{\partial x^*} + v^* \frac{\partial \theta_f}{\partial y^*} + w^* \frac{\partial \theta_f}{\partial z^*} \right) =$$

$$\frac{\partial^2 \theta_f}{\partial x^{*2}} + \frac{\partial^2 \theta_f}{\partial y^{*2}} + G \dot{\gamma}^{*n+1} e^{-\beta \theta_f} \qquad (5\ 10)$$

SCREW :

$$\frac{\partial^2 \theta_s}{\partial x^{*2}} + \frac{\partial^2 \theta_s}{\partial y^{*2}} = 0 \qquad (5\ 11)$$

The boundary conditions are also obtained in the non-dimensional form as:

at $z^* = 0$,

$$u^* = u^*_{dev}, \ v^* = v^*_{dev}, \ w^* = w^*_{dev} \ , \ \theta_f = \theta_s = 0 \qquad (5.12a)$$

at $y^* = 0$,

$$\frac{\partial \theta_s}{\partial y^*} = 0 \qquad (5.12b)$$

at $y^* = H_d/H$ (i e , at the interface),

$$u^* = 0, \ v^* = 0, \ w^* = 0,$$

$$\frac{\partial \theta_f}{\partial y^*} = \frac{K_s}{K_f} \frac{\partial \theta_s}{\partial y^*}, \ \theta_s = \theta_f \qquad (5\ 12c)$$

at $y^* = 1 + H_d/H$ (at the barrel surface),

$$u^* = V_{bx}/V_{bz} = \frac{V_b \sin\phi}{V_b \cos\phi} = \tan\phi, \ v^* = 0, \ w^* = 1, \ \theta_f = 1 \qquad (5\ 12d)$$

at $x^* = 0$, and W/H,

$$u^* = 0, \ v^* = 0, \ w^* = 0,$$

$$\frac{\partial \theta_f}{\partial x^*} = \frac{\partial \theta_s}{\partial x^*} = 0 \ (\text{ adiabatic condition }) \qquad (5\ 12e)$$

The constraint on the flow in the downstream direction in the dimensionless form are,

$$\int_0^{W/H} \int_{H_d/H}^{1+H_d/H} w^* \ dx^* \ dy^* = \frac{Q}{H \ W \ V_{bz}} = q_v \qquad (5.13)$$

5.4 METHOD OF SOLUTION

As mentioned earlier in section 5 2, when the pressure field is split in the manner indicated by Eq. (5 8)-(5.9c), two distinct

velocity-pressure couplings result In the first of these, associated with the in-plane velocity and pressure distributions, it is required to determine what distribution of p* should be used in Eq.(5.9a) and (5 9b) such that the resulting u* and v* velocities satisfies the equation of conservation of mass, Eq (5 8). For the second coupling, associated with the velocity distribution and pressure gradient in the parabolic direction, it is required to determine the value of $\partial p^*_{av}/\partial z^*$ that should be used in Eq (5 9c), together with the boundary conditions, such that the resulting velocity distributions yields the correct dimensionless volumetric flow rate q_v as specified in Eq (5.13) in the z-direction The methods of handling these two couplings are presented in susequent sections of this chapter

5.4.1 DOMAIN DISCRETIZATION

The computational domain in the x-y plane is discretized to obtain the finite difference equation The pressure term does not appear explicitly in the momentum equations Instead, the pressure gradient is present and through satisfying the continuity equation, pressure is calculated. If the velocity components and pressure are at the same location and interpolated linearly for evaluation at the control volume faces, the resulting discretized equations may result in a physically unrealistic solution (Patankar, 1980). So to avoid such possibility, different grids are chosen for velocity components and pressure and they are suitably staggered with respect to each other. The locations where

the pressure and other dependent variables (temperature and w-velocity) are calculated, are designated as main grid points In practice, for computational domain discretization, the main control volume boundaries are first drawn in an arbritarily non-uniform manner and the main grid points are then placed at their geometric centres In this practice, the main control volume faces are not located midway between adjacent grid points, which represents less accurate finite difference representation of the derivatives In spite of this, the above practice is adopted here due to the following desirable features

(a) The grid point at the geometric centre of the control volume represents the control volume better than any other point,

(b) half control volume does not occur adjacent to a boundary,

(c) discontinuities in thermophysical properties, boundary conditions and the source terms are easier to handle.

The grid points corresponding to the velocity components are displaced with respect to the main grid points in such a way that they are located on the faces of the main control volume. The u-control volumes are staggered horizontally backwards (i e. in the x-direction) with respect to the main control volume, while the v-control volumes are staggered vertically downwards (i.e., in the y-direction). This staggering is done in such a way that the

displaced faces pass through the main grid points, while non-displaced faces lie along the main control volume faces Hence the resultant shape of the control volume used to compute velocity components and other dependent variables becomes inverted L shape as shown in Fig 5 2 In this figure, the main grid points are denoted by dots identified by letters P, W, E, S, N, SW, SE, NW, NE whereas u-velocity locations are denoted by arrows ($\rightarrow$) identified by P', W', E', S', N', $S'W'$, $S'E'$, $N'W'$ and $N'E'$ and v-velocity locations are denoted by arrows ($\uparrow$) identified by P'', W'', E'', S'', N'', $S''W''$, $S''E''$, $N''W''$ and $N''E''$ The u and v locations are referred to as staggered points. In the same Fig 5 2, the main control volume, u-control volume and v-control volume are respectively identified by inclined, vertical and horizontal hatch lines. The type of control volume used for velocities near the boundaries is different as shown in Fig.5 3. A complete picture of the discretized computational domain used is shown in Fig.5.4 in which NI and NJ are the total number of main grid points used for discretizing the computational domain, respectively, in the x- and y-directions In this figure, boundaries of the main control volume are shown as dashed lines The various geometrical quantities needed for discretizing the governing equations are also shown in Fig.5 2, 5.3 and 5 6 in FORTRAN variables. Attention will now be focussed on deriving the discretized form of Eqs (5.8-5.11)
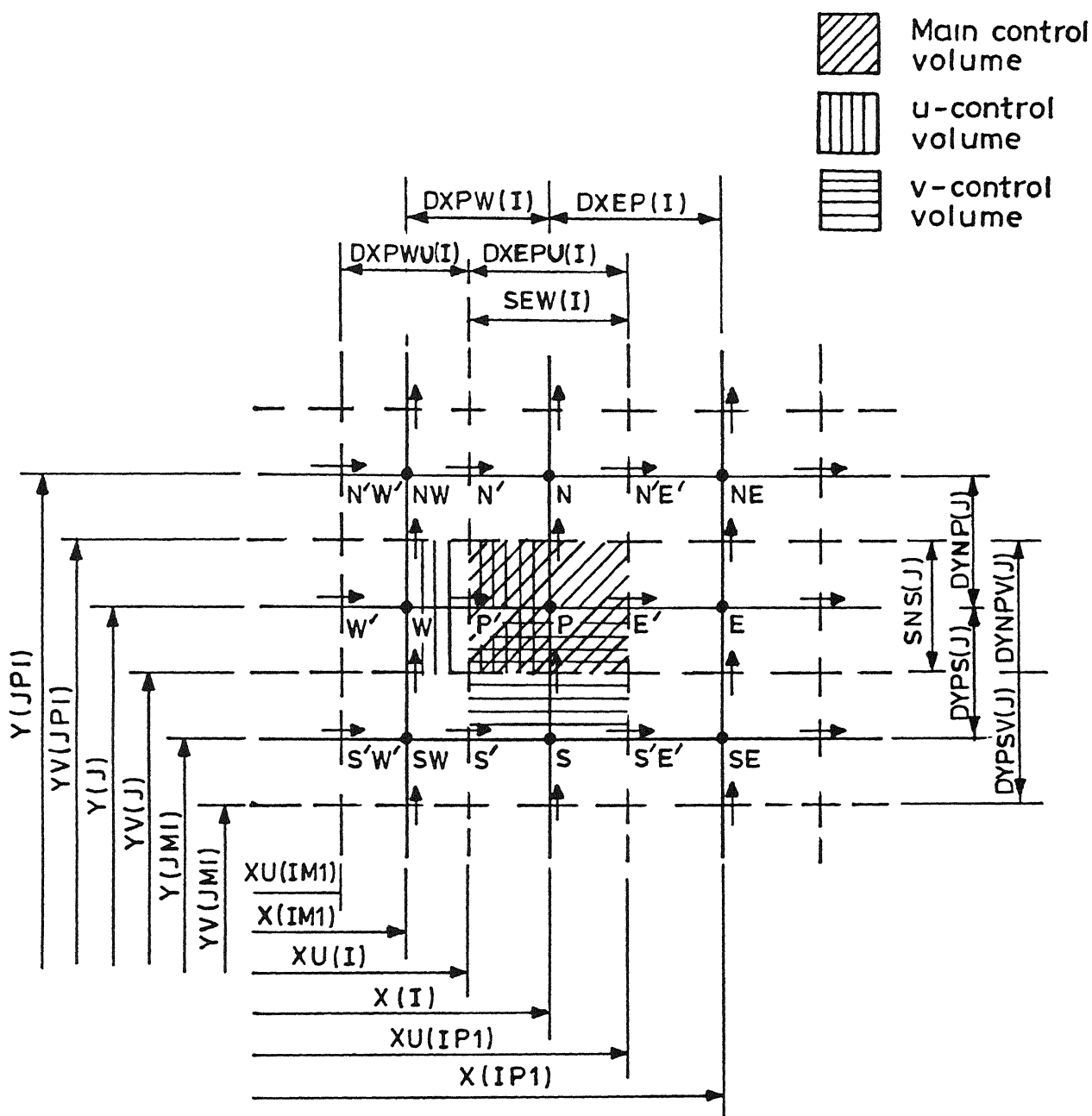
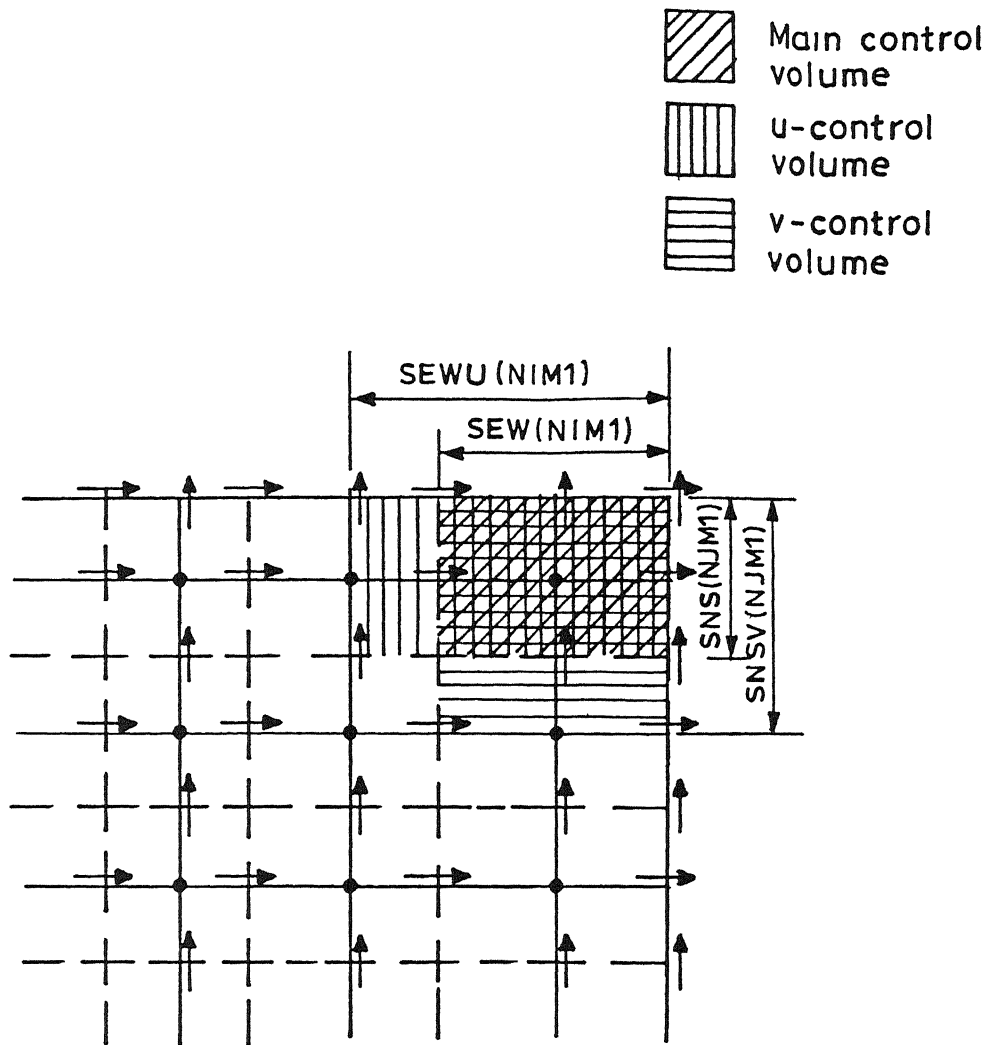Fig. 5.2 Type of the control volume used.
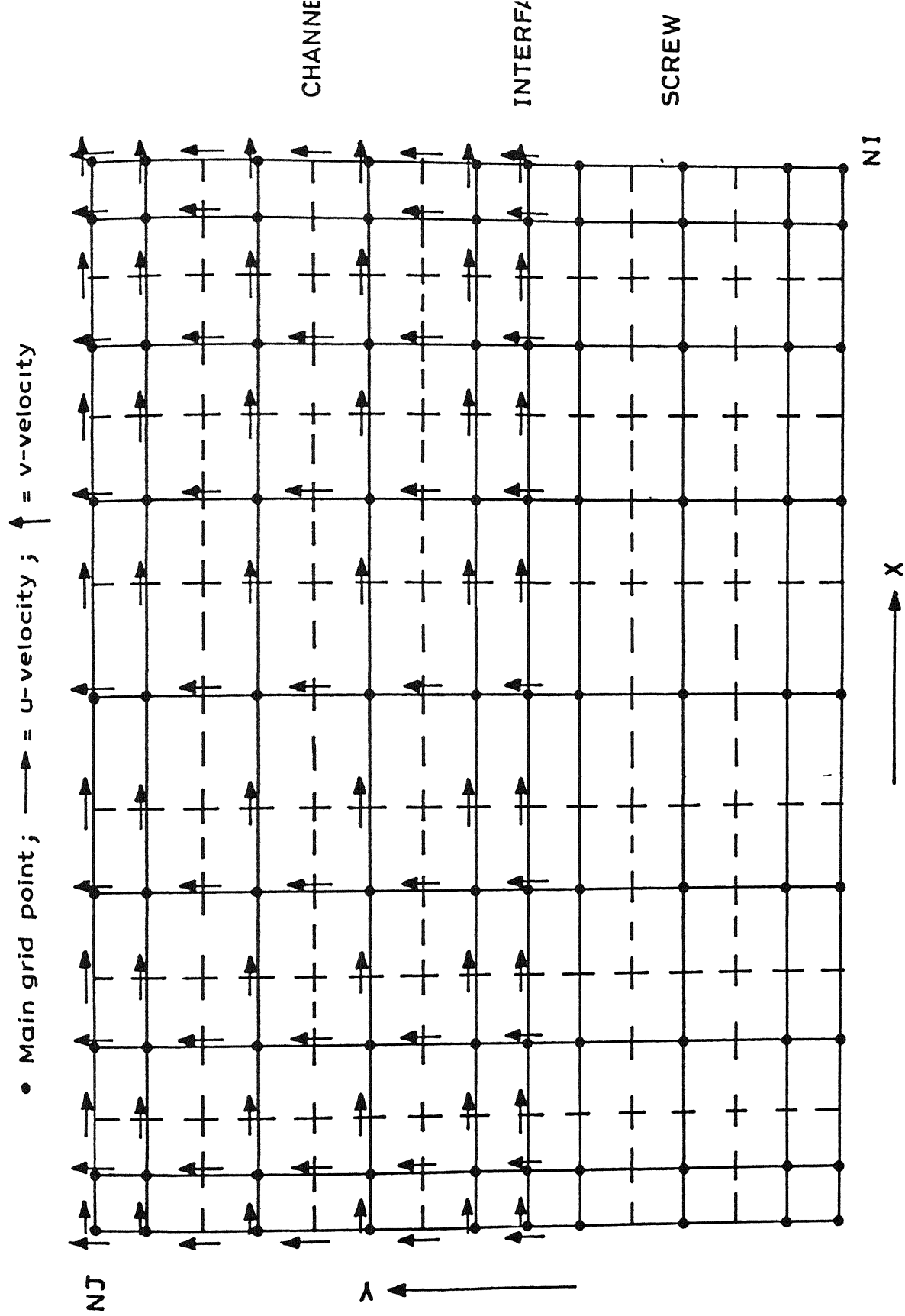
Fig 5.3 Type of the control volume at the boundary.

Fig. 5.4(a) Complete picture of the discretized computational domain.
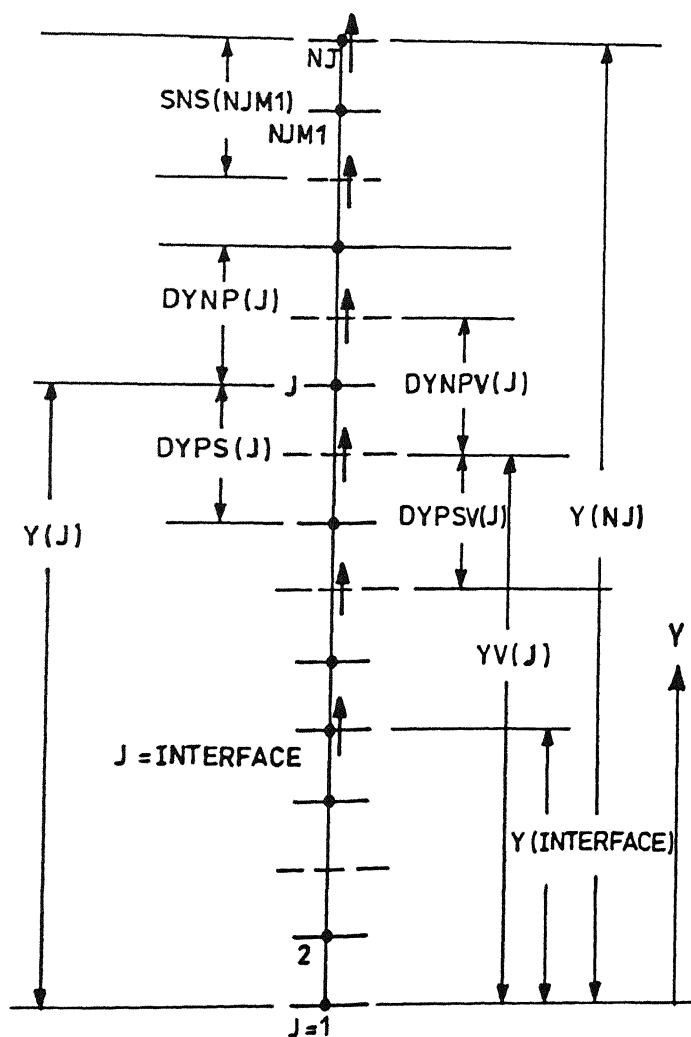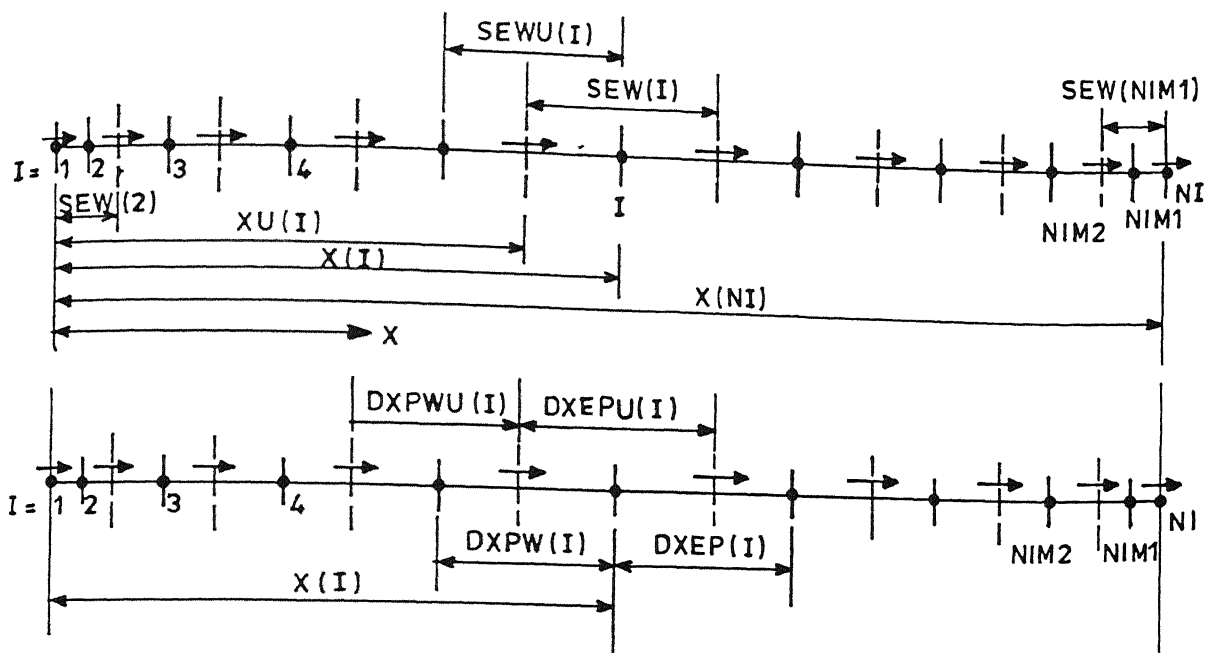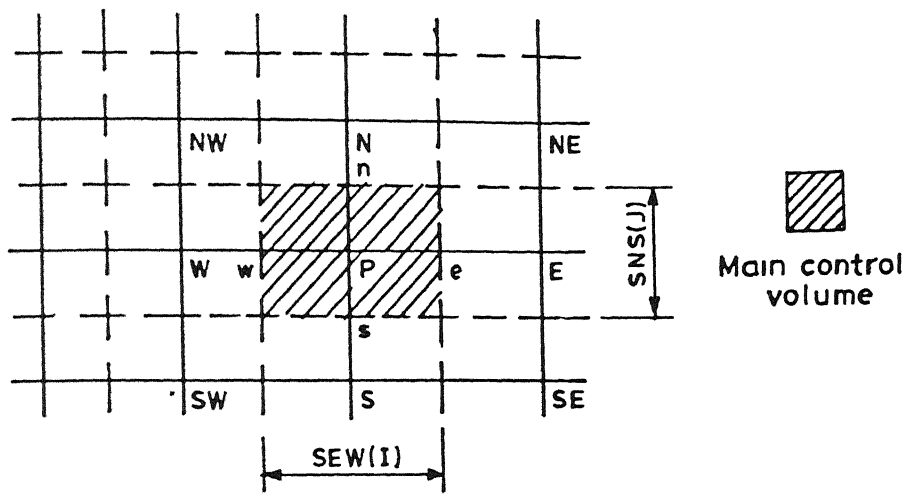
Fig 5.4(b) Various grid quantities.
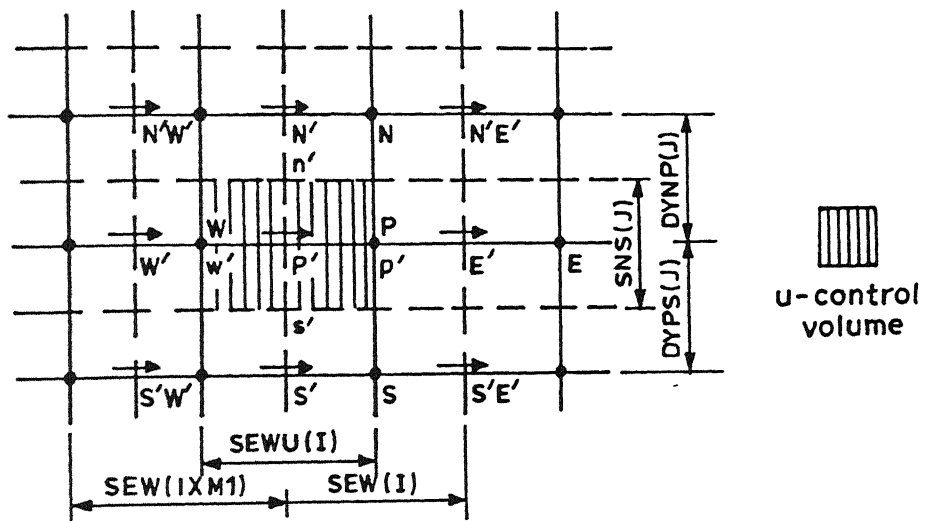
Fig. 5.5 Main control volume.

Fig. 5.6 u-control volume.
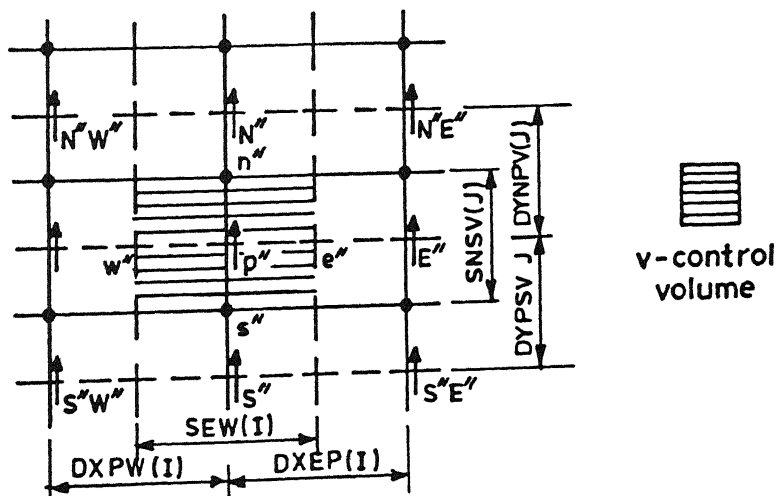
Fig. 5.7 v-control volume

5.5 The finite difference equations

The differential Eqs.(5 8)-(5 11) are integrated over the respective control volume to obtain the following finite difference forms. For the sake of simplicity, the superscripts (*) have been dropped

5.5.1 X-momentum

The x-momentum equation may be rewritten from Eq (5 8a):

$$\frac{\partial p}{\partial x} = 2 \frac{\partial}{\partial x} \left(\dot{\gamma}^{n-1} e^{-\beta\theta} f \frac{\partial u}{\partial x} \right) + \frac{\partial}{\partial y} \left\{ \dot{\gamma}^{n-1} e^{-\beta\theta} f \left(\frac{\partial u}{\partial y} + \frac{\partial v}{\partial x} \right) \right\}$$

(5 14)

$$\text{and let } A = \dot{\gamma}^{n-1} e^{-\beta\theta} f$$

(5 14a)

The Eq.(5.14) is integrated over the u-control volume shown in Fig.5 6,

$$\int_{s'}^{n'} \int_{w'}^{p'} \frac{\partial p}{\partial x} \, dx \, dy = 2 \int_{s'}^{n'} \int_{w'}^{p'} \frac{\partial}{\partial x} \left(A \frac{\partial u}{\partial x} \right) \, dx \, dy +$$

$$\int_{s'}^{n'} \int_{w'}^{p'} \frac{\partial}{\partial y} \left\{ A \left(\frac{\partial u}{\partial y} + \frac{\partial v}{\partial x} \right) \right\} \, dx \, dy$$

(5.15)

This may be rewritten as,

$$(p_p - p_w)\,SNS(J) = 2\,0\,\left\{ \left(A\frac{\partial u}{\partial x} \right)_{p'} - \left(A\frac{\partial u}{\partial x} \right)_{w'} \right\} SNS(J)$$

$$+ \left\{ \left(A\frac{\partial u}{\partial y} \right)_{n'} - \left(A\frac{\partial u}{\partial y} \right)_{s'} \right\} SEWU(I) +$$

$$\left\{ \left(A\frac{\partial v}{\partial x} \right)_{n'} - \left(A\frac{\partial v}{\partial x} \right)_{s'} \right\} SEWU(I) \quad (5\ 16)$$

The Eq.(5 16) is further discretized to obtain the final discretized equation,

$$a_{P'}u_{P'} = a_{E'}u_{E'} + a_{W'}u_{W'} + a_{N'}u_{N'} + a_{S'}u_{S'} + S_u + (p_W - p_P)\,SNS(J)$$

$$(5.17)$$

where,

$$a_{E'} = \frac{2\ SNS(J)}{SEW(I)}\ A_{uP'} \tag{5 17a}$$

$$a_{W'} = \frac{2\ SNS(J)}{SEW(IXM1)}\ A_{uP'} \tag{5 17b}$$

$$a_{N'} = \frac{2\ SEWU(I)}{DYNP(J)}\ A_{uP'} \tag{5 17c}$$

$$a_{S'} = \frac{2\ SEWU(I)}{DYPS(J)}\ A_{uP'} \tag{5 17d}$$

$$a_{P'} = a_{E'} + a_{W'} + a_{N'} + a_{S'} \tag{5.17e}$$

$$S_u = A_{uP'}\left[\left\{ v(I,J+1) - v(I-1,J+1) \right\} - \left\{ v(I,J+1) - v(I-1,J+1) \right\} \right]$$

$$(5.17f)$$

$$S_{c'} = S_u + (p_W - p_P)\ SNS(J) \qquad (5\ 17g)$$

$A_{uP'}$ is the non-dimensional viscosity term This term is assumed as constant over the control volume domain and calculated where the variable is located. This helps in linearising the non-linear terms in the finite difference equation

5.5.2 Y-MOMENTUM

The y-momentum equation may be rewritten from Eq (5.8b)

$$\frac{\partial p}{\partial y} = 2 \frac{\partial}{\partial y}\left(\dot{\gamma}^{\,n-1} e^{-\beta\theta}f\ \frac{\partial v}{\partial y}\right) + \frac{\partial}{\partial x}\left\{\dot{\gamma}^{\,n-1} e^{-\beta\theta}f\left(\frac{\partial u}{\partial y}+\frac{\partial v}{\partial x}\right)\right\}$$

$$(5.18)$$

$$\text{and let } A = \dot{\gamma}^{\,n-1} e^{-\beta\theta}f \qquad (5\ 18a)$$

The Eq (5.18) is integrated over the v-control volume shown in Fig 5.7,

$$\int_{s'}^{n'}\int_{w'}^{p'}\frac{\partial p}{\partial y}\ dx\ dy = 2\int_{s'}^{n'}\int_{w'}^{p'}\frac{\partial}{\partial y}\left(A\frac{\partial v}{\partial y}\right)dx\ dy +$$

$$\int_{s'}^{n'}\int_{w'}^{p'}\frac{\partial}{\partial x}\left\{A\left(\frac{\partial u}{\partial y}+\frac{\partial v}{\partial x}\right)\right\}dx\ dy \qquad (5\ 19)$$

This may be rewritten as,

$$(p_p - p_s) \, SEW(I) = 2 \, 0 \left\{ \left(A \frac{\partial v}{\partial y} \right)_{n''} - \left(A \frac{\partial v}{\partial y} \right)_{s''} \right\} SEW(I)$$

$$+ \left\{ \left(A \frac{\partial u}{\partial y} \right)_{p''} - \left(A \frac{\partial u}{\partial y} \right)_{w''} \right\} SNSV(J) +$$

$$\left\{ \left(A \frac{\partial v}{\partial x} \right)_{p''} - \left(A \frac{\partial v}{\partial x} \right)_{w''} \right\} SNSV(J) \qquad (5 \ 20)$$

The Eq (5.20) is further discretized to obtain the final discretized equation,

$$a_{P''} v_{P''} = a_{E''} v_{E''} + a_{W''} v_{W''} + a_{N''} v_{N''}$$
$$+ a_{S''} u_{S''} + S_v + (p_S - p_P) \, SEW(I) \qquad (5 \ 21)$$

where,

$$a_{E''} = \frac{SNSV(J)}{DXEP(I)} A_{vP''} \qquad (5.21a)$$

$$a_{W''} = \frac{SNSV(J)}{DXEP(I)} A_{vP''} \qquad (5.21b)$$

$$a_{N''} = \frac{2 \, SEW(I)}{DYNPV(J)} A_{vP''} \qquad (5.21c)$$

$$a_{S''} = \frac{2 \, SEW(I)}{DYPSV(J)} A_{vP''} \qquad (5.21d)$$

$$a_{P''} = a_{E''} + a_{W''} + a_{N''} + a_{S''} \qquad (5.21e)$$

$$S_v = A_{vP''} \left[\left\{ u(I+1,J) - u(I+1,J-1) \right\} - \left\{ u(I,J) - u(I,J-1) \right\} \right]$$
$$(5.21f)$$

$$S_{c''} = S_v + (p_S - p_P) \, SEW(I) \qquad (5\ 21g)$$

$A_{vP''}$ is the non-dimensional viscosity term which is assumed as constant over the control volume domain   It is defined and calculated at the grid point of the v-velocity control volume   This helps in linearising the non-linear terms in the finite difference equation.

5.5.3 CONTINUITY EQUATION

The control volume of specific interest in this case is that which surrounds the main grid point P in Fig 5 5 (main control volume in Fig.5.2). The continuity Eq.(5 8) is integrated between surfaces e, w, and n, s. The integration is performed by regarding those values as constant over each face to obtain,

$$\int_s^n \int_w^e \frac{\partial u}{\partial x} \, dx \, dy + \int_s^n \int_w^e \frac{\partial v}{\partial y} \, dx \, dy = 0 \qquad (5.22)$$

which yeilds,

$$(\ u_{E'} - u_{P'}\ )\ SNS(J) + (\ v_{N''} - v_{S''}\ )\ SEW(I) = 0 \qquad (5.23)$$

Before deriving the pressure-correction equation at this stage, let us discuss the necessity of using under-relaxation factor for solving the finite difference Eqs.(5 17), (5.21), (5.23).

5.6 Under-relaxation

The generalized form of the Eq (5.17), Eq (5 21) for a control volume is given by,

$$(a_1 - S_1)\phi_1 = \sum a_{nb} \phi_{nb} + S_{\phi 1} \qquad (5\ 24)$$

where, ϕ stands for u, v, $S_{\phi 1}$ stands for $S_{c'}$ or $S_{c''}$, and 1 indicates for point P', P'' respectively, for the u-momentum, and v-momentum.

Eq. (5.24) appears to be linear. However, the co-efficients of Eq. (5.24) may themselves depend on one or more of the dependent variables represented by ϕ. To account for the resulting inter-equation linkages and non-linearities, repeated solutions of the nominally linear form of Eq (5 24) are required Each of these iterative solutions is defined herein as a 'cycle' At the beginning of each cycle, the co-efficients are evaluated using the ϕ values obtained in the previous cycle. With the cycle by cycle change in co-efficients of Eq (5.24), the resulting changes in the ϕ values can be quite large, and this may cause slow convergence or even divergence. To moderate the changes in successive solutions for ϕ, and thereby improve convergence, under-relaxation is used.

Patankar (1980) introduces under-relaxation into Eq. (5.24)

through α_R as follows,

$$\frac{a_1 - S_1}{\alpha_R}\phi_1 = \sum a_{nb}\phi_{nb} + S_{\phi_1} + \frac{1 - \alpha_R}{\alpha_R}\left(a_1 - S_1\right)\phi_1^0 \qquad (5\ 25)$$

where, ϕ_1^0 is the value of ϕ_1 from the previous cycle, whereas VanDoormal and Raithby (1984) introduce under-relaxation through the use of an E-factor according to the following revised form of Eq.(5.25),

$$(a_1 - S_1)(1 + \frac{1}{E})\phi_1 = \sum a_{nb}\phi_{nb} + S_{\phi_1} + \frac{1}{E}(a_1 - S_1)\phi_1^0$$
$$(5\ 26)$$

$$\text{or, } D_1\phi_1 = \sum a_{nb}\phi_{nb} + S_{\phi_1} + \frac{1}{E}(a_1 - S_1)\phi_1^0 \qquad (5\ 27)$$

$$\text{where, } D_1 = (a_1 - S_1)(1 + \frac{1}{E}) \qquad (5.27a)$$

From Eq (5 25) and (5 26), we may write,

$$\alpha_R = \frac{E}{1 + E} \qquad (5.28)$$

Under-relaxation through the use of E-factors has better physical meaning than that using α_R, as discussed by VanDoormal and Raithby (1984). In order to accelerate convergence, values of E well in excess of unity are desirable In fact values in the range of 1 to 20 were found to be useful for the present problems

5.7 DERIVATION OF THE PRESSURE CORRECTION EQUATION

SIMPLEC procedure (VanDoormal and Raithby, 1984) has been used for handling the velocity-pressure linkages In this method pressure field is first guessed With this guessed pressure field, coefficients of the momentum equations can be evaluated allowing these equations to be solved to obtain the flow field. In general this flow field does not satisfy the continuity Eq (5.23) Therefore this guessed pressure field is corrected so that the resulting velocity field satisfies the continuity Eq (5.23) This is accomplised by the pressure correction equation which is derived in accordance with VanDoormal and Raithby (1984) by combining the continuity equation with truncated forms of the momentum equatin. After solving the pressure correction equation following the recommendation given in VanDoormal and Raithby (1984), the velocity and pressure fields are corrected, and the procedure is repeated until the flow field satisfies both the continuity and momentum equations Details of the above outline follow.

Let us say that for the guessed pressure distribution p*, the u* and v* velocity distribution obtained [1], by solving the u-momentum and v-momentum equations respectively, satisfies

---

[1]These asterix are different from the non-dimensional asterix. All the calculation are carried out with the non-dimensional values.

$$D_{P'} u_{P'}^* = \sum a_{nb} u_{nb}^* + S_u + A_{uP'}(p_W^* - p_P^*) + \frac{1}{E} a_{P'} u_{P'}^0 \qquad (5.29)$$

$$D_{P''} v_{P''}^* = \sum a_{nb} v_{nb}^* + S_v + A_{vP''}(p_S^* - p_P^*) + \frac{1}{E} a_{P''} v_{P''}^0 \qquad (5.30)$$

While the u- and v-velocities obtained from Eq (5.25) using the correct (but unknown) pressure distribution p satisfy the continuity equation, the u^* and v^* velocities obtained from Eq.(5.29) and (5.30) do not in general satisfy the continuity equation Correction of the guessed pressure by $p' = p - p^*$ is therefore necessary to correct the u^* field by $u' = u - u^*$ and v-field by $v' = v - v^*$ The relation between p' and u' is obtained by subtracting Eq (5.29) from Eq (5.24) which yields to,

$$D_{P'} u_{P'}' = \sum a_{nb} u_{nb}' + A_{uP'}(p_W' - p_P') \qquad (5.31)$$

The pressure p and velocity u that satisfy both the continuity and the momentum equations are,

$$u = u^* + u' \qquad (5.32)$$

$$p = p^* + p' \qquad (5.33)$$

Attention will now be given to that method to find p'. The exact equation for p' derived from Eq.(5.31) and (5.32) and the continuity eqution, is complicated and unsuitable for economic calculation. In the SIMPLE method (Patankar, 1980), the term $\sum a_{nb} u_{nb}'$ in Eq.(5.31) is ignored whereas a term of similar

magnitude on the left hand side is retained, leading to inconsistency of the method

For a 'consistent' approximation, leading to a suitable simple expression for p', the term $\sum a_{nb} u'_{nb}$ is subtracted from both the sides of Eq (5 31) This yields

$$\left(D_{P'} - \sum a_{nb} \right) u'_{P'} = \left(\sum a_{nb} u'_{nb} - \sum a_{nb} u'_{P'} \right) + A_{uP'} \left(p'_W - p'_P \right)$$

(5 34)

In this method, termed 'SIMPLEC' by VanDoormal and Raithby (1984), the term $\left(\sum a_{nb} u'_{nb} - \sum a_{nb} u'_{P} \right)$ is neglected With this approximation, Eq.(5 34) becomes,

$$(D_{P'} - \Sigma a_{nb}) u'_{P'} = A_{uP'} (p'_W - p'_P)$$

(5 35)

i.e.,

$$u'_{P'} = d_{P'} (p'_W - p'_P)$$

(5.36)

where,

$$d_{P'} = \frac{A_{uP'}}{D_{P'} - \Sigma a_{nb}}$$

(5.37)

Thus,

$$u_{P'} = u_{P'} + d_{P'} (p'_W - p'_P)$$

(5.38)

Eq (5 38) is an intermediate step to link velocity with pressure, and is called the velocity correction equation. A similar expression can be obtained for $u_{E'}$.

$$u_{E'} = u_{E'} + d_{E'}(p_P' - p_E')$$ (5.39)

where,

$$d_{E'} = \frac{A_{uE'}}{D_{E'} - \Sigma a_{nb}}$$ (5 40)

Now, in a manner similar to that used for deriving Eq.(5 38) and Eq (5 39), we have (using Eq (5 30)),

$$v_{P''} = v_{P''} + d_{P''}(p_S' - p_P')$$ (5 41)

$$v_{N''} = v_{N''} + d_{N''}(p_P' - p_N')$$ (5 42)

where,

$$d_{P''} = \frac{A_{vP''}}{D_{P''} - \Sigma a_{nb}}$$ (5 43)

$$d_{N''} = \frac{A_{vN''}}{D_{N''} - \Sigma a_{nb}}$$ (5 44)

Substituting Eqs.(5.38), (5 39), (5 41) and (5 42) in the continuity Eq (5.23), we have,

$$(u^{*}_{E'} - u^{*}_{P'})SNS(J) + (v^{*}_{N''} - v^{*}_{P''})SEW(I) +$$

$$(u'_{E} - u'_{P'})SNS(J) + (v'_{N''} - v'_{P''})SEW(I) = 0$$ (5.45)

This equation may be written as,

$$a_P p'_P = a_E p'_E + a_W p'_W + a_N p'_N + a_S p'_S + B \qquad (5\ 46)$$

where,

$$a_E = d_{E'}\ SNS(J) \qquad (5\ 47a)$$

$$a_W = d_{P'}\ SNS(J) \qquad (5\ 47b)$$

$$a_N = d_{N''}\ SEW(I) \qquad (5\ 47c)$$

$$a_S = d_{P''}\ SEW(I) \qquad (5\ 47d)$$

$$a_P = a_E + a_W + a_N + a_S \qquad (5\ 47e)$$

$$B = -[(u^*_{E'} - u^*_{P'})SNS(J) + (v^*_{N''} - v^*_{P''})SEW(I)] \qquad (5\ 47f)$$

where, $d_{P'}$, $d_{E'}$, $d_{N''}$, $d_{P''}$ are given by Eqs (5.37), (5 40), (5.43), (5.44) respectively

The direct solution on the line I in Fig.(5 4a) can be obtained with one application of the Thomas algorithm by suitably guessing the off line dependent values. Such a line by line solution is the basis of an iteration scheme that solves along each I-line and then along J-line, and repeats the pattern until convergence is acheived The rate of convergence of such a scheme depends crucially on the treatment of the off line values of the

dependent varible.

Let us suppose that in the current iteration, Eq(5 46) is to be solved along an I line, sweeping in the direction of increasing I According to Patankar's suggestion (1980), the avilable estimate of p_E' is from the previous iteratuin i e , $[p_E']^0$, but according to Vandoormal and Raithby (1984), the best estimate of p_E' is,

$$p_E' = [p_E']^0 + (\theta - 1)(p_E' - [p_E']^0) \qquad (5.48)$$

$$p_E' \approx [p_E']^0 + (\theta - 1)(p_P' - [p_P']^0) \qquad (5.49)$$

In the expression θ is a relaxation parameter such that for $\theta = 1$, p_E' is taken as $[p_E']^0$ This approximatation in Eq.(5.49) is therefore introduced into Eq (5.46) to obtain,

$$a_P p_P' = a_E p_E' + a_W p_W' + a_N p_N' + a_S p_S' + B \qquad (5\ 50)$$

or,
$$a_P p_P' = a_E [[p_E']^0 + (\theta - 1)(p_P' - [p_P']^0)] [p_E']^0$$

$$+ a_W p_W' + a_N p_N' + a_S p_S' + B \qquad (5.51)$$

A similar estimate is made for solutions along J-lines.

$$a_P w_P = a_E w_E + a_W w_W + a_N w_N + a_S w_S - D_W \frac{\partial p_{av}}{\partial z} \qquad (5\ 55)$$

where,

$$a_E = \frac{A_{wp}\ SNS(J)}{DXEP(I)} \qquad (5\ 55a)$$

$$a_W = \frac{A_{wp}\ SNS(J)}{DXPW(I)} \qquad (5\ 55b)$$

$$a_N = \frac{A_{wp}\ SEW(I)}{DYNP(J)} \qquad (5.55c)$$

$$a_S = \frac{A_{wp}\ SEW(I)}{DYPS(J)} \qquad (5\ 55d)$$

$$D_W = SEW(I)\ SNS(J) \qquad (5\ 55e)$$

The under-relaxation scheme as described in section 5.6 is used here to solve the Eq.(5 55). So the Eq (5 55) becomes with the under-relaxation method as described,

$$D_P w_P = \sum a_{nb} w_{nb} - D_W \frac{\partial p_{av}}{\partial z} + \frac{1}{E}\ a_P w_P^0 \qquad (5.56)$$

$$\text{where, } D_P = a_P \left(1 + \frac{1}{E}\right) \qquad (5.56a)$$

Initially $\frac{\partial p_{av}}{\partial z}$ is not known So, $\frac{\partial p_{av}}{\partial z}$ is guessed and subsequently it is corrected by the method described below.

5.8.2 PRESSURE-VELOCITY COUPLING IN THE PARABOLIC DIRECTION : THE LONGITUDINAL PRESSURE GRADIENT

The $\frac{\partial p_{av}}{\partial z}$ in the Eq (5 56) is regarded as uniform over a cross-section. $\frac{\partial p_{av}}{\partial z}$ is obtained from the integral mass-conservation equation in the following manner

At first we make an estimate of $\frac{\partial p_{av}}{\partial z}$ which is denoted by $\frac{\partial p_{av}^{*}}{\partial z}$. This enables us to compute w_P^{*} field from Eq.(5 56) The corresponding volume flow rate is

$$\dot{Q}^{*} = \sum_{\text{all } P} \Delta x \; \Delta y \; w_P^{*} \qquad (5 \; 57)$$

where, all P denotes all the w-control volume in Fig 5 5 For a correct value of $\frac{\partial p_{av}}{\partial z}$, the velocity field w_P will be found that yields the correct cross-sectional flow rate $\dot{Q}$:

$$\dot{Q} = \sum_{\text{all } P} \Delta x \; \Delta y \; w_P \qquad (5 \; 58)$$

According to Raithby and Schneider (1979), the proposals made by Patankar and Spalding (1972) for finding $\frac{\partial p_{av}}{\partial z}$ does not guarantee the satisfaction of both Eq.(5.56) and Eq.(5.58) at given z-locations. Though Briley's (1974) scheme does result in an exact solution that requires three solutions to Eq.(5.56), Raithby and Scheineder (1979) found that the alternative method proposed by them yields the 'exact' result with about one-third less computational effort than Briley's method.

Motivated by the linear relation[2] between w and $\frac{\partial p_{av}}{\partial z}$, for a fixed set of co-efficients, an equation for the rate of change of w with $\frac{\partial p_{av}}{\partial z}$ is sought. Defining,

$$R = - \frac{\partial p_{av}}{\partial z}, \ f_P = \frac{\partial v_p}{\partial R}, \tag{5 59}$$

if the f_P's were known, the correct velocities would be related to the w's by,

$$w_P = w_P^* + f_P \Delta R \tag{5 60}$$

where,

$$\Delta R = - \left[\left(\frac{\partial p_{av}}{\partial z} \right) - \left(\frac{\partial p_{av}^*}{\partial z} \right) \right] \tag{5 60a}$$

The ΔR value is chosen to make the total volume flow rate correct, i.e.,

$$\Delta R = \frac{\dot{Q} - \dot{Q}^*}{\sum_{all \ P} \Delta x \ \Delta y \ f_P} \tag{5 61}$$

This permits both w_P and $\frac{\partial p_{av}}{\partial z}$ to be found from Eq. (5.60). the equation for f_P is found by differentiating Eq (5.55) with respect

[2] As the co-efficients of the Eq. (5 56) are linearized using the previous iteration values of the velocities, Eq. (5.56) becomes linear between w and $\frac{\partial p_{av}}{\partial z}$.

to R to obtain,

$$A_P f_P = A_E f_E + A_W f_W + A_N f_N + A_S f_S + D_W \qquad (5\ 62)$$

The velocity boundary conditions have been used to obtain the w_P^* solutions so that, to maintain the same conditions on w_P, $f = 0$ is applied on boundaries where the velocity is specified

5.9 Discretization of Energy Equations of Fluid and Screw Body

5.9.1 Energy Equation of the Fluid

The non-dimensional energy equation of the fluid may be rewritten from Eq.(5 10) as,

$$Pe\left(u\frac{\partial\theta}{\partial x} + v\frac{\partial\theta}{\partial y} + w\frac{\partial\theta}{\partial z}\right) = \frac{\partial^2\theta}{\partial x^2} + \frac{\partial^2\theta}{\partial y^2} + G\ \dot{\gamma}^{n+1} e^{-\beta\theta} \qquad (5.63)$$

Using the continuity equation (Eq.(5 1) and $\partial w/\partial z=0$,for developed velocity profile) Eq (5 63) may be rewritten in the weak conservation form as,

$$Pe\left\{\frac{\partial(u\theta)}{\partial x} + \frac{\partial(v\theta)}{\partial y} + \frac{\partial(w\theta)}{\partial z}\right\} = \frac{\partial^2\theta}{\partial x^2} + \frac{\partial^2\theta}{\partial y^2} + G\ \dot{\gamma}^{n+1} e^{-\beta\theta} \qquad (5.64)$$

Leaving only the z-direction in the left hand side, one obtains,

$$Pe \frac{\partial(w\theta)}{\partial z} = \frac{\partial^2\theta}{\partial x^2} + \frac{\partial^2\theta}{\partial y^2} + G\,\dot\gamma^{n+1}e^{-\beta\theta} - Pe\left\{\frac{\partial(u\theta)}{\partial x} + \frac{\partial(v\theta)}{\partial y}\right\} \quad (5\ 65)$$

The discretized equation is now derived by integrating Eq (5 65) over the main control volume shown in Fig 5 5 and over the interval from z and z+dz. Thus,

$$Pe \int_s^n \int_w^e \int_z^{z+dz} \frac{\partial(w\theta)}{\partial z}\,dz\,dx\,dy = \int_z^{z+dz}\int_s^n\int_w^e \frac{\partial}{\partial x}\left(\frac{\partial\theta}{\partial x}\right)\,dx\,dy\,dz +$$

$$\int_z^{z+dz}\int_w^e\int_s^n \frac{\partial}{\partial y}\left(\frac{\partial\theta}{\partial y}\right)\,dy\,dx\,dz + \int_z^{z+dz}\int_s^n\int_w^e G\,\dot\gamma^{n+1}e^{-\beta\theta}\,dx\,dy\,dz$$

$$- Pe\int_z^{z+dz}\int_s^n\int_w^e \frac{\partial(u\theta)}{\partial x}\,dx\,dy\,dz - Pe\int_z^{z+dz}\int_w^e\int_s^n \frac{\partial(v\theta)}{\partial y}\,dy\,dx\,dz$$

$$(5\ 66)$$

where, the order of the integration is choosen according to the nature of the term. For the representation of the term $\frac{\partial(w\theta)}{\partial z}$, we shall assume that the grid point value of $(w\theta)$ prevails throughout the control volume. Fully implicit scheme has been used in the integration from z to z+dz. The old values at z at the grid points will be denoted by superscript ^{o}. The new values of z+dz at the grid points will be denoted without any superscript. Then we obtain from Eq.(5.66),

$$Pe \left[(w\theta) - (w\theta)^0 \right] \frac{SEW(I)\ SNS(J)}{dz} = \left[\left(\frac{\partial\theta}{\partial x} \right)_e - \left(\frac{\partial\theta}{\partial x} \right)_w \right] SNS(J) +$$

$$\left[\left(\frac{\partial\theta}{\partial y} \right)_n - \left(\frac{\partial\theta}{\partial y} \right)_s \right] SEW(I) + \left[G\ \dot{\gamma}^{n+1}\ e^{-\beta\theta} \right]\ SEW(I)\ SNS(J)$$

$$- Pe \left[(u\theta)_e - (u\theta)_w \right] SNS(J) - Pe \left[(v\theta)_n - (v\theta)_s \right] SEW(I)$$

$$(5\ 67)$$

The third term on the right hand side is the viscous dissipation term This term is assumed to be constant throughout the control volume. The last two terms of Eq (5 67) are convective terms which are discretized following the 'upwind scheme' (Patankar, 1980) . The value of u at an interface is equal to the value of u at the grid point on the upwind side of the face This is true for v-velocity also

Thus,

$$(u\theta)_e = \left[u_e, 0 \right]\theta_P - \left[0, -u_e \right]\theta_E \qquad (5\ 68a)$$

$$(u\theta)_w = \left[u_w, 0 \right]\theta_W - \left[0, -u_w \right]\theta_P \qquad (5.68b)$$

$$(v\theta)_n = \left[v_n, 0 \right]\theta_P - \left[0, -v_n \right]\theta_N \qquad (5\ 68c)$$

$$(v\theta)_s = \left[v_s, 0 \right]\theta_S - \left[0, -v_s \right]\theta_P \qquad (5.68d)$$

The notation $\left[a, b \right]$ means that the larger of a and b is to be

used   When   Eq.(5 67)   is   repeated   by   this   concept,   the
discretization equation becomes,

$$a_P \theta_P = a_E \theta_E + a_W \theta_W + a_N \theta_N + a_S \theta_S + S_P \qquad (5.69)$$

where,

$$a_E = \frac{SNS(J)}{DXEP(I)} + Pe \; SNS(J) \; \Big[0,-u_e\Big] \qquad (5\;70a)$$

$$a_W = \frac{SNS(J)}{DXPW(I)} + Pe \; SNS(J) \; \Big[u_w,0\Big] \qquad (5.70a)$$

$$a_N = \frac{SEW(I)}{DYNP(J)} + Pe \; SEW(I) \; \Big[0,-v_n\Big] \qquad (5\;70c)$$

$$a_S = \frac{SEW(I)}{DYPS(J)} + Pe \; SEW(I) \; \Big[v_s,0\Big] \qquad (5\;70a)$$

$$a_P = a_E + a_W + a_N + a_S +$$

$$Pe \; SNS(J) \; \left[\Big[u_e,0\Big] - \Big[0,-u_e\Big] + \Big[0,-u_w\Big] - \Big[u_w,0\Big]\right] +$$

$$Pe \; SEW(I) \; \left[\Big[v_n,0\Big] - \Big[0,-v_n\Big] + \Big[0,-v_s\Big] - \Big[v_s,0\Big]\right] +$$

$$\frac{Pe \; w_P \; SEW(I) \; SNS(J)}{\Delta z}$$

$$(5.70e)$$

On rearranging,

$$a_P = a_E + a_W + a_N + a_S + Pe \ [(u_e - u_w) \ SNS(J) +$$

$$(v_n - v_s) \ SEW(I)] + \frac{Pe \ w_P \ SEW(I) \ SNS(J)}{\Delta z} \qquad (5 \ 70f)$$

$$S_P = G \ \dot{\gamma}^{n+1} \ e^{-\beta\theta} \ SEW(I) \ SNS(J) +$$

$$\frac{Pe \ w_P^0 \ \theta_P^0 \ SEW(I) \ SNS(J)}{\Delta z} \qquad (5.70g)$$

5.9.2 ENERGY EQUATION OF THE SCREW BODY

The energy equation of the screw body is written as:

$$\frac{\partial^2\theta}{\partial x^2} + \frac{\partial^2\theta}{\partial y^2} = 0 \qquad (5.71)$$

This equation is integrated in the main contol volume (Fig.5.5) to yield the discretized finite difference equation:

$$\int_s^n \int_w^e \frac{\partial^2\theta}{\partial x^2} \ dx \ dy + \int_w^e \int_s^n \frac{\partial^2\theta}{\partial y^2} \ dx \ dy = 0 \qquad (5.72)$$

which may be written as:

$$\left[\left(\frac{\partial\theta}{\partial x}\right)_e - \left(\frac{\partial\theta}{\partial x}\right)_w\right] SNS(J) - \left[\left(\frac{\partial\theta}{\partial x}\right)_n - \left(\frac{\partial\theta}{\partial x}\right)_s\right] SEW(I) = 0 \qquad (5.73)$$

On further discretization, Eq.(5 73) takes the form as

$$a_P \theta_P = a_E \theta_E + a_W \theta_W + a_N \theta_N + a_S \theta_S \qquad (5\ 74)$$

where,

$$a_E = \frac{SNS(J)}{DXEP(I)} \qquad (5\ 75a)$$

$$a_W = \frac{SNS(J)}{DXPW(I)} \qquad (5\ 75b)$$

$$a_N = \frac{SEW(I)}{DYNP(J)} \qquad (5.75c)$$

$$a_W = \frac{SEW(I)}{DYNP(J)} \qquad (5\ 75d)$$

$$a_P = a_E + a_W + a_N + a_S \qquad (5.75e)$$

5.9.3 DISCRETIZED EQUATION AT THE FLUID-SCREW INTERFACE

In this section, a discretized equation at the fluid-screw interface is derived using the energy equation of the fluid and the screw and the compatibility conditions at the interface. The details of the derivation are given below (Carnahan et.al , 1969). The main advantage of this method is that the fluid and screw temperature are obtained in a single computational domain.

Now, in the main control volume shown in the Fig 5.5 and Fig.(5.8), $\theta_{i,j+1}$ in the fluid and $\theta_{i,j-1}$ in the screw body are expanded into Taylor series form dropping terms beyond the second

Fig. 5.8 Type of control volumes near the interace

order

FLUID :

$$\theta_{i,j+1} = \theta_{i,j} + \left.\frac{\partial\theta}{\partial y}\right|_{i,j}\frac{\Delta y_f}{2} + \left.\frac{\partial^2\theta}{\partial y^2}\right|_{i,j}\frac{(\Delta y_f/2)^2}{2} \qquad (5.76)$$

$$\text{i e.,} \qquad \left.\frac{\partial\theta}{\partial y}\right|_{i,j} = \frac{\theta_{i,j+1} - \theta_{i,j}}{(\Delta y_f/2)} - \left.\frac{\partial^2\theta}{\partial y^2}\right| \frac{\Delta y_f}{4} \qquad (5\ 76a)$$

SCREW :

$$\theta_{i,j-1} = \theta_{i,j} - \left.\frac{\partial\theta}{\partial y}\right|_{i,j}\frac{\Delta y_s}{2} + \left.\frac{\partial^2\theta}{\partial y^2}\right|_{i,j}\frac{(\Delta y_s/2)^2}{2} \qquad (5\ 77)$$

$$\text{i.e }, \left.\frac{\partial\theta}{\partial y}\right|_{i,j} = \frac{\theta_{i,j+1} - \theta_{i,j}}{(\Delta y_s/2)} + \left.\frac{\partial^2\theta}{\partial y^2}\right|_{i,j}\frac{\Delta y_s}{4} \qquad (5\ 77a)$$

The compatibility conditions, Eq.(5 12c) are re-written here as Eq.(5.78) shown below:

$$\left.\frac{\partial\theta}{\partial y}\right|_s = \frac{K_f}{K_s}\left.\frac{\partial\theta}{\partial y}\right|_f, \text{ and } \theta_{i,j}\Big|_s = \theta_{i,j}\Big|_f \qquad (5.78)$$

Substituting Eq.(5.76a) and (5.77a), one obtains.

$$\left[\frac{\theta_{i,j} - \theta_{i,j-1}}{\Delta y_s/2} + \frac{\partial^2 \theta}{\partial y^2}\bigg|_{i,j} \frac{\Delta y_s}{4} \right]_s =$$

$$\frac{K_f}{K_s} \left[\frac{\theta_{i,j+1} - \theta_{i,j}}{\Delta y_f/2} - \frac{\partial \theta^2}{\partial y^2}\bigg|_{i,j} \frac{\Delta y_f}{4} \right]_f \qquad (5\ 79)$$

The terms $\dfrac{\partial^2 \theta}{\partial y^2}\bigg|_{i,j}$ in the fluid and $\dfrac{\partial^2 \theta}{\partial y^2}\bigg|_{i,j}$ in the screw are substituted from Eq.(5 64) and (5 71) respectively Eq (5 64) is rewritten here as Eq.(5 80) and shown below

$$Pe\left\{ \frac{\partial(u\theta)}{\partial x} + \frac{\partial(v\theta)}{\partial y} + \frac{\partial(w\theta)}{\partial z} \right\} = \frac{\partial^2 \theta}{\partial x^2} + \frac{\partial^2 \theta}{\partial y^2} + G\,\dot{\gamma}^{n+1} e^{-\beta\theta} \qquad (5\ 80)$$

At the screw-fluid inteface, the velocity boundary condition is given by, $u = v = w = 0$. Therefore, the left hand side of Eq.(5.80) becomes zero, which yields,

$$\frac{\partial^2 \theta}{\partial y^2} = - \left[\frac{\partial^2 \theta}{\partial x^2} + + G\,\dot{\gamma}^{n+1} e^{-\beta\theta} \right] \qquad (5\ 81)$$

Now energy equation of the screw is

$$\frac{\partial^2 \theta}{\partial x^2} + \frac{\partial^2 \theta}{\partial y^2} = 0 \qquad (5.82)$$

$$\therefore \qquad \frac{\partial^2 \theta}{\partial y^2} = - \frac{\partial^2 \theta}{\partial x^2} \qquad (5.83)$$

When Eq (5 81) and Eq (5 83) are substituted in Eq (5 79), the following equation results

$$
\left[\frac{\theta_{i,j} - \theta_{i,j-1}}{(\Delta y_s/2)} - \left.\frac{\partial^2\theta}{\partial x^2}\right|_{i,j} \frac{\Delta y_s}{4} \right]_s =
$$

$$
\frac{K_f}{K_s} \left[\frac{\theta_{i,j+1} - \theta_{i,j}}{(\Delta y_f/2)} + \left(\frac{\partial^2\theta}{\partial x^2} + \dot{\gamma}^{n+1} e^{-\beta\theta} \right) \frac{\Delta y_f}{4} \right]_f \qquad (5.84)
$$

The Eq.(5 84) is integrated between e and w over the interface line:

$$
\int_w^e \left[\frac{\theta_{i,j} - \theta_{i,j-1}}{(\Delta y_s/2)} - \left.\frac{\partial^2\theta}{\partial x^2}\right|_{i,j} \frac{\Delta y_s}{4} \right]_s dx =
$$

$$
\frac{K_f}{K_s} \int_w^e \left[\frac{\theta_{i,j+1} - \theta_{i,j}}{(\Delta y_f/2)} + \left(\frac{\partial^2\theta}{\partial x^2} + \dot{\gamma}^{n+1} e^{-\beta\theta} \right) \frac{\Delta y_f}{4} \right]_f dx \qquad (5\ 85)
$$

Dropping the subscripts s and f we obtain,

$$
\left[\frac{\theta_P - \theta_S}{DYPS(J)} SEW(I) - \frac{DYPS(J)}{2} \left\{ \left(\frac{\partial\theta}{\partial x}\right)_e - \left(\frac{\partial\theta}{\partial x}\right)_w \right\} \right] =
$$

$$
\frac{K_f}{K_s} \left[\frac{\theta_N - \theta_P}{DYNP(J)} SEW(I) - \frac{DYNP(J)}{2} \left\{ \left(\frac{\partial\theta}{\partial x}\right)_e - \left(\frac{\partial\theta}{\partial x}\right)_w \right\} + \right.
$$

$$
\left. \left(G\,\dot{\gamma}^{n+1} e^{-\beta\theta} \right)_P SEW(I) \frac{DYNP(J)}{2} \right] \qquad (5.86)
$$

where,

$$\Delta y_s/2 = DYPS(J)$$

$$\Delta y_s/2 = DYNP(J)$$

The Eq (5.86) is expressed in the form

$$a_P \theta_P = a_E \theta_E + a_W \theta_W + a_N \theta_N + a_S \theta_S + S \qquad (5.87)$$

where,

$$a_E = \frac{DYPS(J)}{2\ DXEP(I)} + \frac{K_f}{K_s}\ \frac{DYNP(J)}{2\ DXEP(I)} \qquad (5\ 87a)$$

$$a_W = \frac{DYPS(J)}{2\ DXPW(I)} + \frac{K_f}{K_s}\ \frac{DYNP(J)}{2\ DXPW(I)} \qquad (5\ 87b)$$

$$a_N = \frac{K_f}{K_s}\ \frac{SEW(I)}{DYNP(J)} \qquad (5.87c)$$

$$a_S = \frac{K_f}{K_s}\ \frac{SEW(I)}{DYPS(J)} \qquad (5.87d)$$

$$a_P = a_E + a_W + a_N + a_S \qquad (5.87e)$$

$$S = \frac{K_s}{K_s}\ G\ \left(\dot{\gamma}^{\,n+1}\ e^{-\beta\theta}\right)_P\ \frac{SEW(I)\ DYNP(J)}{2.0} \qquad (5.87f)$$

Eq (5 87) is the desired discretized equation at the interface.

5.10 SOLUTION ALGORITHM

The overall solution algorithm is as follows

(1) Calculate u^*, v^*, w^*, p^* and $(\partial p^*_{av}/\partial z^*)$ for the isothermal flow $(\theta_f=0)$ at the inlet in the x-y plane by solving Eqs.(5.8)-(5.9c) subject to satisfying Eq (5 13)

(2) Guess u^*, v^*, w^*, θ, $(\partial p^*_{av}/\partial z^*)$, p^* in the x-y plane at the next z-station

(3) Solve Eq.(5.9a) and Eq.(5 9b) to obtain u^* and v^* in the said x-y plane. This implies solution of Eq.(5 17) and Eq.(5.21) in the x-y plane. SIMPLE algorithm of Patankar (1980) has been used to compute u^* and v^*.

(4) Obtain the corrected pressure distribution in the plane using pressure correction term This means that Eq.(5.46) is solved to obtain the pressure correction term p'. Adding p' to p gives correct pressure distribution in the plane Correct u^* and v^* using Eq.(5.38) and Eq.(5.41) respectively.

(5) Solve Eq.(5 9c) to obtain w^*. This implies of solution of Eq.(5.55).

(6) Correct the pressure gradient $(\partial p^*_{av} /\partial z^*)$ and w^* by checking whether Eq.(5.13) is satisfied or not This means that Eq.(5 62) is solved to obtain f. Using Eq (5 60a) the pressure gradient $(\partial p^*_{av} /\partial z^*)$ is corrected. w^* is corrected by using Eq.(5.60). Solve Eqs.(5 69),(5.74), and (5 87) simultaneously to obtain θ

(7) Solve Eq.(5.10) and Eq (5.11) simultaneously to obtain θ This means Eqs.(5.69), (5.87) and (5.74) are solved in the entire x-y domain at a particular z-station to obtain θ-distribution.

(8) The maximum difference between the previous iteration value and the current iteration value is calculated for u^*, v^*, w^*, and θ. If this value is less than a specified small value 'eps', then the solution is converged Go to Step 10

(9) Otherwise, go to Step 3.

(10) Print u^*, v^*, w^*, θ, p^*, $(\partial p^*_{av}/\partial z^*)$.

(11) Compute p^*_{av}, θ_{bulk}, Nu_H.

(12) If z^* less than 250 0, go to Step 2 and the procedure is repeated for next z^* locations.

(13) STOP.

CHAPTER 6

RESULTS AND DISCUSSIONS

CHAPTER 6

In this Chapter, the results based on the quasi three-dimensional model developed by the present author (see Chapter 5) are presented The isotherms in the screw channel and screw body in the y-z plane, the transverse temperature (θ) and u* and w* velocity profiles (i.e., variables as functions of y only) at various z* locations are compared with those obtained on the basis of the quasi two-dimensional model Also, velocity vector plots and isotherms in the x-y plane have been shown at four z* locations. Finally screw surface temperature, bulk temperature, Nusselt number, pressure gradient, and pressure along downchannel direction based on all three models, namely, the quasi two-dimensional model, the fully two-dimensional model and the present quasi three-dimensional model, have been compared

It is important to note that the temperature (θ), w* and u* velocities used for comparison are the integrated average values over x* at each y* (see Eqs (6.1)-(6 3)) in the case of quasi three-dimensional model.

$$\theta(y^*) = \frac{1}{(W/H)} \int_0^{W/H} \theta(x^*, y^*) dx^* \qquad (6\ 1)$$

$$w^*(y^*) = \frac{1}{(W/H)} \int_0^{W/H} w^*(x^*, y^*) dx^* \qquad (6\ 2)$$

$$u^*(y^*) = \frac{1}{(W/H)} \int_0^{W/H} u^*(x^*,y^*)dx^* \qquad (6\ 3)$$

The input data are the same as those used for the quasi two-dimensional and fully two-dimensional models However, for the quasi three-dimensional model, the finite width (W/H) of the screw channel has been considered. A typical W/H equal to 5 (Palit and Fenner, 1972) has been used in this study. It is to be kept in mind that away from the walls of the channel in the x^* direction, the gradients of the unknowns are expected to be small Therefore, a non-uniform grid spacings gradually increasing in the x^*-direction have been used. In the y^*-direction, i.e , along the height of the channel, grid spacing is uniform The computations have been carried out over 23 × 17 grids and 23 × 21 grids in the x-y plane (i.e., the cross-section) of the channel and the screwbody respectively. Δy_f^* and Δy_s^* are 0.0667 and 0 5263 respectively. However, a better resolution of the temperature gradients in the y^* direction of the screw body would have been obtained if a finer grid spacing adjacent to the screw surface were taken. Δz^* is 2.5 as before and the computations stop at $z^* = 250.0$. Sufficient numerical experimentation have been performed for the choice of optimum number of grid points.

6.1 TEMPERATURE AND VELOCITY FIELDS

Fig.6.1 shows the isotherms in the screw channel for the quasi two-dimensional and the quasi three-dimensional model on the
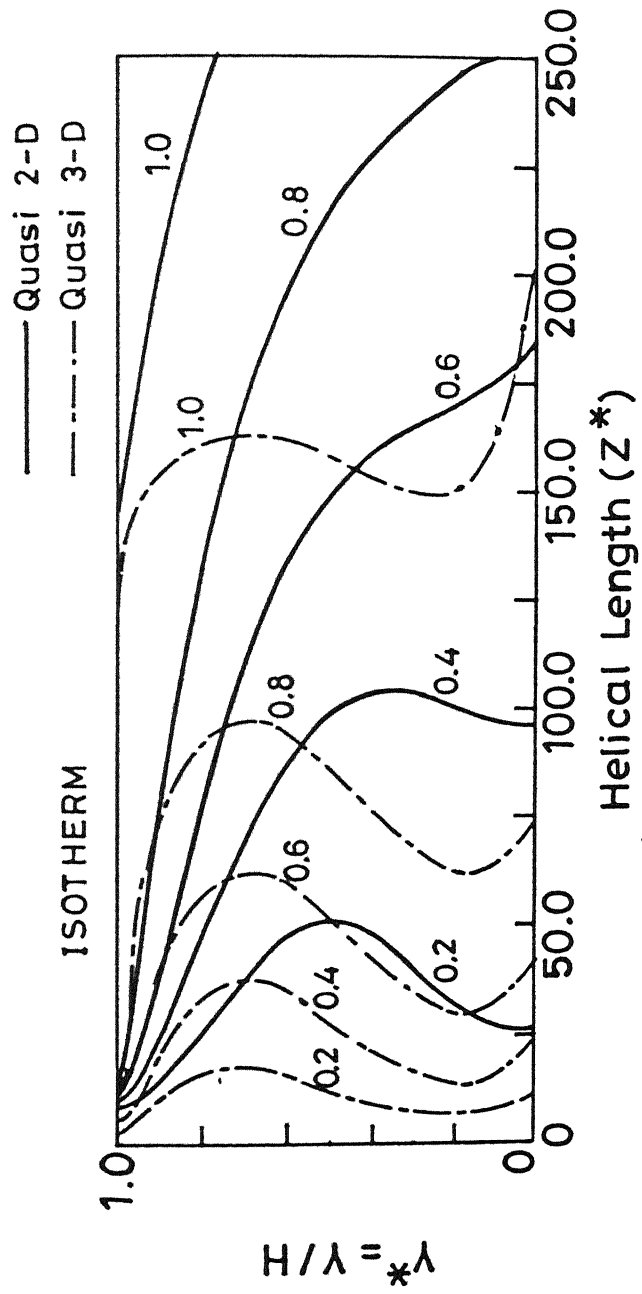
Fig 6.1 Isotherms in the screw channel for the quasi two-dimensional and quasi three-dimensional models.

same plot A comparison reveals that the temperature profile develops much faster for the quasi three-dimensional model In other words, the fluid temperatures are much greater in a larger portion of the channel in the downchannel direction This is physically expected as in the quasi three-dimensional model the cross convection effect has been taken into account Fig.6 2 shows that the nature of the isotherms in the screw body for the quasi three-dimensional model is consistent with those in the channel Fig.6 3 and Fig.6.4 show a comparison of transverse temperature profiles at four downstream locations in the fluid and the screw body respectively. The graphs in Fig.6 3 indicate that as z^* increases, more uniformity in the fluid temperature distribution is achieved in t · case of the quasi three-dimensional model This better uniformity can be attributed to better mixing due to the cross convection effect. The quasi two-dimensional model does not show this level of uniformity in the temperature profiles because of non-inclusion of the thermal convection normal to the screw flights in the same. Also, the fluid temperature is higher for the quasi three-dimensional model. However, the difference with respect to the quasi two-dimensional model is higher in the middle and gradually decreases towards the exit of the channel As expected, Fig.6.4 shows that the screw temperature profiles are almost uniform at each z^* location and the screwbody temperatures are higher in the case of the quasi three-dimensional model.

Fig.6.5 depicts the isovelocity (w^*) lines in the screw channel for the quasi two-dimensional and the quasi
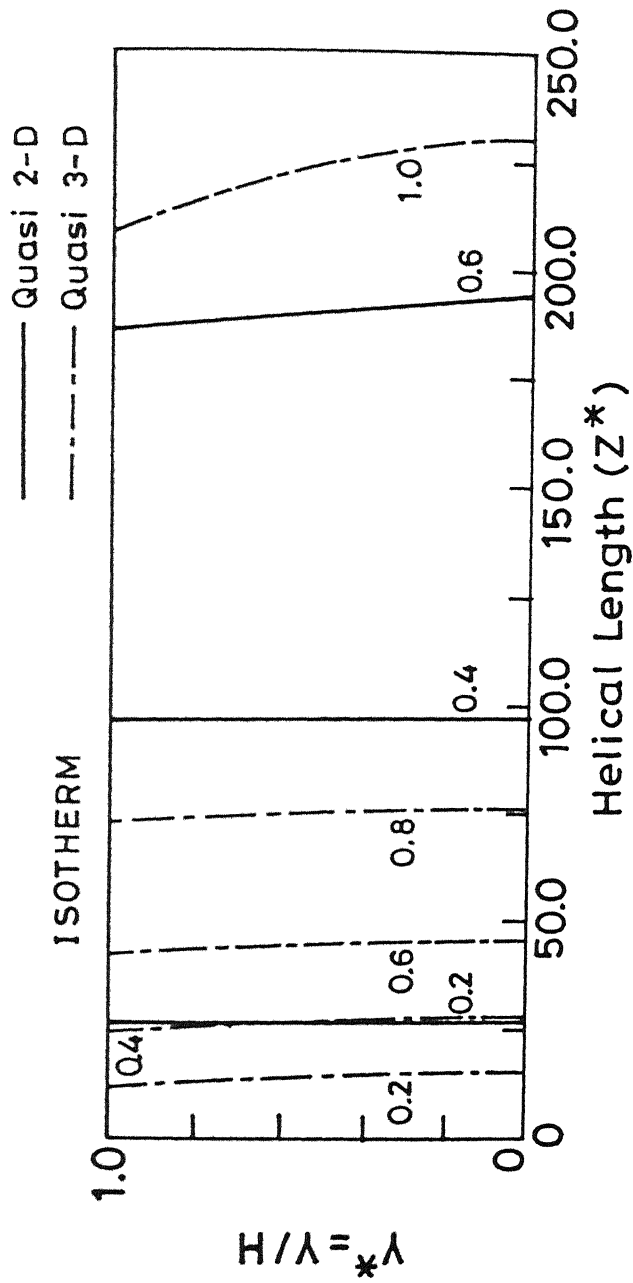
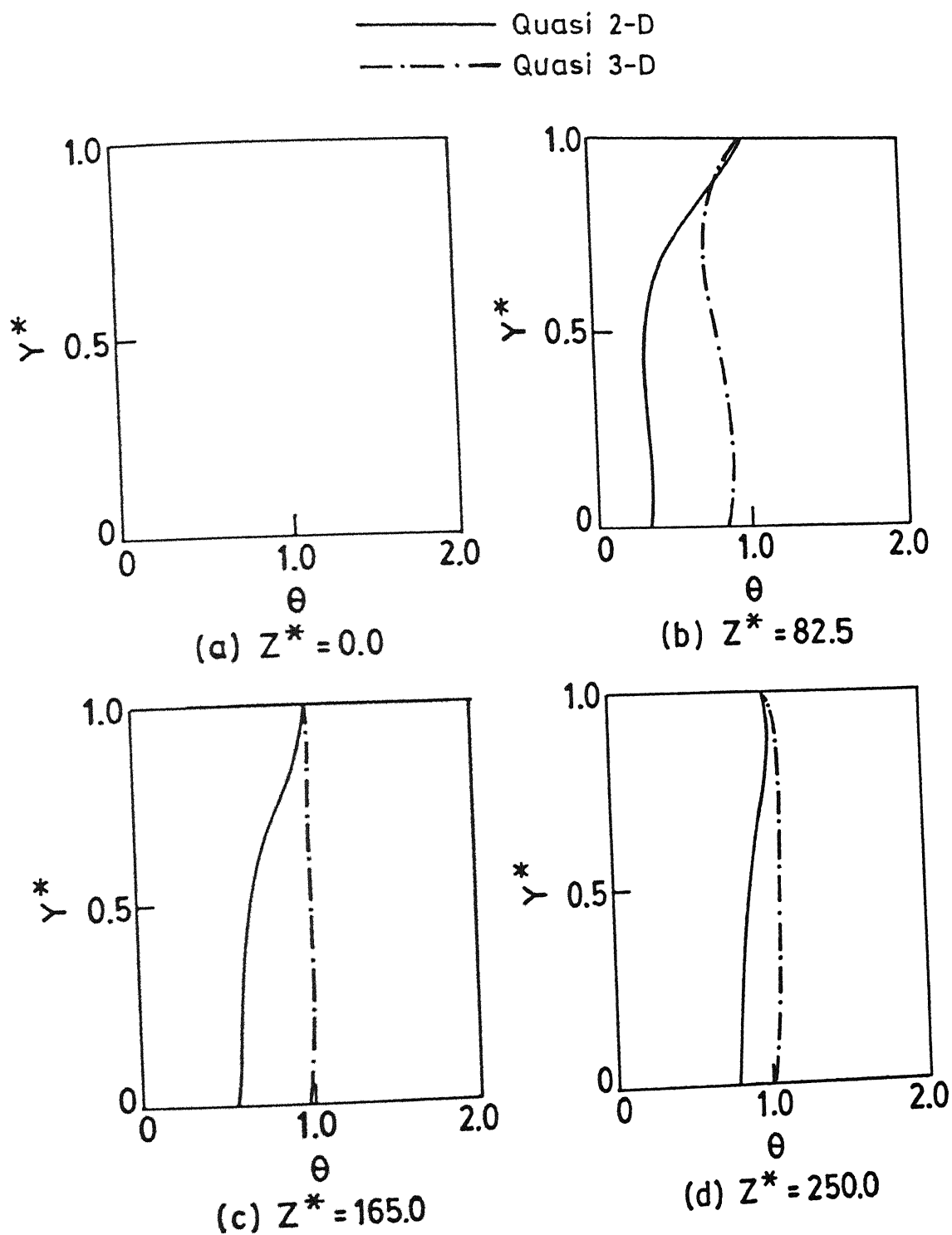Fig. 6.2 Isotherms in the screw body for the quasi two-dimensional and quasi three-dimensional models.

Fig. 6.3 Transverse temperature profiles in the screw channel at four down strem locations based on the quasi two-dimensional and quasi three-dimensional models.
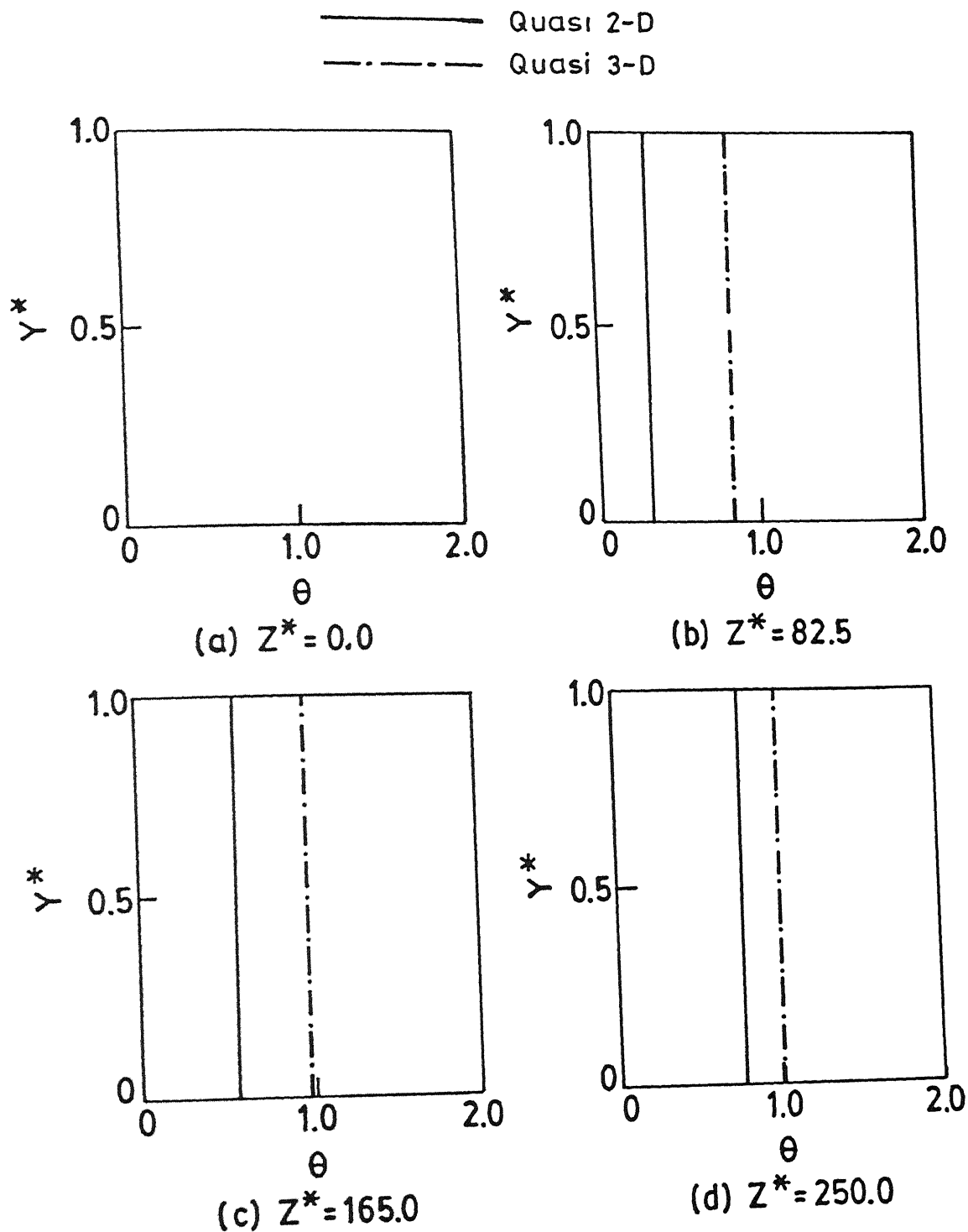
Fig. 6.4 Transverse temperature profiles in the screw body at four downstream locations based on the quasi two-dimensional and quasi three-dimensional models.
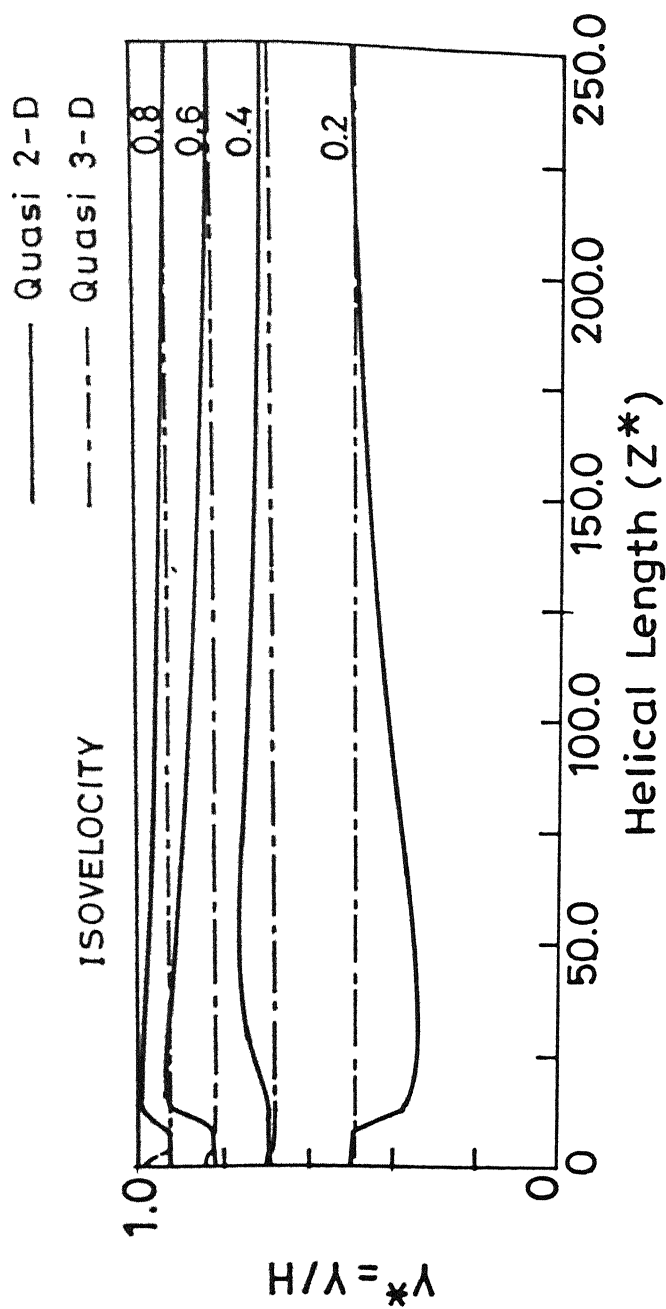
Fig. 6.5 Lines of constant velocity components w for the two models based on the quasi two-dimensional and quasi three-dimensional models.

three-dimensional model on the same plot A comparison reveals that w^* velocities based on the quasi three-dimensional model are higher in the upper half of the channel in the middle of the channel length but they coincide with the quasi two-dimensional w^*-velocities towards the channel exit. This is clearly revealed in Fig 6.6 This is because higher fluid temperature result in drop in viscosity which in turn increases the flow velocity Near the entry and the exit, the temperature difference is small and hence the w^* velocities for the two models almost coincide.

Fig.6.7 shows the development of u^* velocity profiles along the downchannel direction. While for the two models, u^*-velocities differ in the middle of the channel length as well as at the inlet, the former coincide at the exit The higher u^*-velocities for the quasi three-dimensional model in the middle of the channel length is attributed to the higher fluid temperature resulting in drop in viscosity whereas near the exit the temperature difference corresponding to the two models is small and hence the u^*-velocity profiles for the quasi two-dimensional and the quasi three-dimensional models become identical. As for the deviation at the inlet, the reason is as follows. The inlet velocity u^* has been taken as zero for the quasi two-dimensional case whereas for the quasi three-dimensional model, the u^* and v^* and w^* profiles are obtained by solving Eqs.(5.8)-(5.9c) subject to satisfying Eq.(5.13) by putting $\theta_f=0$ in Eqs.(5.9a)-(5.9c).
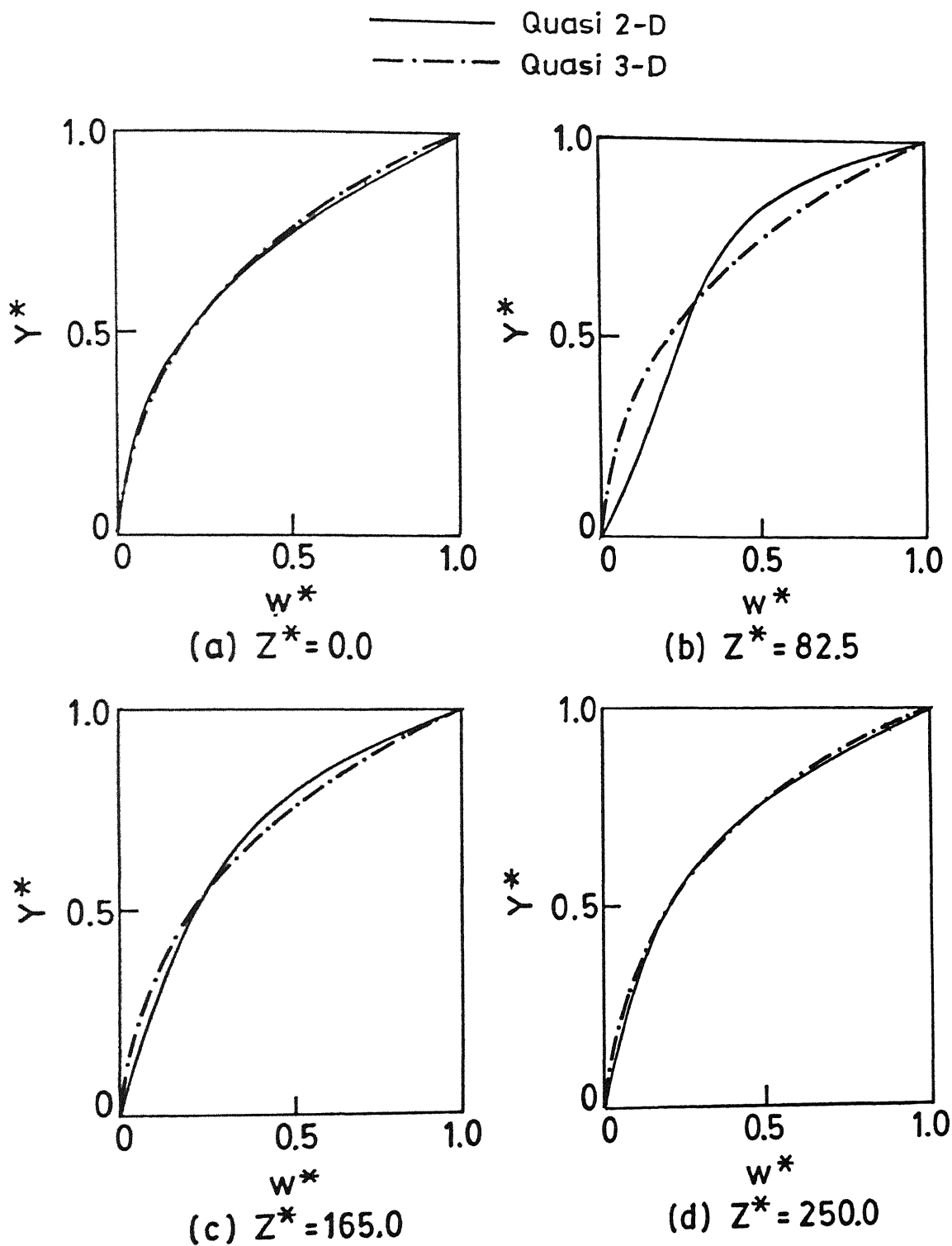
Fig. 6.6 Downchannel velocity w* profiles at four
downstream locations based on the quasi
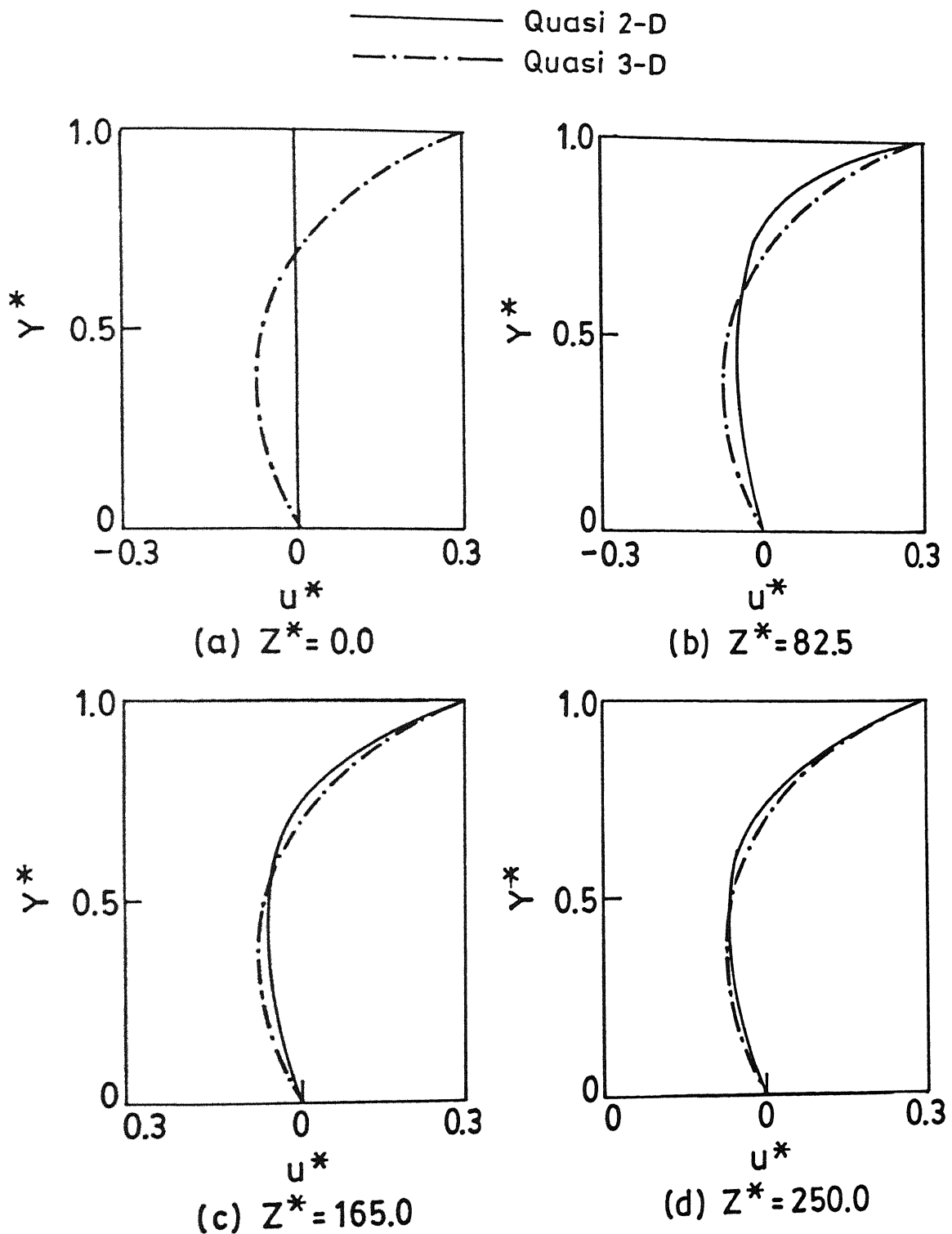two-dimensional and quasi three-dimensional
models.

Fig. 6.7 Crosschannel velocity u* profiles at four
downstream locations based on quasi
two-dimensional and quasi three-dimensional
models.

6.2 Velocity Vector Plots and Isotherms in X-Y Plane of the Channel

Fig 6 8 shows the velocity vector plots in the x-y plane at four downstream locations The plots clearly show the circulatory nature of the flow in the cross-sectional plane of the extruder This circulation results in the cross thermal convection enhancing the overall mixing process It is also noticed that v^* velocities are negligible except near the right and left boundary walls meaning a very weak flow and thermal convection normal to the channel base Fig 6 9 shows isotherm plots in the x-y planes at four locations in the downchannel direction. The figure depicts visually the increase of fluid temperatures as the fluid moves towards the exit of the channel At $z^* = 12.5$, i.e., near the inlet of the channel, it is seen a large core of relatively cold fluid sandwiched between hot fluids in the upper and lower region of the channel cross-section Near the right and left boundaries, temperatures are large because the sides are assumed to be insulated At higher z^*, i e , at $z^* = 82\ 5$, a dramatic rise in the fluid temperature is noticed This is due to the fact that more heating of the fluid is now taking place as the fluid is exposed to larger surface of the heated barrel and the effect of viscous heat generation is now more pronounced The temperature gradient in the y-direction as well as in the x-direction decreases which means that compared to that at $z^* = 12\ 5$, fluid is better mixed. At $z^*=165\ 0$, more uniformity in the temperature distribution is achieved and a major portion of the
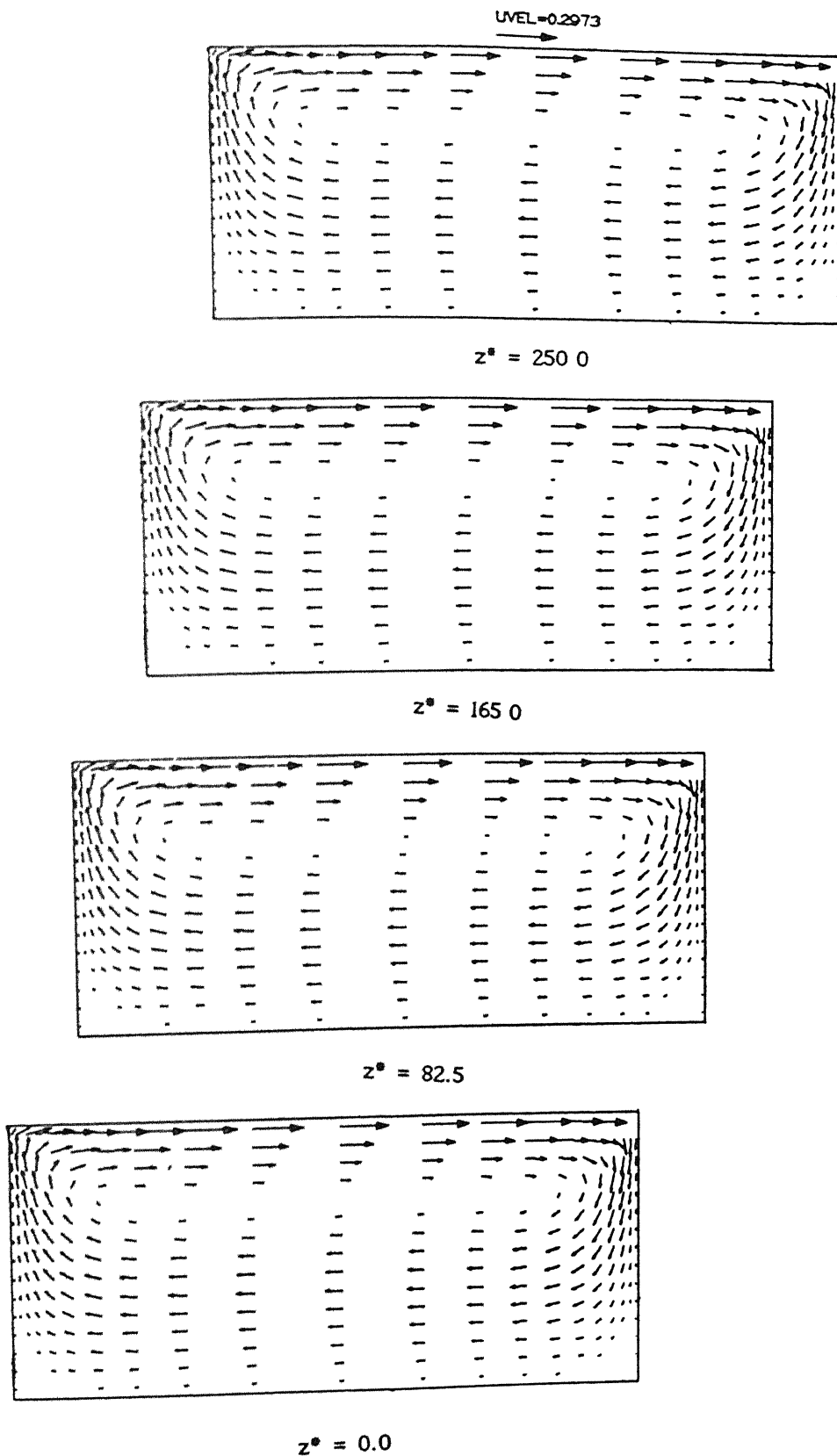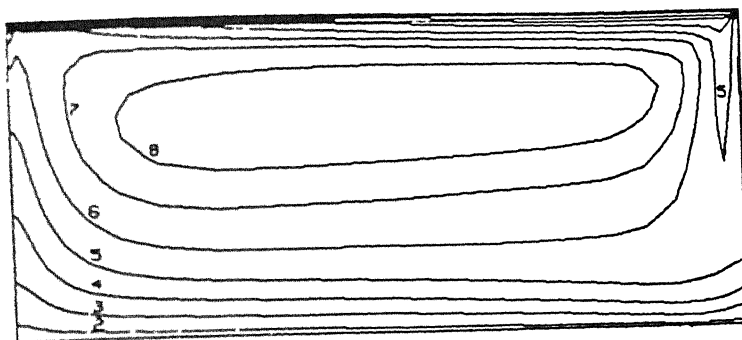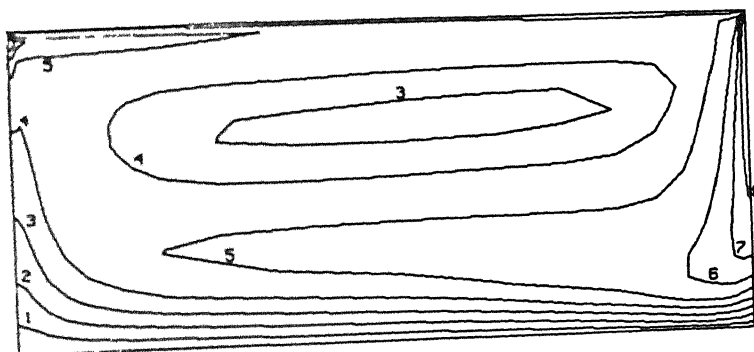
UVEL=0.2973

$z^* = 250\ 0$

$z^* = 165\ 0$

$z^* = 82.5$

$z^* = 0.0$

Fig. 6.8 Velocity vector plots in the cross-sectional
(x-y) planes at four down stream locations
for the quasi three-dimensional model.

1	1 013
2	1 025
3	1 038
4	1 050
5	1 063
6	1 075
7	1 088
8	1 101
9	1 113

$z^* = 250\ 0$

1.	977
2.	986
3.	995
4.	1 005
5.	1.014
6	1 023
7.	1 033
8	1 042
9.	1 051

$z^* = 165\ 0$
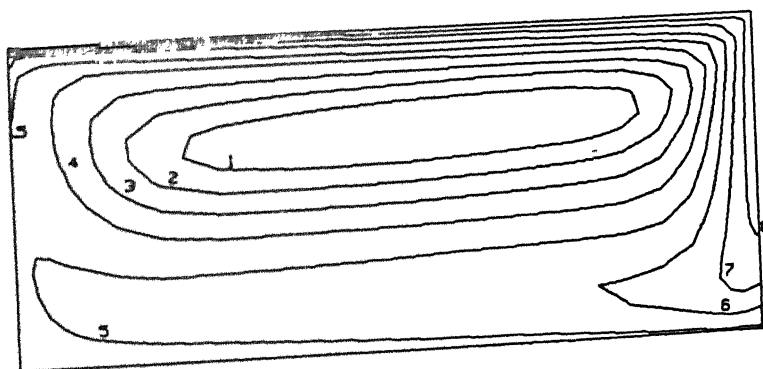
1	734
2	767
3	800
4	834
5.	.867
6	900
7.	.933
8	.967
9.	1.000

$z^* = 82\ 5$
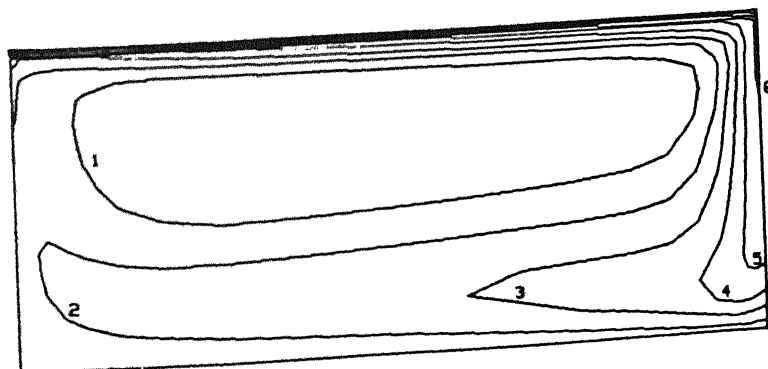
1	.191
2	.292
3	.393
4	.494
5.	.595
6	697
7.	798
8	899
9.	1.000

$z^* = 12.5$

Fig. 6.9 Isotherm plot in the cross-sectional (x-y) plane at four downstream locations for the quasi three-dimensional model.

fluid (except near the screw surface) is at temperatures higher than that at the barrel This is due to greater viscous dissipation At $z^*=250.0$, i e., at the exit of the channel, it is clearly seen that the entire fluid in the x-y plane is at a temperature higher than that at the barrel The fluid is now at almost uniform temperature, i e , thoroughly mixed To obtain a well-mixed fluid at the die is one of the main objectives Also, since near the exit, barrel is being heated by the fluid, appropiate amount of heat must be removed from the barrel to maintain it at a fixed temperature Another important and interesting observation is that at the exit the isotherms take the shape of streamlines (as is evident from the vector plots of Fig 6.8). This phenomenon revealed by the present numerical study matches also with the expectation of Griffith (1962)

6.3   COMPARISON OF RESULTS BASED ON THE QUASI TWO-DIMENSIONAL, FULLY TWO-DIMENSIONAL AND QUASI THREE-DIMENSIONAL MODELS

Finally, screw surface temperature, pressure gradient, pressure, Nusselt number and bulk temperature along downchannel direction z^* based on the quasi two-dimensional, fully two-dimensional and quasi three-dimensional models have been compared in order to see how the quasi three-dimensional model fares in contrast with the other two models.

Fig.6.10 shows that the screw surface temperature is close to barrel temperature ($\theta_b=1.0$) beyond $z^*=70.0$ and greater than barrel
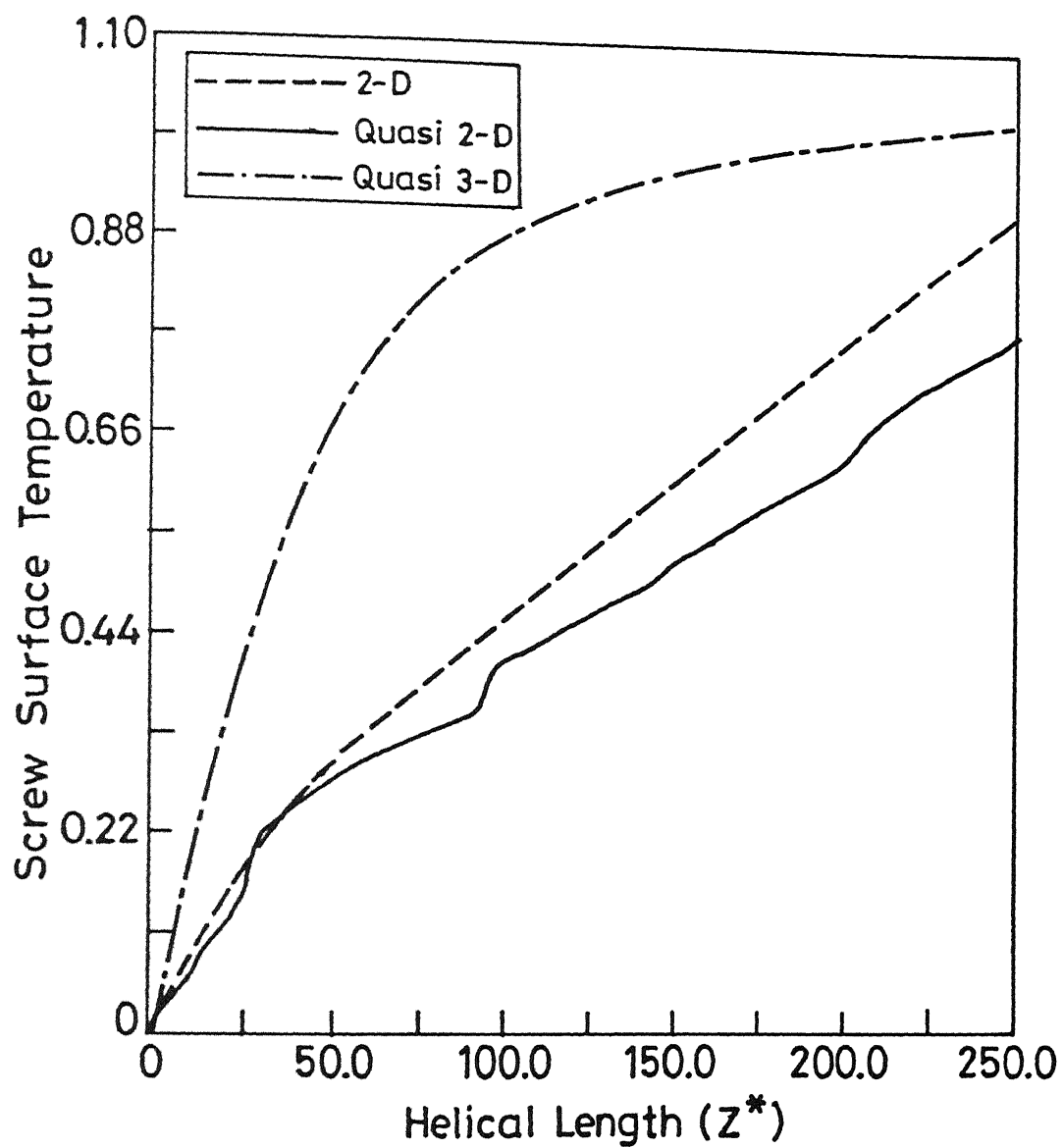
Fig. 6.10 Screw surface temperature variations along
the helical length for all three models,
-quasi two-dimensional, fully two-dimen-
sional and quasi three-dimensional.

temperature beyond z*=190.0. In other words, the screw surface temperature is almost equal to or greater than the barrel temperature in most part of the metering section This trend is also confirmed by earlier experimental works of Marshall et al. (1965) and Palit (1972) obtained from 63.5 mm (2.5 inch) extruders processing materials such as LDPE, polypropylene and polyvinyl chloride. Griffith also assumed the screw surface temperature to be equal to the barrel temperature on the ground that very large Peclet number associated with melt flow in a screw channel implies that temperature is constant along a streamline If there is no leakage over the flight tip, the screw and the barrel boundaries form a single continuous streamline.

It is clear that quasi two-dimensional and the fully two-dimensional models have failed to predict physically realistic screw surface temperature behaviour

Fig.6.11 reveals that in sharp contrast with the quasi two-dimensional and fully two-dimensional models, pressure gradient computed by the quasi three-dimensional model never goes to negative value and therefore, pressure continually increases to its final value at the exit of the channel (Fig.6.12) which is according to the physical expectations Another remarkable feature is that pressure predicted by the quasi three-dimensional model is much greater than that by the other two models. Therefore, quasi three-dimensional model in this regard also performs superior to quasi two-dimensional model and fully two-dimensional model. It is
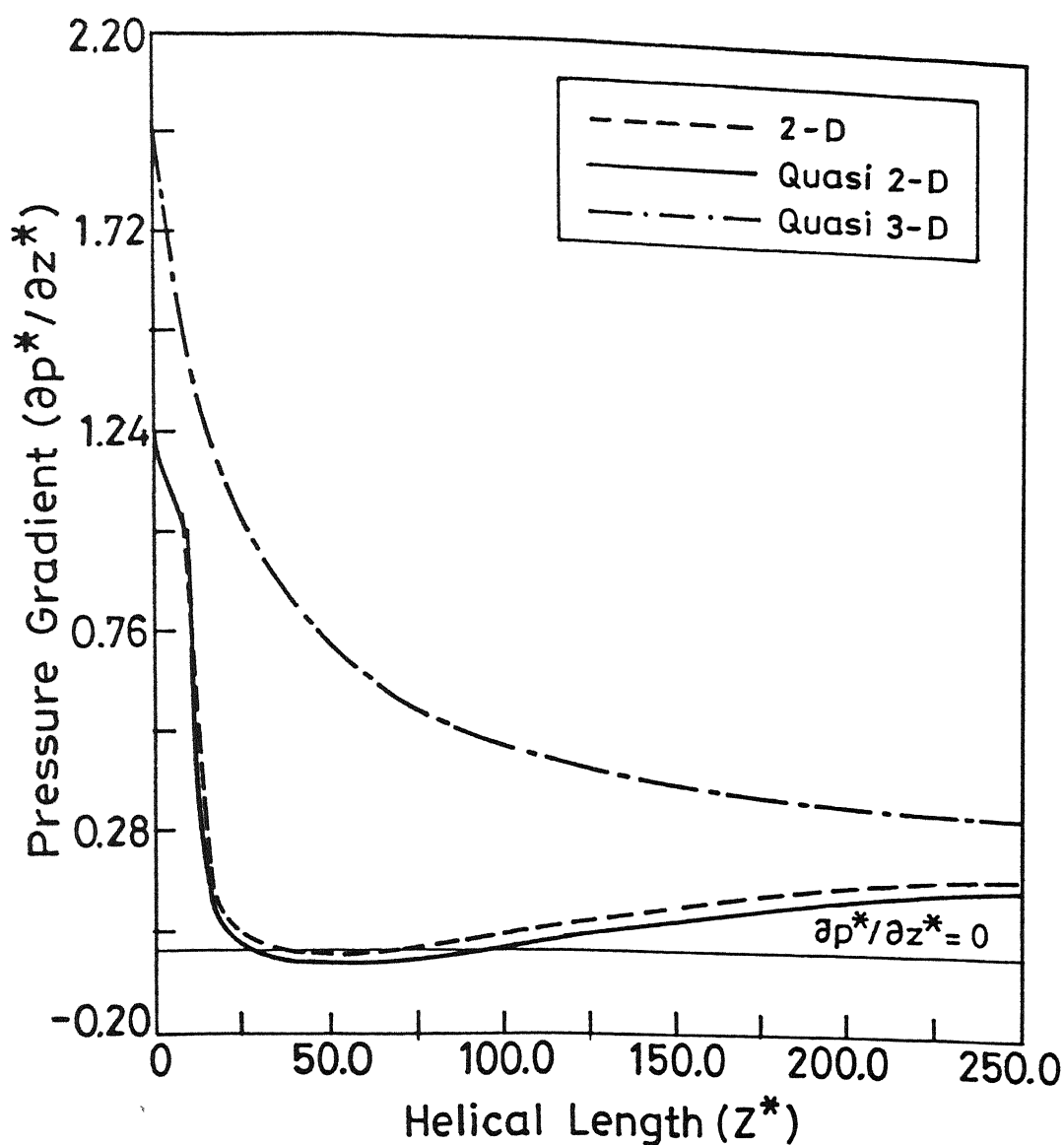
Fig. 6.11 Pressure gradient distribution along the helical length for all three models,-quasi two-dimensional, fully two-dimensional and quasi three-dimensional.
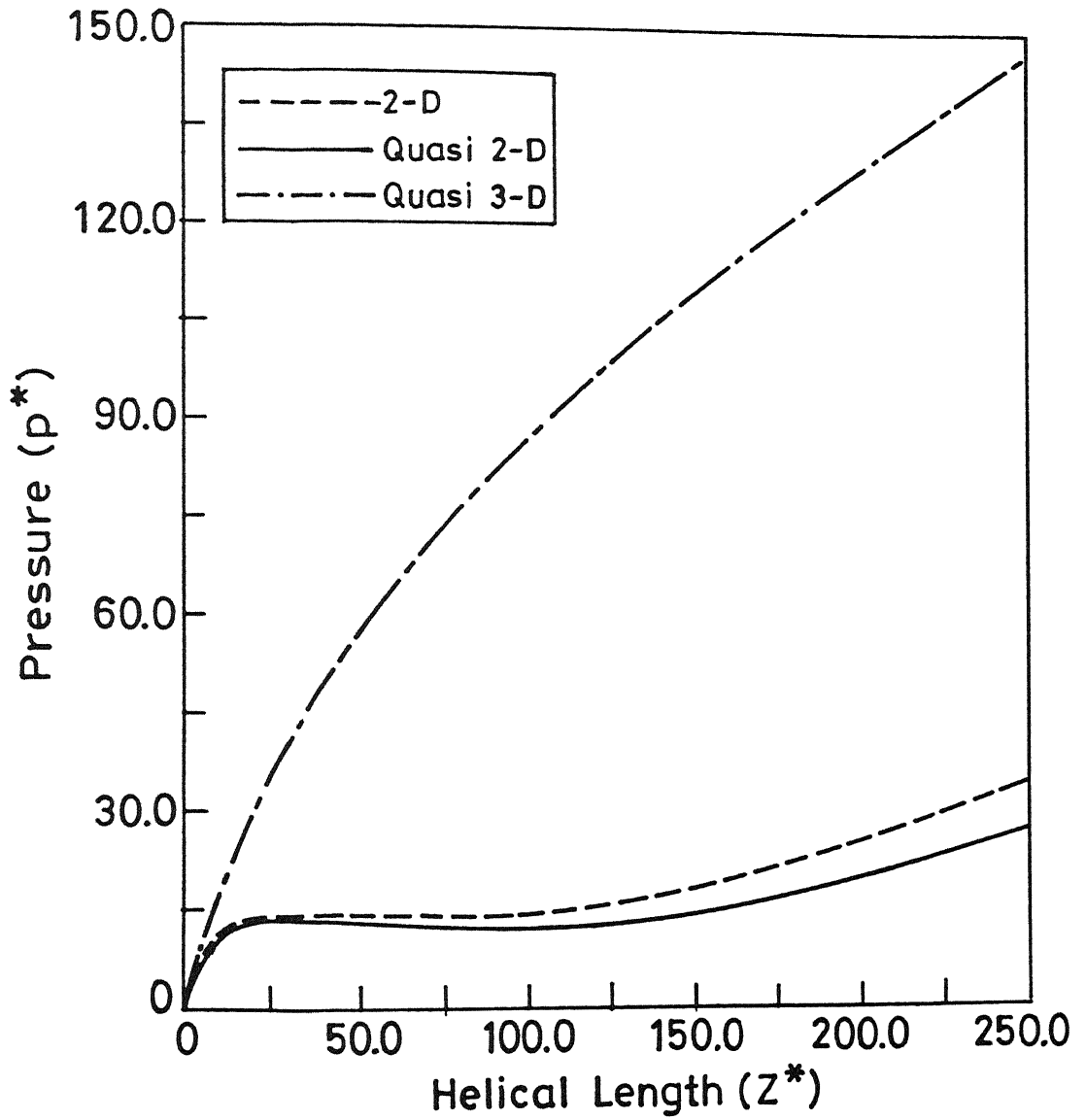
Fig. 6.12 Pressure distribution along the helical length
for all three models,-quasi two-dimensional,
fully two-dimensional and quasi
three-dimensional.

to be noted that pressure predicted by the quasi three-dimensional model is the average pressure (p_{av}) computed from Eq.(5 92) Fig 6 13 depicts that Nusselt number changes its sign from positive to negative (i.e., the fluid temperature near the barrel becomes higher than the barrel temperature) at around $z^*=150\ 0$ for all the three models Furthermore, the quasi three-dimensional model predicts greater Nusselt number It is to be noted at this point that for the quasi two-dimensional and fully two-dimensional models, in order to avoid numerical oscillations, the barrel boundary is taken as adiabatic near the inlet (till $z^*=10$) That is why the Nusselt number is zero at the inlet (i.e , at $z^*=0$) For obvious reason, this is not done in respect of the quasi three-dimensional model

Fig 6.14 shows that the bulk temperature predicted by the quasi three-dimensional model is greater in most part of the metering channel than that predicted by the other two models However, at the exit of the channel, bulk temperature based on the quasi three-dimensional model coincides with that computed by the fully two-dimensional model. This may be due to the effect of axial diffusion considered in the fully two-dimensional model.
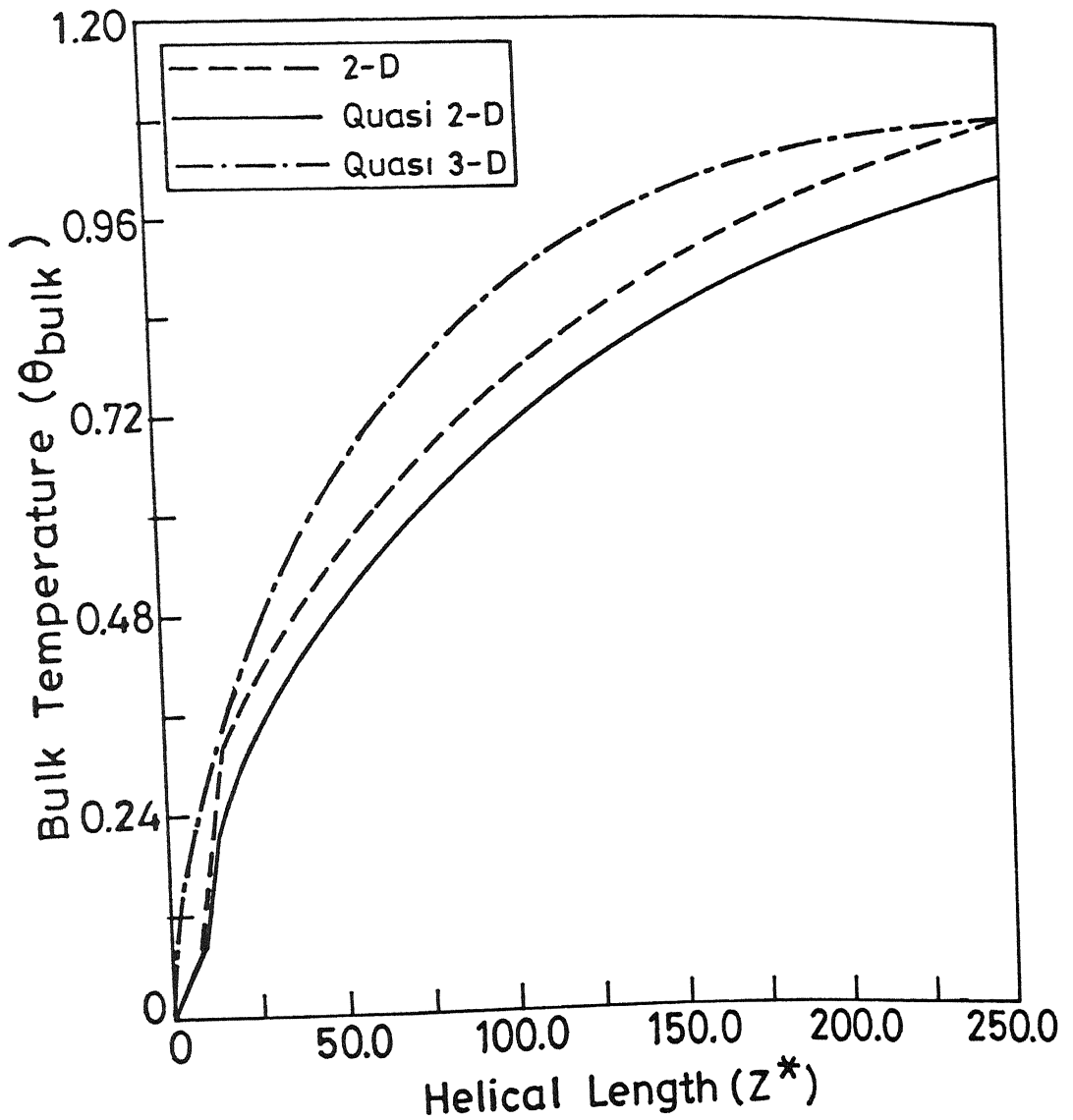
Fig. 6.14 Bulk temperature distribution along the helical length for all three models, - quasi two-dimensional, fully two-dimensional and quasi three-dimensional model.

CHAPTER 7

PARAMETRIC STUDY

CHAPTER 7

It has been shown in Chapter 6 that the quasi three-dimensional model simulates the physical processes in the metering section of a single-screw plasticating extruder in a most realistic manner Therefore, the quasi three-dimensional model can be used for the simulation of the performance of different size extruders with various screws and operating conditions to determine their relative performance in the desired application This procedure will yield an optimized design and valuable information on the performance of the extruder in a variety of operating conditions However,since the aim of this work is not to arrive at an optimized design, the parametric study has been performed on a single screw extruder thus excluding variation of W/H ratio.

The purposes of the present parametric study are two fold: (i) to see whether the quasi three-dimensional model is consistently behaving in a physically realistic manner when operating variables are changed at a time and (ii) to gain a great deal of insight and information on the process

The effect of three variables, namely, non-dimensional volumetric flow rate (q_v), power law index (n) and screw speed (N), on pressure gradient, pressure, Nusselt number and bulk temperature of a screw extruder (processing LDPE) have been

investigated It is to be noted that input data for q_v and n variations are taken from Karwe and Jaluria (1990) and have been listed in Table-1 The input data for N variations are taken from Fenner (1979) and have been listed in Table-2.

7.1 EFFECT OF DIMENSIONLESS FLOW RATE (q_v)

Fig.7 1 and Fig 7.2 show the effect of variation of q_v i e , the flow rate (keeping all other variables such as frequency of screw rotation, screw geometry, etc., constant) on the pressure gradient and pressure along the downchannel direction respectively. It is seen from Fig 7 1 that for q_v = 0 3, 0 35 and 0.4, the pressure gradient is positive and is decreasing monotonically. For q_v = 0 45, the pressure gradient is slightly negative indicating that the drag flow situation has arrived. Also, as q_v increases, pressure gradient decreases. Consequently, from Fig.7.2 it is revealed that pressure rise decreases as the volumetric flow rate increases. The trend may be explained as follows.

In the laboratory, various flow rates can be obtained by a variable resistance in the discharge end of the extruder. This is accomplished by opening or closing the valve at the die end Now at low flow rates (i.e., q_v = 0 3, 0.35, 0 4) the pressure profiles increase monotonically This is caused by the ability of the barrel to drag more polymer than the net flow rate of the melt at each location in the extruder channel. Therefore, the pressure gradient higher at lower flow rates. As flow rate is increased
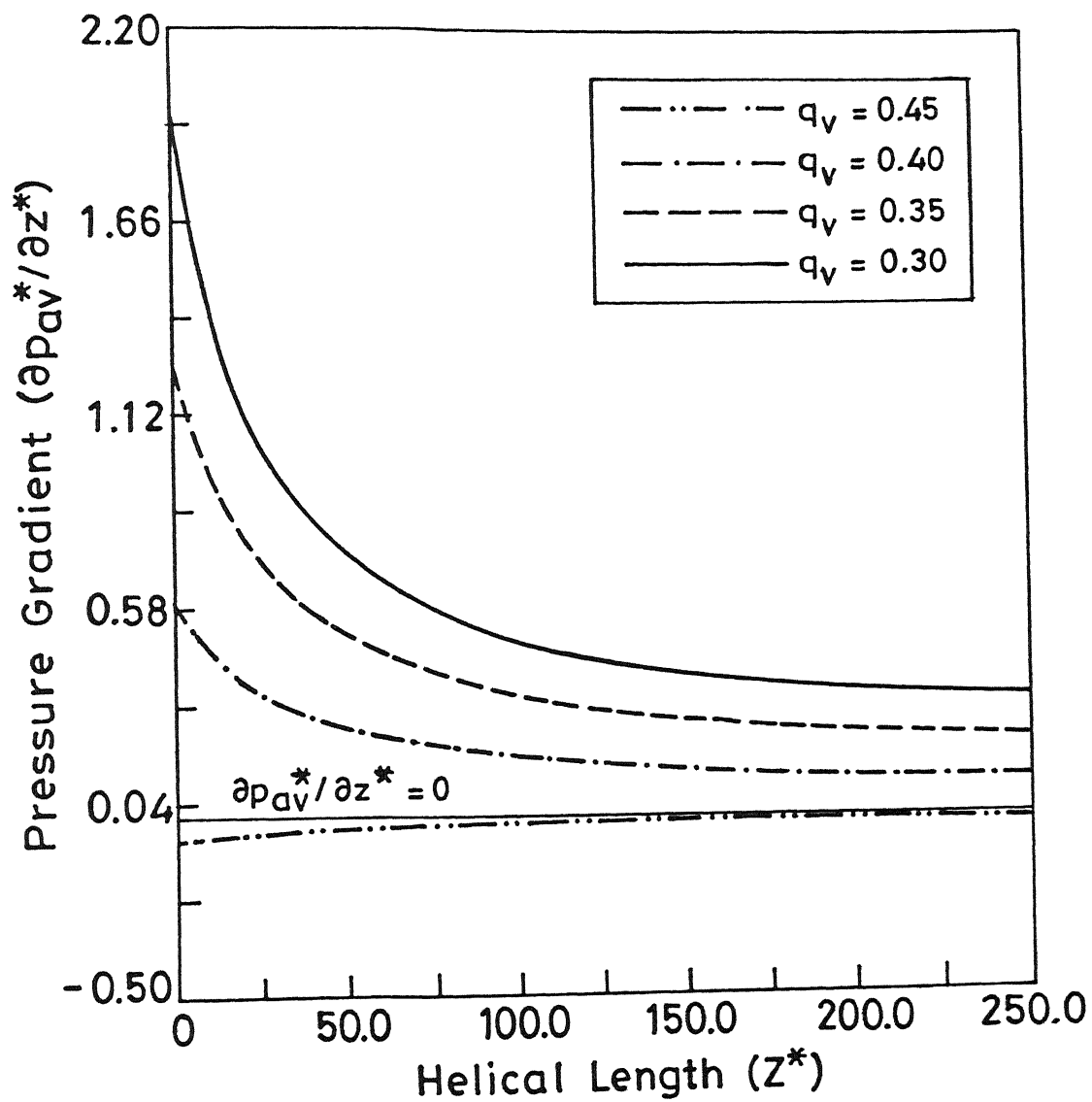
Fig. 7.1 Pressure gradient distribution along the
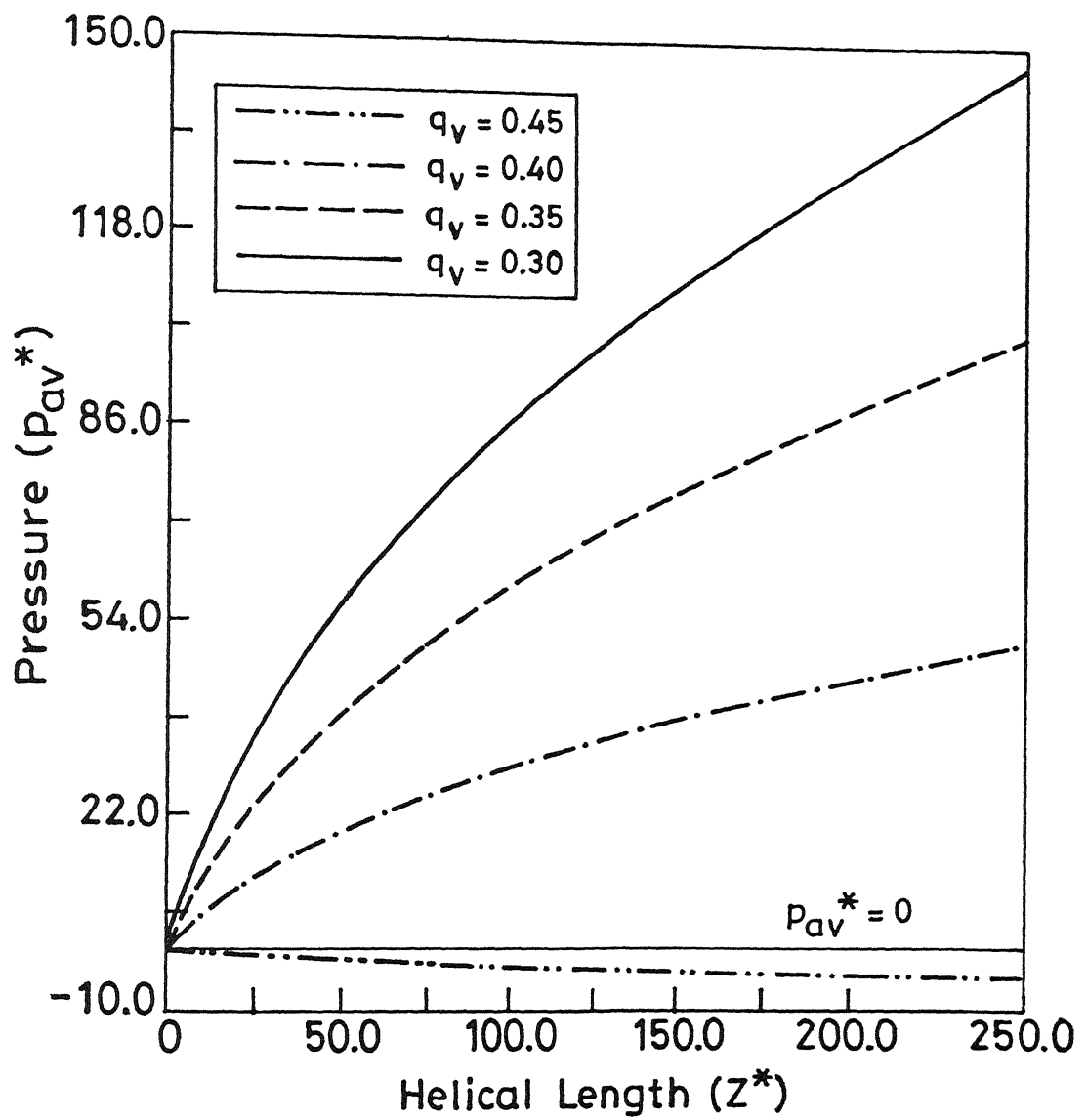helical length for $q_v = 0.3, 0.35, 0.4, 0.45$.

Fig. 7.2 Pressure distribution along the helical length
for $q_v = 0.3, 0.35, 0.4, 0.45$.

(q_v=0 45 case) by opening a valve (at constant screw speed), the pressure gradient decreases, reaching a value at a certain point in the extruder where the drag flow generated by the advancing barrel equals the flow rate (net flow rate) No pressure gradient is developed at this point and further down the channel, negative pressure gradient is exhibited In the present case, since the metering section is the last section of the channel, no maxima is seen in the pressure curve and at $z^* = 0$, the pressure gradient is already negative and remains negative till the channel exit Hence, $q_v = 0$ 45, the pressure continues to decrease up to the die end (Fig 7.2). That is why, a value for q_v between about 0 4 and 0.5 corresponds to the drag flow situation, where no pressure gradient is generated. For this reason, the limiting value of q_v on the higher side is taken as 0 4.

Fig 7.3 shows the Nusselt number (Nu_H) distribution along the downchannel direction for $q_v = 0$ 3, 0 35, 0 4, and 0.45 As expected, Nusselt number is higher for higher flow rates. This is because, with rise in flow rate, the residence time distribution of the polymer material decreases which means that the fluid is heated less and therefore, the fluid temperature is lower. Therefore Nusselt number (Nu_H) being indicative of the temperature gradient at the barrel surface increases.

Fig7.4 depicts the bulk temperature (θ_{bulk}) distribution along the downchannel direction for $q_v = 0$ 3, 0.35, 0.4, and 0.45. As expected, the bulk temperature at any z^*-location is higher for lower volumetric flow rates. The reason has been already stated in
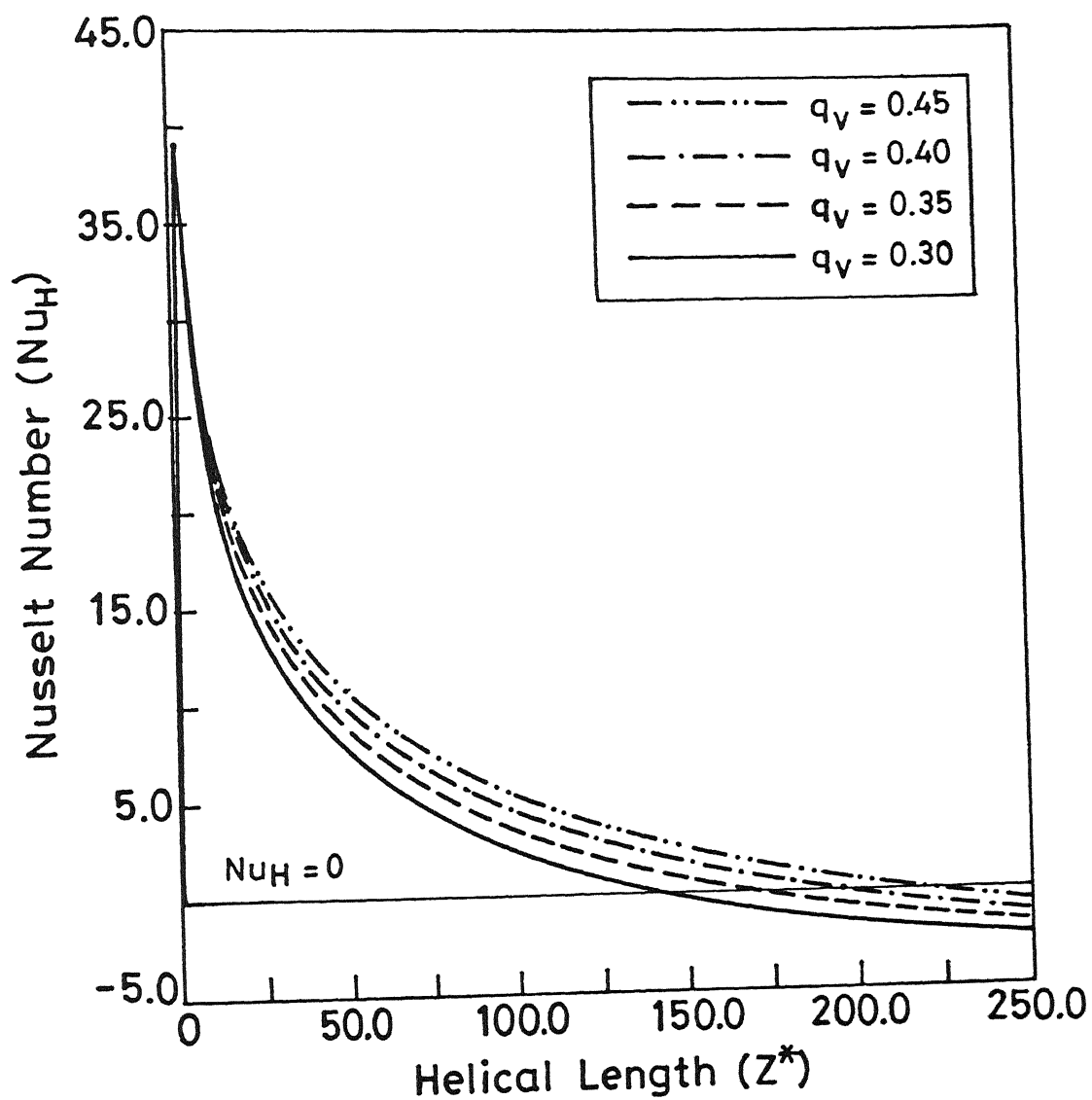
Fig 7.3 Nusselt number distribution along the helical
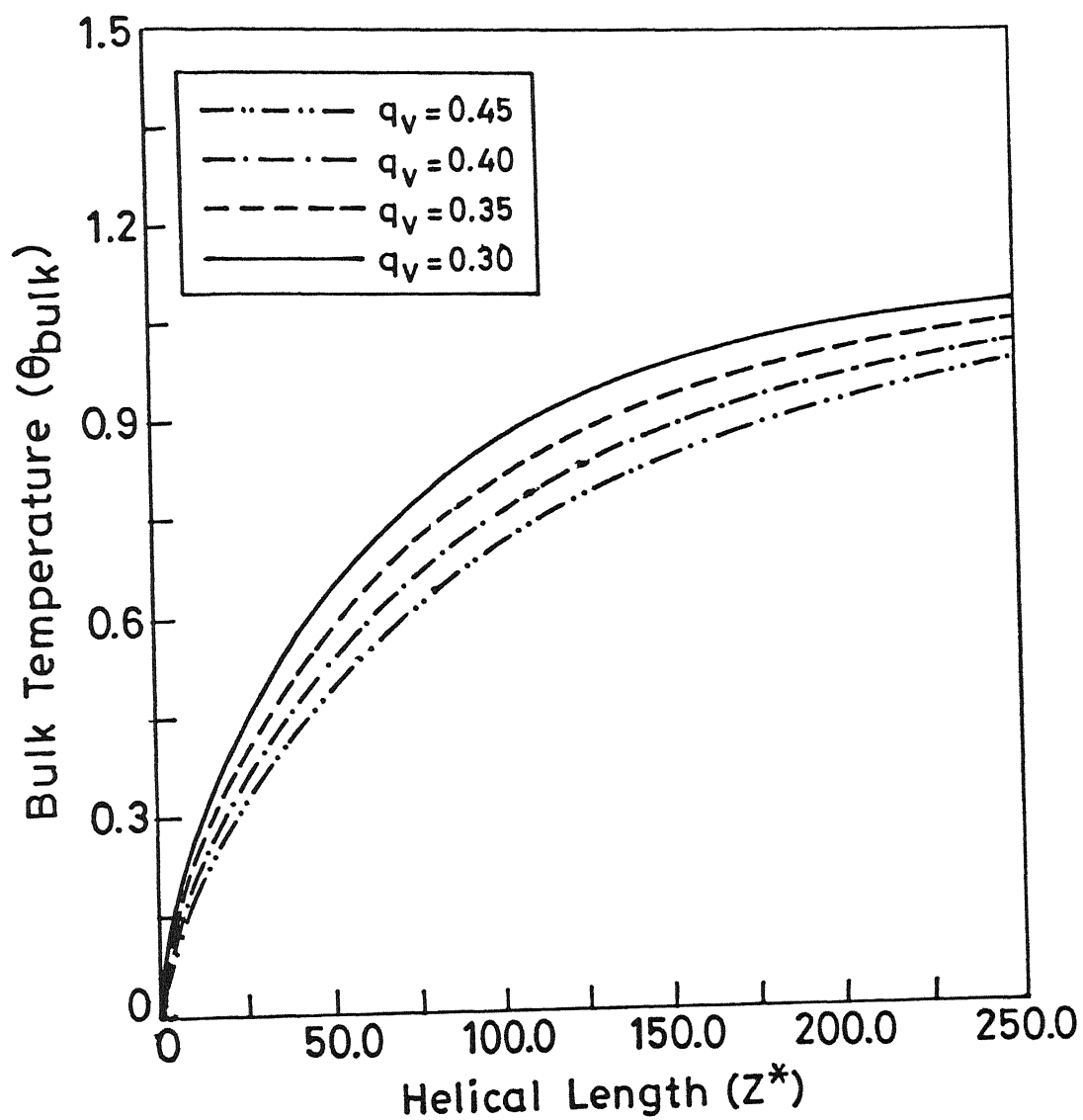length for $q_v = 0.3, 0.35, 0.4, 0.45$.

Fig 7.4 Bulk temperature distribution along the helical length for $q_v = 0.3, 0.35, 0.4, 0.45$.

the foregoing paragraph

<div align="center">TABLE-1</div>

Parameter	Value
Power law index (n)	0 5
Screw helix angle (ϕ)	16 54°
Griffith number (G)	10 0
Peclet number (Pe)	5000 0
Temperature co-efficient of viscosity (β)	1.61

7.2 EFFECT OF POWER-LAW INDEX (n)

Fig 7.5 and Fig 7.6 show that the effect of variation of power-law index n, on the pressure gradient ($\partial p^*/\partial z^*$) and pressure ($p^*$) along the downchannel direction respectively It is to be noted that n=0 5 and n=0.3 represent different grades of LDPE (i e., of different melt flow index, MFI) The viscosity of the fluid having n=0.3 is greater than that for n=0.5. On the other hand n=1.0 represents a Newtonian fluid. It is evident that viscosity of a Newtonian fluid does not depend on the strain-rate. Furthermore, the viscosity of a Newtonian fluid (e.g. lubricating oil) is several orders of magnitude lower than that of molten polymers.

Inspection of Fig 7.5 reveals that pressure gradient for n=1 0 is lowest in comparison with that for n=0.3 and 0.5. This is because for n=1.0, viscosity is lowest and therefore, lowest
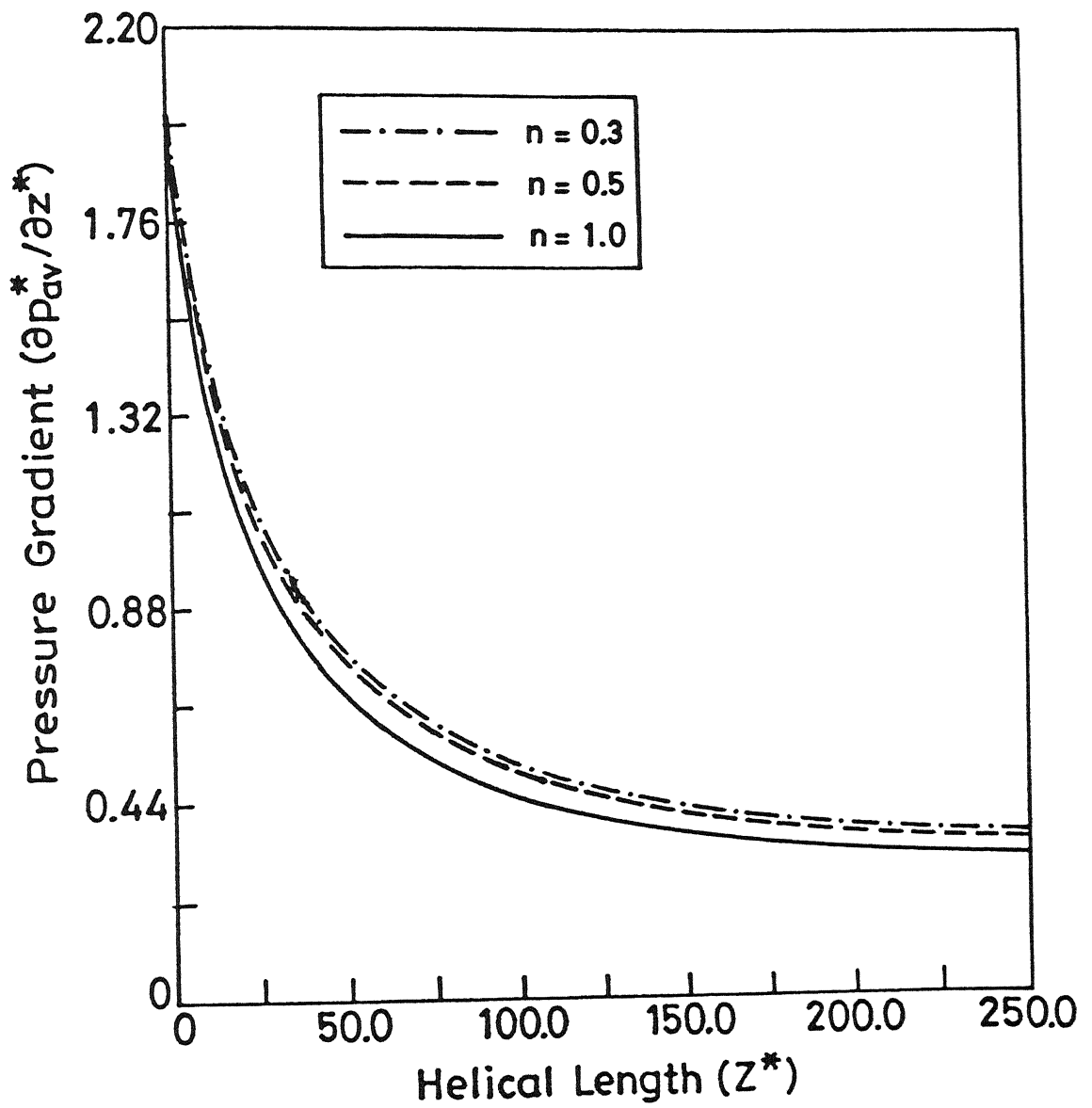
Fig. 75 Pressure gradient distribution along the
helical length for n = 0.3, 0.5, 1.0 .

pressure gradient is generated For the aforementioned reason, it is seen from Fig 7 6 that pressure rise from inlet to outlet is maximum for the fluid with n=0 3, followed by fluids with n=0 5 and n=1 0 respectively

Fig.7.7 depicts the Nusselt numbers, Nu_H variations along the downstream direction of the channel. Nusselt number is lowest for the Newtonian fluid because of higher fluid temperature, the reason being greater strain rate leading to overall greater viscous heating although viscosity is low The strain rate is large because the fluid moves with greater velocity as the viscosity is smaller with respect to fluids with n=0 3 and n=0 5. The net effect is greater viscous heat dissipation (also evident from the term $G \; \dot{\gamma}*^{n+1}$ in the non-dimensional energy equation of the fluid, where for Newtonian fluid n=1.0 as compared to n<1 for other two fluids, G remaining same for all three). It is also noticed that Nu_H becomes negative for the Newtonian fluid earlier in the downchannel length meaning greater heating of the fluid so that the fluid temperature near the barrel becomes greater than the barrel temperature.

Fig.7.8 shows that as expected, for the Newtonian fluid the bulk temperature rise is highest for the reasons mentioned in the previous paragraph.

7.3 EFFECT OF FREQUENCY OF SCREW ROTATION (N)

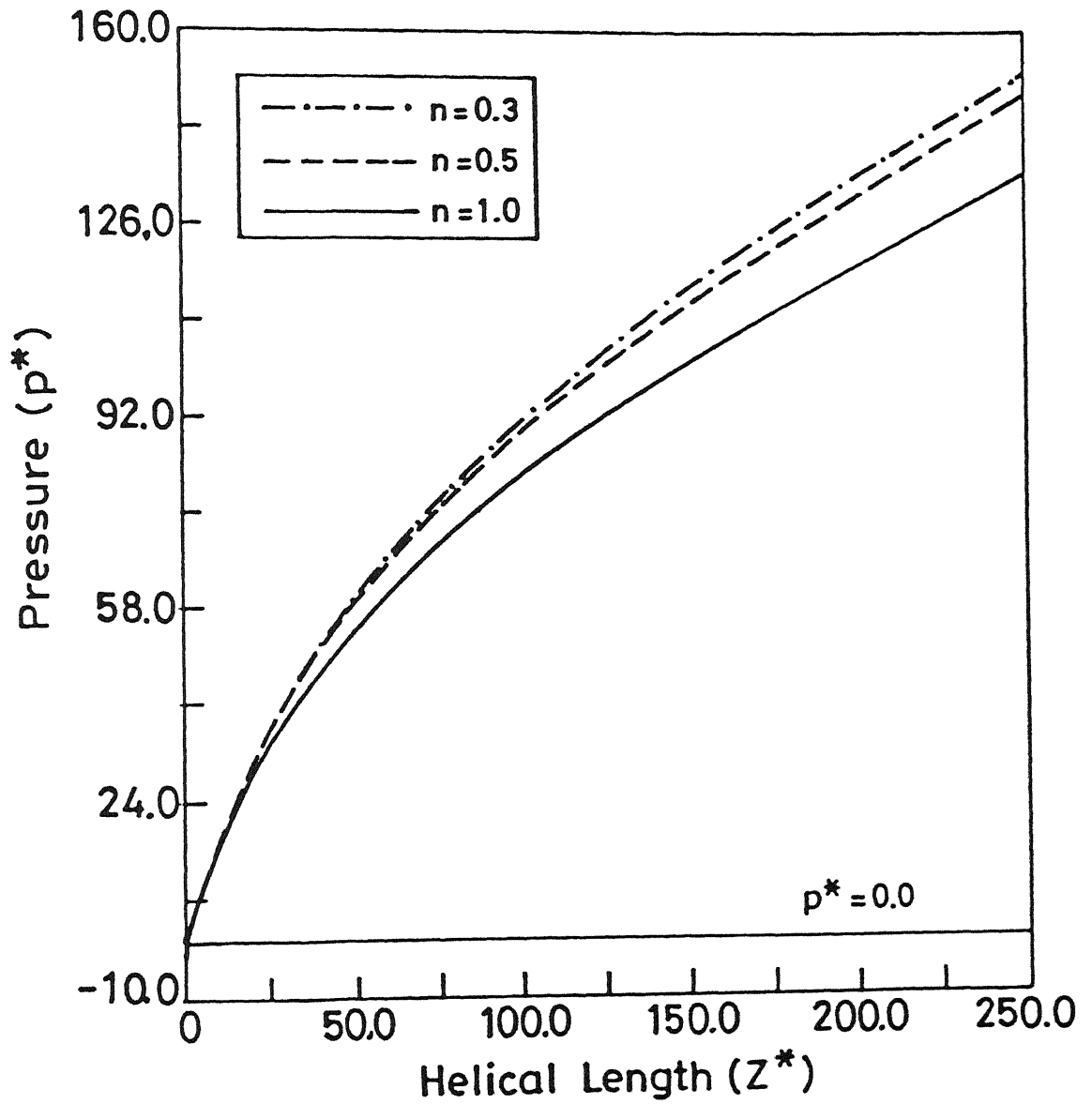The frequency of screw rotation is the single most important

Fig 7.6 Pressure distribution along the helical length
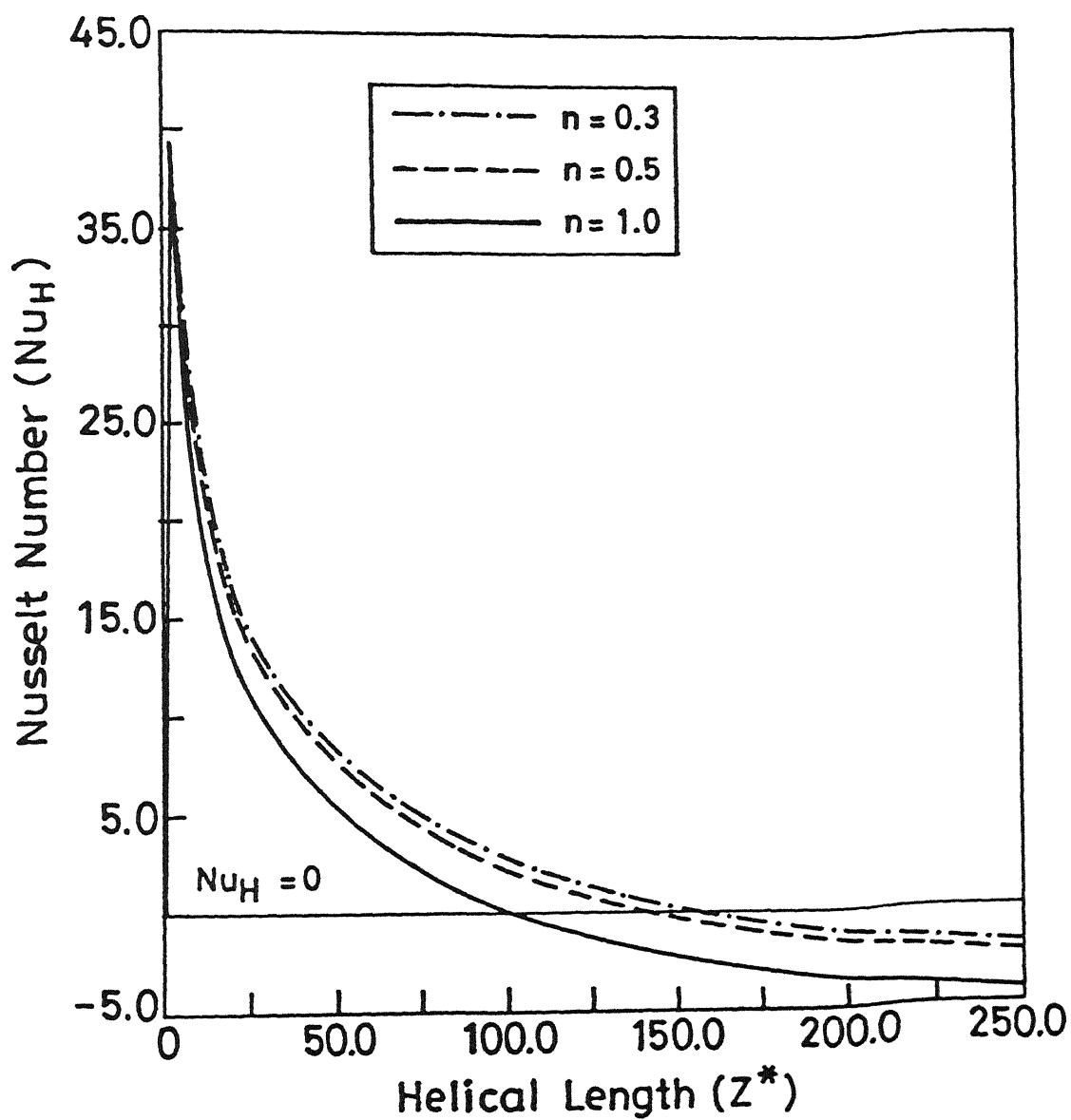for n = 0.3, 0.5, 1.0

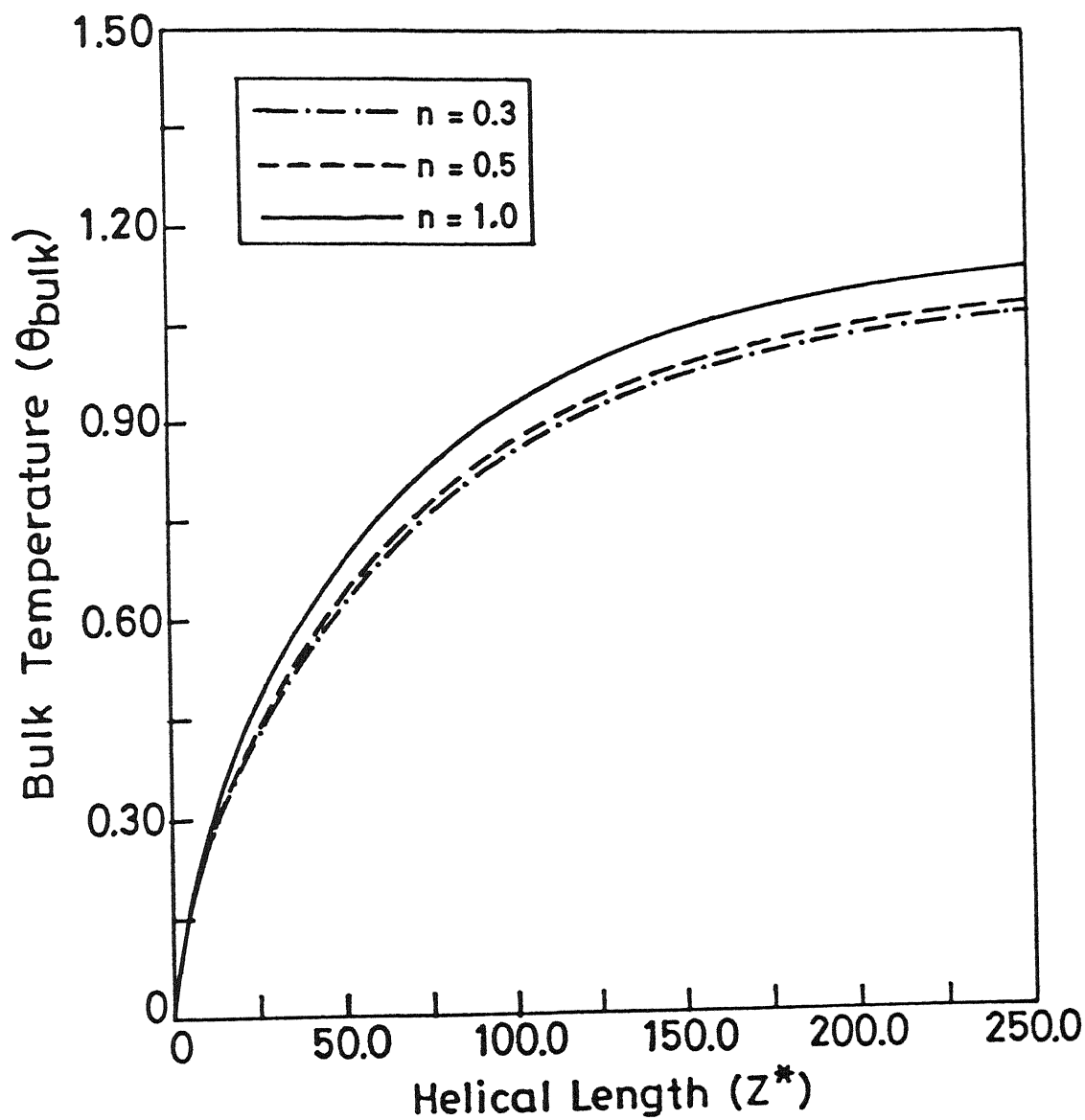**Fig. 7.7 Nusselt number distribution along the helical length for n = 0.3, 0.5, 1.0**

Fig 7.8 Bulk temperature distribution along the
helical length for n = 0.3, 0.5, 1.0

variable, because it can be controlled best and is also most often varied The input data is listed in Table-2 Note that for this parametric study, data for a different extruder handling a different grade LDPE (i e., with different power-law index, n) have been used Three screw speeds of 90, 100, 110 r.p.m have been selected because usually most plasticating screw extruders operate in this range The dimensional flow rate Q is kept constant. (Note that, in the laboratory this can be achieved by means of a valve at the die-end) However, in this case, q_v will be changing since N is changing (meaning V_{bz} is different for different N's)

Fig.7.9 shows the pressure gradient variations along the downchannel direction for N = 90, 100, 110 r.p m . It is readily seen that lower screw speed results in lower pressure gradients and hence lower pressure rise in the extruder (Fig.7.10) and vice-versa This is because at higher screw speeds the barrel drags more amount of fluids but since constant Q is maintained the valve opening is reduced at the channel exit resulting in higher pressure gradient and hence, higher pressure rise

Fig.7.11 shows Nusselt number (Nu_H) variations along the downchannel direction for various screw speeds It is interesting to note that for N = 90 r.p.m , Nu_H at the channel exit is still positive unlike those for N = 100 and 110 r.p.m. in which cases Nu_H's are negative. This is because for lower r.p.m. (N = 90, in this case) viscous heat dissipation is less and hence the fluid temperature near the barrel at the die end has not reached a value
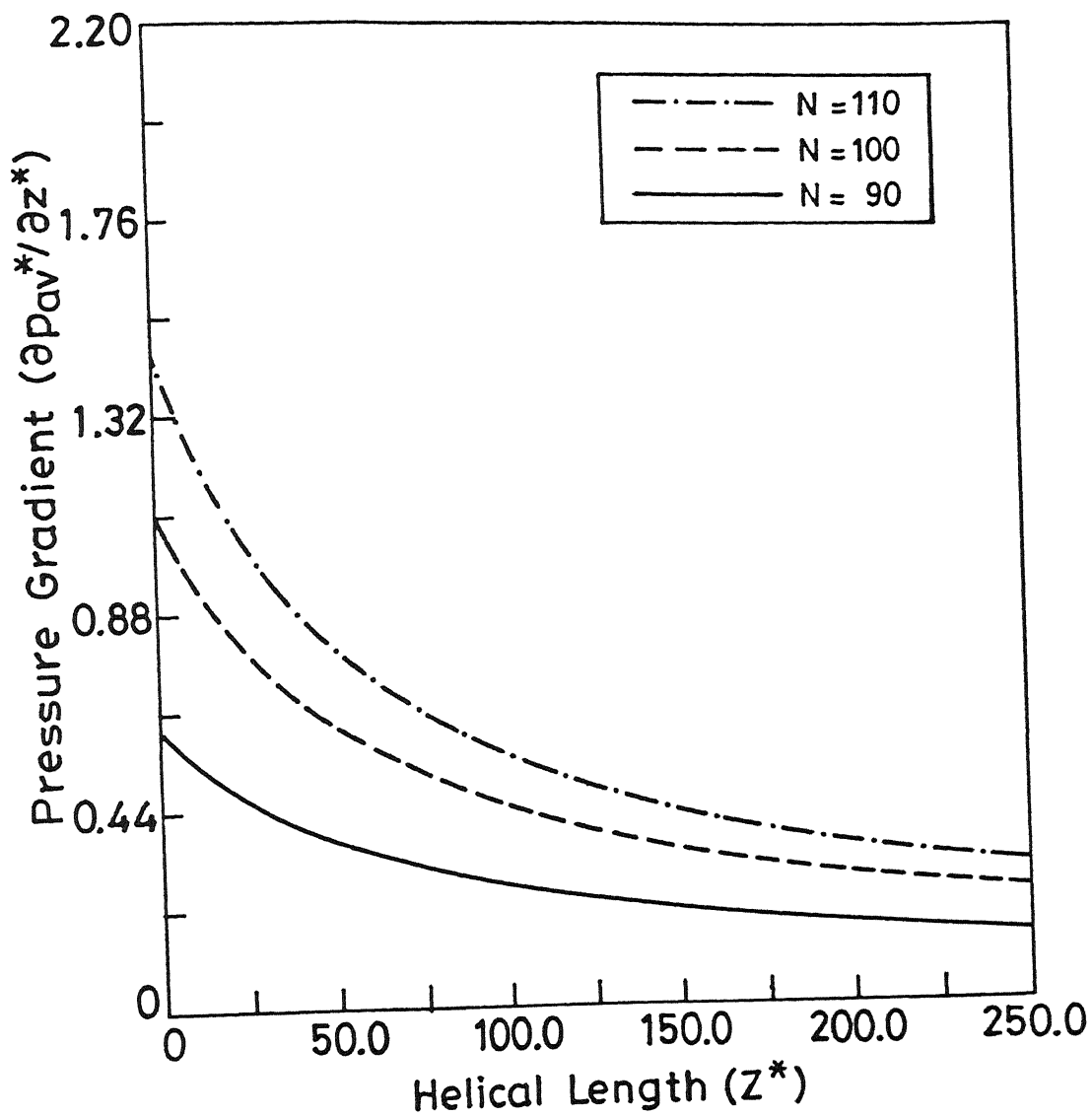
Fig 7.9 Pressure gradient distribution along the
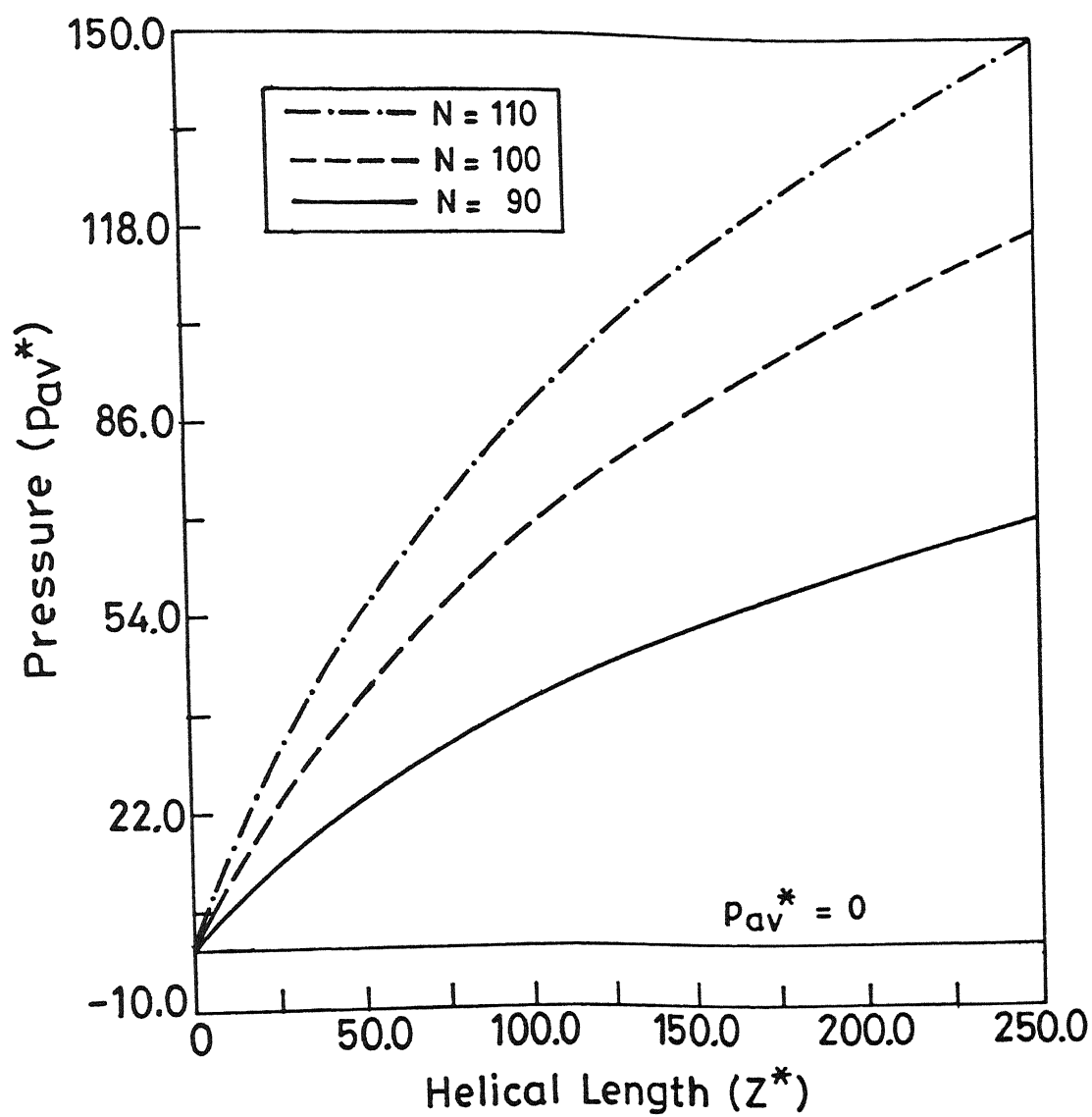helical length for N = 90, 100, 110

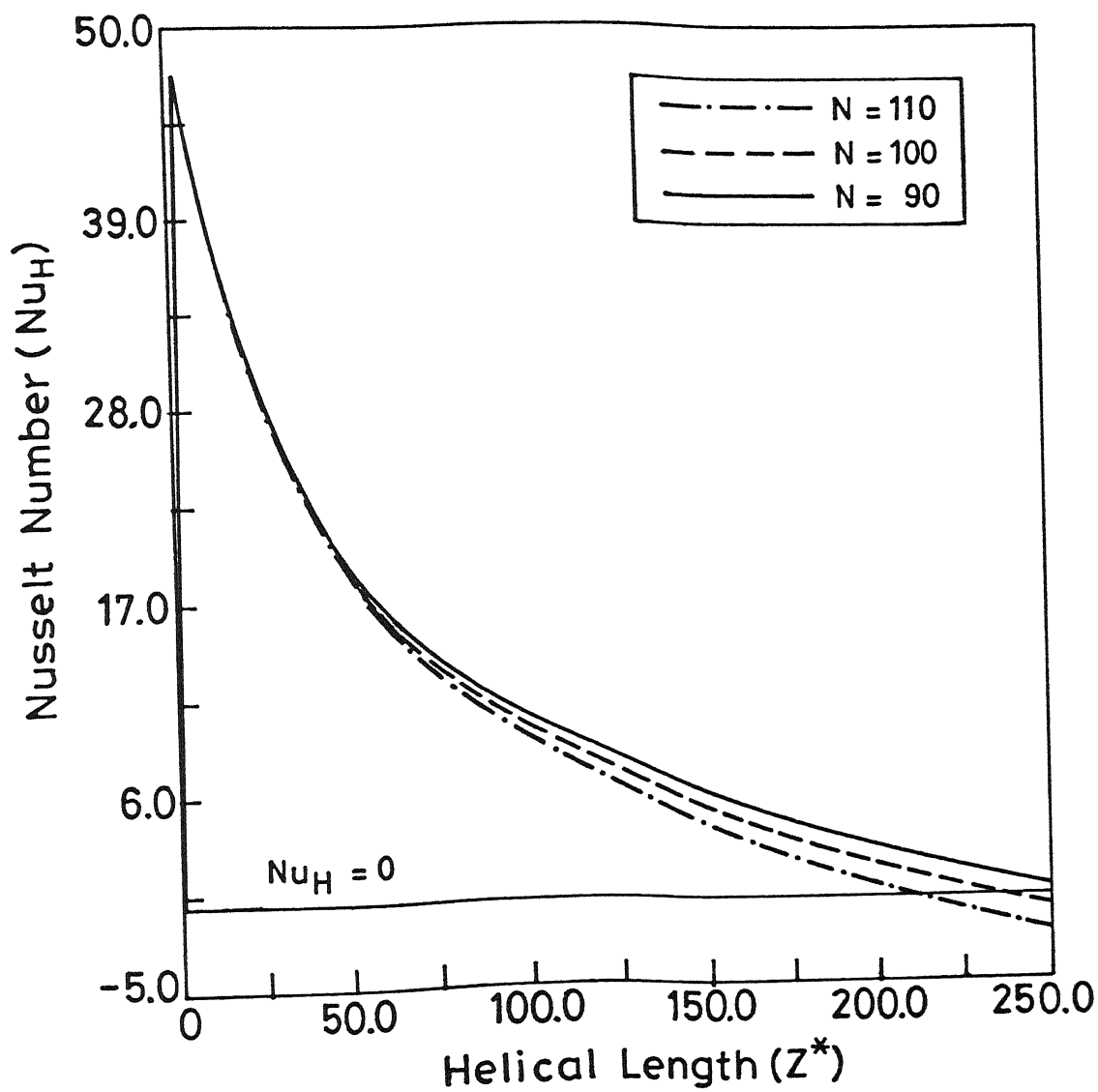Fig 7.10 Pressure distribution along the helical
length for all N = 90, 100, 110

Fig. 7.11 Nusselt number distribution along the helical length for N = 90, 100, 110

greater than or equal to the barrel temperature in sharp constrast to other two cases where viscous dissipations are higher

Finally, Fig 7 12 shows the bulk temperature (θ_{bulk}) rise along the extruder, which, as expected, indicates higher value for higher screw speeds, the reason being greater viscous heat dissipation for larger screw speeds

TABLE 2

| Parameter	Value
Barrel inner diameter, D	120mm
Screw channel depth, H	6mm
Flight width, e	12mm
Axial length, L	480mm
Screw helix angle (ϕ)	17 66^{0}
Flow rate, Q	510 kg/hr
Power law index, n	0 36
Reference viscosity, μ_0	10 8 kNs/m^2
Reference strain rate, γ_0	1 0 s^{-1}
Temperature coefficient of viscosity, b	0.022 C^{-1}
$T_{b(ref)} - T_1$	10 C
$T_i - T_0$	10 C
Specific heat, C_p	2000 J/kg K
Density, ρ	990 kg/m^3
Thermal conductivity, K_f	0 3 W/m K
Thermal conductivity, K_s	45 0 W/m K
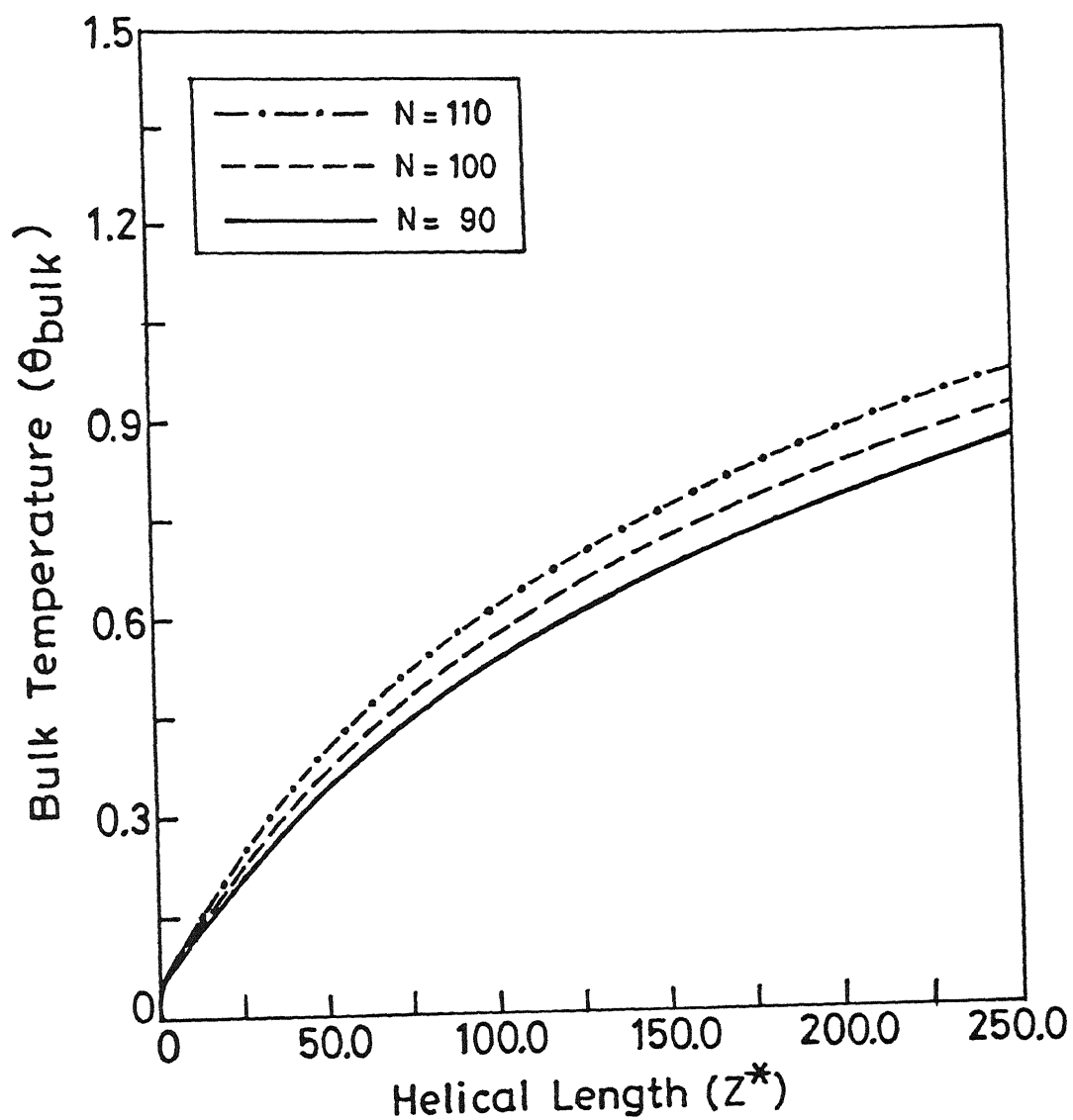
Fig 7.12 Bulk temperature distribution along the
helical length for N = 90, 100, 110

CHAPTER 8

CONCLUSIONS

CHAPTER 8

CONCLUSIONS

A detailed numerical study of thermal transport processes in the metering section of a single-screw plasticating extruder processing non-Newtonian power-law fluids has been carried out Unlike in the earlier works, conduction from the hot melt to the screw body has been taken into account. In the process, three computer models of increasing complexity have been developed and results based on each compared and contrasted with each other

The main achievement of this work is the development of a quasi three-dimensional computer model that includes the important cross-convection (i e., convection normal to the screw flights) thus leading to a very realistic prediction of screw surface temperature and pressure distribution in the downchannel direction. The nature of the screw surface temperature profile matches very well with the trend observed in experiments conducted by earlier researchers in this field. This clearly establishes the superiority of the present three-dimensinal model in its ability to predict flow, thermal and pressure fields in the screw channel over earlier two-dimensional models. However, the two most important outcomes of the comparative study of the quasi-two dimensional and fully two-dimensional models also developed by the

present author are: (a) development of an efficient and novel numerical technique for computing the pressure graients accurately in the case of the fully two-dimensional model and (b) showing that the flow becomes locally fully developed at a short distance from the inlet, - thus confirming the earlier use of fully developed velocity profiles in the quasi two-dimensional model as the inlet boundary condition to be not physically unrealistic The main limitation of both the models is that they do not take into account the thermal convection normal to the screw flights and thus fail to predict realistically the screw surface temperature. The necessity of realistic prediction of screw surface temperature as well as pressure distribution is the motivation behind the development of the quasi-three dimensional model

The velocity vector plots in the cross-sectional planes of the channel at various downstream locations reveal the circulation normal to the screw flights is much stronger as compared to that normal to the screw root. Consequently, thermal convection normal to the screw flights plays a major role in the mixing of the fluid and hence, in bringing the screw surface temperature very close to the barrel temperature This is also confirmed by the isotherm plots in the cross-sectional planes at various downstream locations which show almost uniform temperature near the exit of the channel indicating that the melt is throughly mixed.

The parametric study based on the quasi three-dimensional model reveals that for values of dimensionless volumetric flow rate (q_v) greater than 0.4, pressure gradient ($\partial p^*/\partial z^*$) is

negative (close to zero) which is not desirable because the very purpose of raising the fluid pressure from inlet to outlet will be defeated Therefore, the limiting value of q_v should be 0 4 on the higher side It is also seen that for Newtonian fluid (n=1.0) pressure rise is low and bulk temperature rise is high as compared to two other grades of LDPE (n=0 3 and n=0.5). Also, higher screw speed results in higher pressure rise and higher bulk temperature rise along the downchannel direction of the extruder and vice-versa.

The present quasi three-dimensional model has also formed a firm basis for a realistic design and optimization study of single-screw extruders

REFERENCES

REFERENCES

1   Agur, E E , and Vlachopoulos, J , 1982, Numerical Simulation of Single-Screw Plasticating Extruder, _Polymer Eng Sci_, Vol 22, No 17, pp 1084-1094

2   Bigg, D M , and Middleman, S , 1974, Mixing in a Screw Extruder, Model for Residence Time Distribution and Strain, _Ind Eng Chem Fundam_, Vol 13, pp.66-71

3   Briley, W R , 1974, Numerical Methods for Predicting Three-Dimensional Steady Viscous Flow in Ducts, _J Comp Physics_, Vol 14, pp 8-28.

4   Bruin, S , Van Zuilichem, D J , and Stolp, W , 1978, A Review of Fundamental and Engineering Aspects of Extrusion of Biopolymers in a Single Screw Extruder, _J Food Process Engg_, Vol 2, pp 1-37.

5   Carnahan, B , Luther, H A., and Wilkes, J.O , 1969, _Applied Numerical Methods_, John Wiley & Sons, New York

6   Elbirli, B , and Lindt, J T , 1984, A Note on the Numerical Treatment of the Thermally Developing Flow in Screw, _Polymer Eng Sci_, vol.24, No.7, pp.482-487

7. Fenner, R.T., 1979, _Principles of Polymer Processing_, Chemical Publishing, New York.

8. Fenner, R.T., 1977, Developments in the Analysis of Steady Screw Extrusion of Polymers, _Polymer_, Vol 18, pp.617-635.

9   Gopalakrishna, S , and Jaluria, Y , 1990, Computational Study of Heat and Mass Transfer in a Single Screw Extruder for non-Newtonian Materials, Proc First International Conference on Advanced Computational Methods in Heat Transfer, Portsmouth, U K , pp 363-375

10 Gopalakrishna, S , Jaluria, Y , and Karwe, M V., 1992, Heat and Mass Transfer in a Single Screw Extruder for non-Newtonian Materials, Int J Heat Mass Transfer, Vol 35, No 1, pp 221-237.

11 Gupta, M , and Kwon, T.H , 1990, 3-d Flow Analysis of non-Newtonian viscous Fluids using "enriched" Finite Elements, Polymer Eng Sci , Vol 30, No 22, pp 1420-1430

12 Griffith, R M , 1962, Fully Developed Flow in Screw Extruders, Ind Eng Chm Fundam , Vol 1, No 3, pp.181-187

13 Harper, J , 1980, Food Extrusion, CRC Press, New York.

14 Holman, J P., 1981, Heat Transfer, McGraw Hill International Book Company.

15 Karwe, M V., and Jaluria, Y., 1988, Numerical Simulation of Fluid Flow and Heat Transfer in a Single Screw Extruder for non-Newtonian Fluids, Proc. ASME Winter Annual Meeting, Chicago

16. Karwe, M V , and Jaluria, Y., 1990, Numerical Simulation of Fluid Flow and Heat Transfer in a Single Screw Extruder for non-Newtonian Fluids, Numerical Heat Transfer, Part A, Vol.17, pp.167-190

17 Lappe, H , and Potente, H , 1983, Inestigations into the Throughput Behaviour of Conventional Single Screw Machines, SPE Tech Paper, Vol.29, pp 174-177

18   Lidor, G , and Tadmor, Z , 1976, Theoretical Analysis of Residence Time Distribution Functions and Strain Distribution Functions in Plasicating Screw Extruders, Polymer Eng_ Sci_, Vol 16, pp 450-462

19   Marshall, D I , Klein, I , and Uhl, R H , 1965, SPE J_, Vol 21, pp 1192

20   Martin, B , 1970, Heat Transfer Coupling Effects Between a Dissipative Fluid Flow and its Containing Metal Boundaries, Report to Working Party "Non-Newtonian Liquid Processing" of the European Federation Chemical Engineering

21   Martin, B , 1969, Ph D Thesis, Cambridge University, London

22   Mohamed, I O , and Morgan, R G , 1986, Average Heat Transfer Coefficients in Single Screw Extruders of non-Newtonian Food Materials, AIChE Summer National Meeting, Boston, Mass

23   Mokhtarian, F , and Erwin, L, 1982, Computer Analysis of Mixing in Single Screw Extruders, SPE Tech_ Paper, Vol 28, pp 476-479

24   Palit, Kalipada, and Fenner, Roger T , 1972, Finite Element Analysis of Slow Non-Newtonian Channel Flow, AIChE J_, Vol 18, pp 628-633

25   Palit, Kalipada, and Fenner, Roger T , 1972, Finite Element Analysis of Two-Dimensional Slow Non-Newtonian Flows, AIChE J_, Vol 18, No 6, pp 1163-1170

26   Palit, K , 1972, Ph D. Thesis, London University

27   Palit, K , 1974, Polymer Processing Research Report No 1, Imperial College, Mechanical Engineering Department, U K

28   Patankar, S V , and Spalding, D B., 1972, A Calculation Procedure for Heat, Mass and Momentum Transfer in Three

Dimensional Parabolic Flows, <u>Int J Heat Mass Transfer,</u> Vol 15, pp 1787-1806

29 Patankar, S V , 1980, <u>Numerical Heat Transfer and Fluid Flow,</u> Hemisphere, Washington D C

30 Pearson, J R A , 1966, <u>Mechanical Principles of Polymer Melt Processing,</u> Pergamon, Oxford

31 Raithby, G D , and Schneider, G E , 1979, Numerical Solution of Problems in Incompressible Fluid Flow Treatment of the Velocity-Pressure Coupling, <u>Numerical Heat Transfer,</u> Vol 2, pp 417-440

32 Rauwendaal, C , 1985, Throughput-Pressure Relationship for Power-law Fluids in Single Screw Extruder, <u>SPE Tech Paper,</u> Vol 31, pp 30-33

33 Schlichting, H , 1979, <u>Boundary Layer Theory,</u> McGraw Hill, New York

34 Tadmor, Z , and Gogos, C , 1979, <u>Principles of Polymer Processing,</u> John Wiley and Sons, New York

35 Tadmor, Z , and Klein, I , 1970, <u>Engineering Principles of Plasicating Extrusion,</u> Van Nostrand Reinhold Co , New York

36. VanDoormaal, J P , and Raithby, G D , 1984, Enhancementsof the SIMPLE Method for Predicting Incompressible Fluid Flows, <u>Numerical Heat Transfer,</u> Vol.7, pp 147-163

37 Yates, B , 1968, Ph D Thesis, Cambridge University, London.

38. Zamodits, H J , and Pearson, J R A , 1969, Flow of Polymer Melts in Extruders, Part 1, The Effect of Transverse Flow and of a Superposed Temperature Profile, <u>Trans soc Rheol,</u> Vol 13, No 3, pp 357-385

APPENDIX A

NON-UNIFORM GRID IN THE X-DIRECTION

.

APPENDIX - A

Non-uniform control volume face spacing is used in the x-direction The spacings are symmetric with respect to the mid-width location of the channel width Therefore, while calculating $\Delta\eta_1$, W/2 is used (see Fig A1).
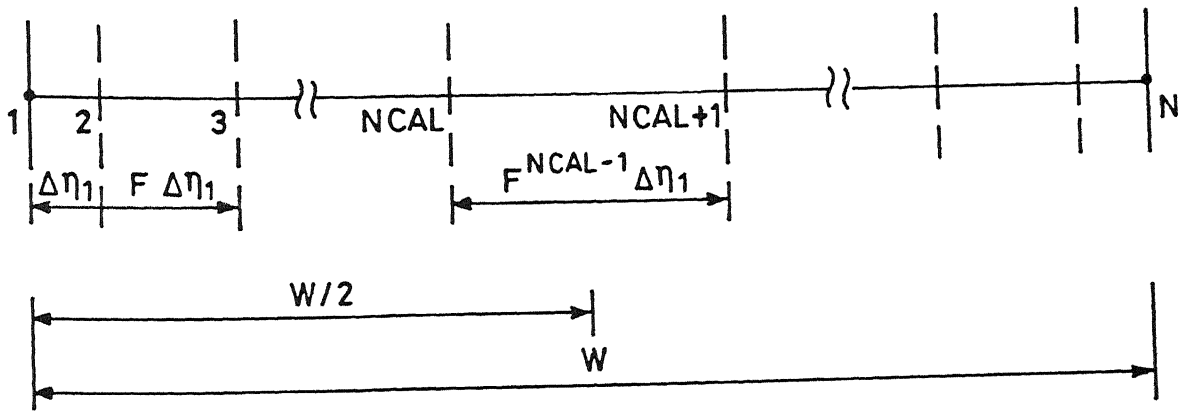

Fig A1 Nonuniform grids in X-direction.

NI = Total number of grid points.

NF = NI - 1 = Number of control volume faces

NCAL = NF/2

F1 = Expansion factor (i e., >1) for grid step length in x-direction

APPENDIX - A

Non-uniform control volume face spacing is used in the x-direction The spacings are symmetric with respect to the mid-width location of the channel width. Therefore, while calculating $\Delta\eta_1$, W/2 is used (see Fig.A1).
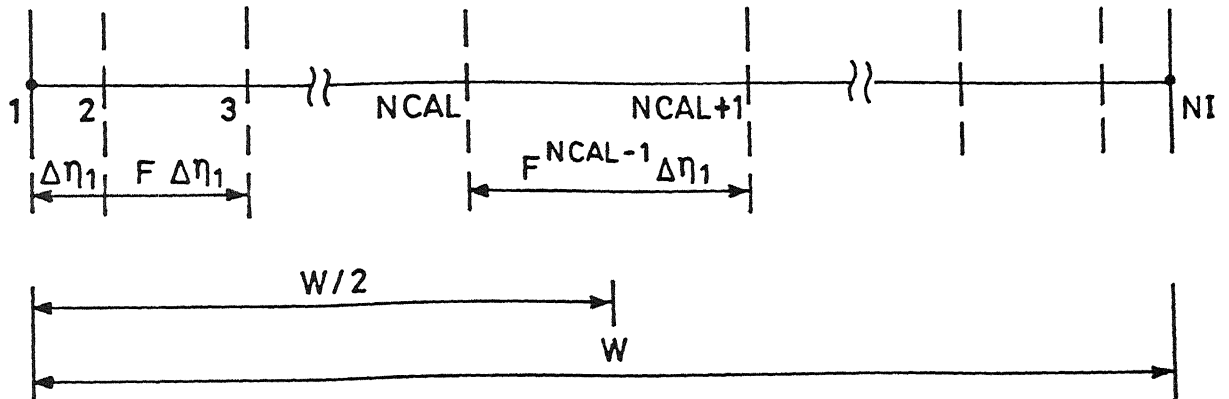

Fig. A1 Nonuniform grids in X-direction.

NI = Total number of grid points

NF = NI - 1 = Number of control volume faces

NCAL = NF/2

F1 = Expansion factor (i e., >1) for grid step length in x-direction

182

$\Delta\eta_1$ = Grid spacing adjacent to the screw flight

As shown in the Fig

$$\frac{W}{2} = \Delta\eta_1 + F_1\Delta\eta_1 + F_1{}^2\Delta\eta_1 + \cdot \ \cdot \ + F_1{}^{NCAL-2}\Delta\eta_1 + \frac{F_1{}^{NCAL-1}\Delta\eta_1}{2}$$

$$= \Delta\eta_1\frac{F_1{}^{NCAL-1} - 1}{F1 - 1} + \Delta\eta_1\frac{F_1{}^{NCAL-1}}{2}$$

$$= \Delta\eta_1\left[\frac{F_1{}^{NCAL-1} - 1}{F1 - 1} + \frac{F_1{}^{NCAL-1}}{2}\right] \tag{A1}$$

$$\text{Let, } A = \left[\frac{F_1{}^{NCAL-1} - 1}{F1 - 1} + \frac{F_1{}^{NCAL-1}}{2}\right] \tag{A2}$$

Therefore,

$$\Delta\eta_1 = (W/2)/A \tag{A3}$$

APPENDIX B

HANDLING OF BOUNDARY CONDITIONS IN THE X-DIRECTION

APPENDIX B

HANDLING OF BOUNDARY CONDITIONS IN THE X-DIRECTION

The temperature boundary conditions at x=0 and W/H are,

$$\frac{\partial \theta}{\partial x} = 0 \qquad (B1)$$

To discretize it, a parabolic profile such as ,

$$\theta = a + bx + c\, x^2 \qquad (B2)$$

is assumed

At $x = x(1) = 0$, (see Fig A2)

$$\theta = \theta_{1,J} \qquad (B3)$$

Therefore,

$$a = \theta_{1,J} \qquad (B4)$$

At $x = x(2)$,

$$\theta = \theta_{2,J} = \theta_{1,J} + bx(2) + cx(2)^2 \qquad (B5)$$

At $x = x(3)$,

$$\theta = \theta_{3,J} = \theta_{1,J} + bx(3) + cx(3)^2 \qquad (B6)$$

Solving Eq.(B5) and (B6),

$$b = \frac{\theta_{2,J}x(3)^2 - \theta_{3,J}x(2)^2}{\{x(3) - x(2)\}x(2)x(3)} - \theta_{1,J}\frac{x(3)+x(2)}{x(2)x(3)} \qquad (B7)$$

Differentiating Eq (B2) w r t x,

$$\frac{\partial \theta}{\partial x} = b + 2cx \qquad (B8)$$

At $x = 0$,

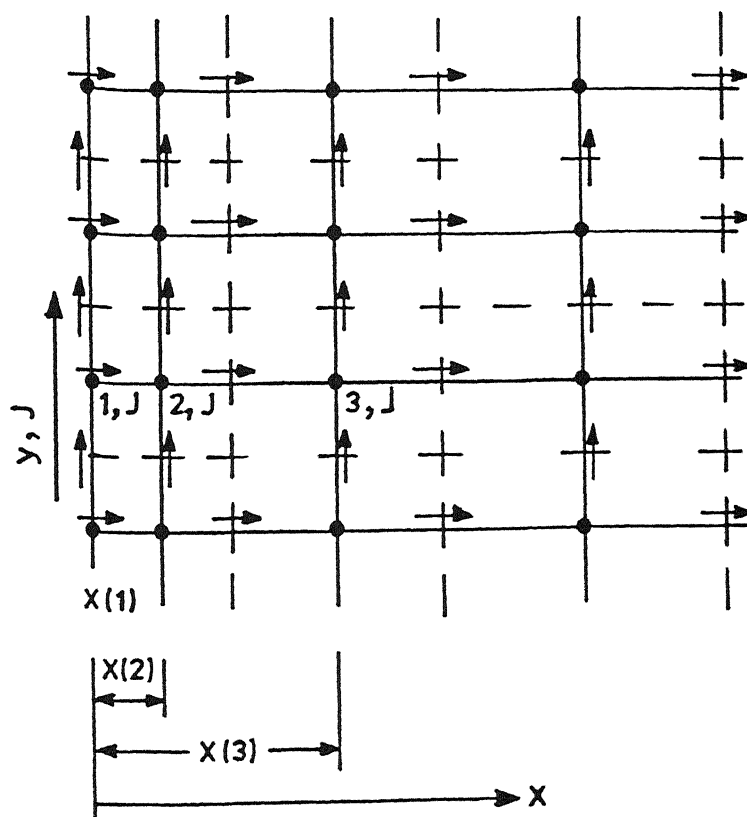$$\frac{\partial \theta}{\partial x} = b \qquad (B9)$$

Fig. A2 Grid numbers at the X-boundary.

Date Slip

This book is to be returned on the
date last stamped